NONLINEAR OPTICAL CHARACTERIZATION OF ORGANIC POLYMERS AND SMALL MOLECULES AND THEIR APPLICATION TOWARDS OPTICAL POWER LIMITING

A Dissertation
Presented to
The Academic Faculty

by

Ariel S. Marshall

In Partial Fulfillment
of the Requirements for the Degree
Doctor of Philosophy in the
School of Chemistry and Biochemistry

Georgia Institute of Technology
August 2014

NONLINEAR OPTICAL CHARACTERIZATION OF ORGANIC POLYMERS AND SMALL MOLECULES AND THEIR APPLICATION TOWARDS OPTICAL POWER LIMITING

Approved by:

Dr. Joseph W. Perry, Advisor
School of Chemistry and Biochemistry
Georgia Institute of Technology

Dr. Jean-Luc Brédas
School of Chemistry and Biochemistry
Georgia Institute of Technology

Dr. David Collard
School of Chemistry and Biochemistry
Georgia Institute of Technology

Dr. Ali Adibi
School of Electrical and Computer Engineering
Georgia Institute of Technology

Dr. Christoph Fahrni
School of Chemistry and Biochemistry
Georgia Institute of Technology

Date Approved: June 30, 2014

To my mother, Lauren, and my loving family and friends

ACKNOWLEDGEMENTS

I would like to express my sincere appreciation to everyone who has helped and supported me during my graduate studies at the Georgia Institute of Technology. Foremost, I would like to acknowledge and express my gratitude to my research advisor, Prof. Joseph W. Perry, for his continuous support of my doctoral research, and for his patience, motivation, enthusiasm, and immense knowledge. It has been a very enjoyable experience to work with Dr. Perry. I could not have imagined having a better advisor and mentor.

I would also like to extend my appreciation to my thesis committee members, Prof. Ali Adibi, Prof. Jean-Luc Brédas, Prof. David Collard, Prof. Cristoph Fahrni, Prof. Bernard Kippelen, and Prof. Seth Marder, for their encouragement, insightful comments, and hard questions.

I would especially like to thank Dr. Joel Hales and Dr. San-hui Chi for their mentorship during my Ph.D. process. Their expertise in chemistry and photophysics, along with their assiduous support was instrumental to my development as a scientist. I also gratefully acknowledge an additional team of mentors in the Perry Research Group: Dr. Vincent Chen, Dr. Mohan Kathaperumal, Dr. Matthew Sartin, Mr. Matteo Cozzuol, and Dr. Philseok Kim. Thank you for your insightful comments, and most importantly, thank you for all your help with LabView! My thanks also go to the current and past members of the Perry Research group for their help and friendship.

I would like to acknowledge my collaborators. My thanks go to Prof. Uwe Bunz, Dr. Evan Davey, and Dr. Anthony Zucchero for supplying the poly(phenylene

ethynylene) polymers and engaging me in thoughtful discussion concerning this work. I also would like to thank Prof. Frieder Jäkle, Xiaodong Yin and Dr. Pangkuan Chen for the organoborane oligomers and all their help. From the Perry Research Group, I gratefully acknowledge Mr. John Tillotson and Mr. Lucas Johnstone for the supply of dyes and the TEM images. I would also like to thank Dr. Nikolay Makarov for his instruction and helpful discussions.

I have been very fortunate to have a wonderful support team during my stay in Atlanta. Thank you to all those at Georgia Tech who served as mentors and as sounding boards for me, especially Dr. Keith Oden, Dr. J. Cameron Tyson, and Ms. Olanda Bryant. Also, thank you to my good friends, Ms. Ellenor Brown and Mr. Marchello Cavitt, and to my "PChem" crew (Dr. O'Neil Smith, Dr. Megan Lydon, Dr. Anthony Giordono, Dr. Sergio Paniagua, Mrs. Jessica Paniagua, Mr. Aaron Danberry, Ms. Emily Herman, Ms. Helen Westbrook, Mr. Anselmo Kim, and Dr. Amy Jablonski) for their laughter and support.

My sincerest gratitude is extended to my dear friend, Mr. Christopher Sutton, for his friendship and support. Thank you for "following" me to Georgia Tech. I am so glad to have gone through my undergraduate and graduate experiences with such a good friend. I would also like to thank my undergraduate advisor, Prof. Patrick Desrochers, for inspiring me to pursue a career in chemistry.

I would like to thank my Arkansas family and friends for their unending support and love. I appreciate every phone call, every visit, and every thoughtful prayer that was sent my way. This would not have been possible without your love and encouragement.

Finally, I would like to thank God for granting me the strength and fortitude to make it through this process.

TABLE OF CONTENTS

LIST OF TABLES

LIST OF FIGURES

LIST OF SYMBOLS

α	Linear polarizability
γ	2nd-order hyperpolarizability
$\chi^{(3)}$	Thrid-order suceptibility
β	Two-photon absorption coefficient
c	Light speed in vacuum
ε	Molar extinction coefficient
Φ_{fl}, η_{fl}	Fluorescence quantum yield
σ_{01}	One-photon absorption cross section
δ	Two-photon absorption cross section
I	Intensity
L	Sample length
λ	Wavelength
n	Refractive index
n_2	Nonlinear refractive index
N	Number density
N_A	Avogadro number
ω	Frequency
A	Pre-exponential factor
τ	Lifetime
τ_{fl}	Fluorescence lifetime
ω_0	beam waist

SUMMARY

This thesis is concerned with the photophysical and nonlinear optical responses, and applications of a set of conjugated polymers and small molecules in the visible and near-IR spectral regions.

Poly(phenylene ethynylene) PPE polymers were substituted with conjugated side-arms in a cruciform fashion to determine the impacts of electronic coupling on the one-photon (1PA), two-photon (2PA), and excited state absorption (ESA) properties of the co-polymer system. The cruciform-like PPEs showed significant changes in their nonlinear and phophysical behavior relative to their linear models, including shifts and splittings of the 1PA bands due to moderate mixing of the lowest singlet excited states, an increase in the 2PA cross section (δ) values, and an increase in the yield of triplet excited-state species. The cruciform-like PPE polymers exhibited effective optical pulse suppression of femtosecond and nanosecond laser pulses over a broad spectral range of ~200 nm in the visible and near-IR. The suppression capability of the cruciform-like PPEs exceeded the best reported value for alkyl-substituted PPE polymers.

The spectroscopic effects due to conjugation length, structural configuration, and intramolecular charge transfer (ICT) are discussed for a family of bent donor-acceptor-donor (D-A-D) -type conjugated oligomers, which incorporate electron-rich triarylamine donors and electron-deficient triarylborane acceptor units into its conjugated structure. These organoborane oligomers are highly fluorescent and exhibit strong 2PA in the visible region with δ values as large as 1410 GM, as well as overlapping ESA bands attributed to singlet-singlet and triplet-triplet absorption. Saturation of the molar

absorptivity, ε, and δ was observed at less than two repeat monomer units due to conformational disorder in the oligomer with increasing length. Positive solvatochromism of fluorescence with solvent shifts as large as ~70 nm was observed as a result of ICT from the arylamine donors to boryl-centered acceptor sites. The excited-state dynamics also show sensitivity to the solvent environment. Experimental findings suggest that these organoborane oligomers may have potential use as nonlinear material for optical power limiting (OPL) and two-photon sensing applications.

The spectral properties of two bis-donor chromophores, (bis(diarylamino)biphenyl (TPD) and distyrylthiophene (DST), were investigated with and without the presence of AgNPs in order to better understand the local-field enhancement and subsequent effects on the photophysics and nonlinear behavior of 2PA dyes. While little changes were observed in the excited-state dynamics, measurements of nanoparticle aggregate-dye composite solutions with TPD revealed a 1.6-enhancement in the two-photon excited fluorescence signal. OPL measurements of nanosecond laser pulses at 532 nm revealed a reduction in threshold energy by a factor of 2 in solutions containing TPD and AgNP aggregates, relative to solutions of TPD alone. DST shows exceptional solubility (>1 M) in several organic solvents and exhibits a 2PA spectrum that overlaps well with its singlet-singlet and triplet-triplet ESA bands. Consequently, DST exhibits effective optical limiting of nanosecond laser pulses through two-photon induced excited-state absorption over a broad spectral range of approximately 200 nm in the red and near-IR.

CHAPTER 1

CONJUGATED ORGANIC SMALL MOLECULE AND POLYMERIC MATERIAL FOR PHOTONIC AND OPTOELECTRONIC APPLICATIONS

1.1. Introduction

Since the invention of the laser, photonics has emerged as a multidisciplinary field of science and technology that has captured the imagination of scientists and engineers because of its potential applications. Photonics is an analog to electronics, where in place of electrons, photons facilitate the generation, transmission, modulation and other processes associated with the manipulation of light [1, 2]. Nonlinear optics is expected to play a large role in future photonic applications as nonlinear media have the ability to modify the frequency, polarization, amplitude or direction of the incident light [3]. Substantial efforts have been directed towards exploiting these nonlinear optical (NLO) phenomena in suitable materials for devices applications [2, 4].

Although all materials can exhibit some form of NLO phenomena under certain excitation conditions, conjugated organic materials are increasingly being recognized for their potential in NLO applications [3, 5, 6]. This is due to the highly delocalized π electrons in the conjugated framework of organics that are sensitive to subtle modifications in molecular structure and the surrounding medium, giving rise to significant changes in the optical and electronic properties [7]. Furthermore, as opposed to traditional inorganic NLO materials (such as GaAs and CdSe), organic materials offer the ability for facile synthetic modification and doping as a means of maximizing and

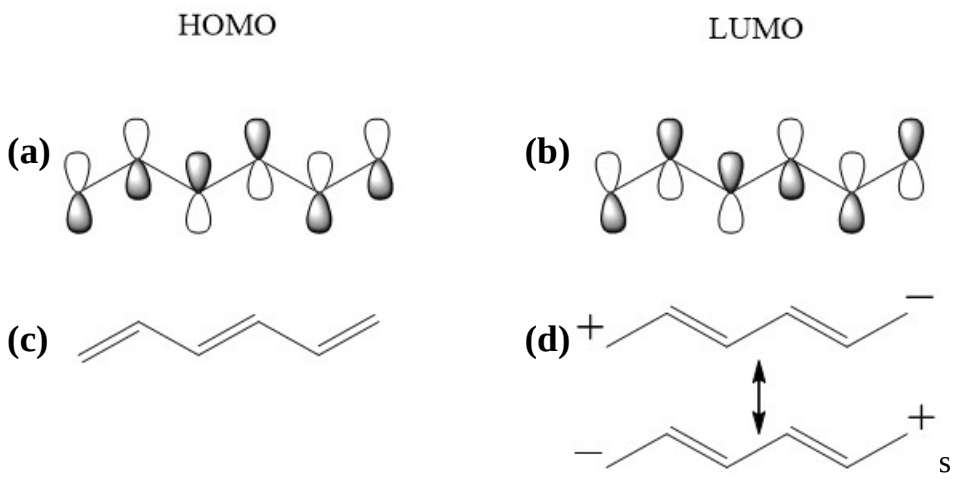

Figure 1.1. HOMO (a) and LUMO (b) wavefunctions along with the ground- (c) and excited-state configurations (d) of hexatriene.

tailoring their NLO and other properties. Organic conjugated materials also offer variety in their fabrication methods for constructing NLO devices. Depending on their molecular structure, conjugated organic molecules or polymers can be grown into single crystals [8, 9] or processed into thin film structures via wet processing methods [10] (such as spin-casting) allowing for potential mass production of NLO devices at relatively low-cost.

To briefly introduce the origin of the linear and NLO responses of conjugated organic materials, we can consider the factors influencing the polarizability associated with the transition between the HOMO and LUMO wavefunctions of a simple polyene molecule. As shown in Figure 1.1a and 1.1b, the bonding and antibonding character of the HOMO wavefunction of hexatriene translates to the double- and single-bond character of the geometry in the ground state. Upon excitation to the first optically-allowed state, there is an instantaneous shift in π-bond density, such that the LUMO (Figure 1.1b) shows a complete reversal of the bonding- and antibonding-character in the polyene. In the case of hexatriene, the shifting of π-bond density results in strong charge

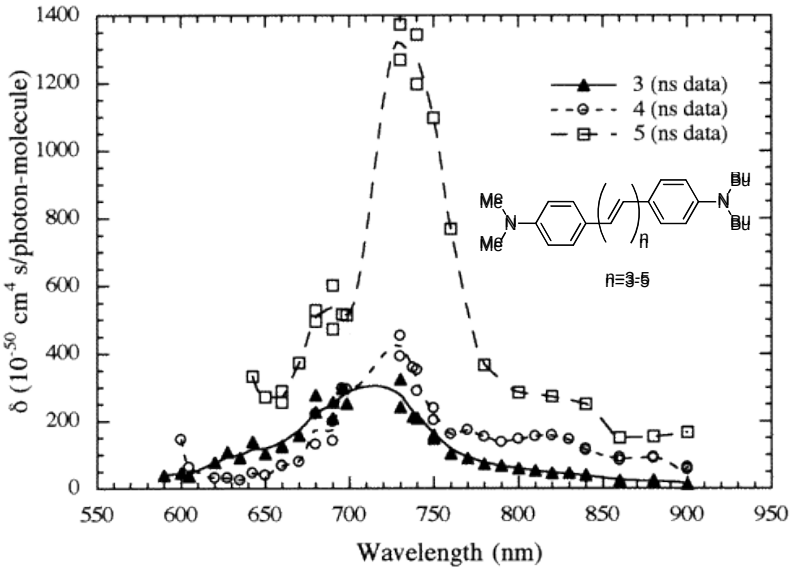

Figure 1.2. Two-photon absorption spectra of D-π-D chromophores with varying π-conjugation lengths. The molecular structure of the chromophores are depicted in the inset of the plot. Reprinted with permission from Mariacristina Rumi; Jeffrey E. Ehrlich, Ahmed A. Heikal, Joseph W. Perry, Stephen Barlow, Zhongying Hu, Dianne McCord-Maughon, Timothy C. Parker, Harald Röckel, Sankaran Thayumanavan, Seth R. Marder, David Beljonne, and Jean-Luc Brédas. J. Am. Chem. Soc. 2000, 122 (39), 9500-9510. DOI: 10.1021/ja994497s. Copyright © 2000 American Chemical Society.

separation (Figure 1.1d). These large changes in electron density upon excitation correlate with large and fast polarizabilities observed in π-conjugated networks [7].

Third-order NLO processes can give rise to a multitude of phenomena including third-harmonic generation, self action (i.e. self-focusing, self defocusing, or self-phase modulation) [7], two-photon absorption [11, 12], degenerate four-wave mixing [13], and coherent Raman effects [14]. These processes are of interest for photonic applications such as all-optical switching (AOS) [15] and optical power limiting (OPL) [16], both of which are particularly important as laser systems are ubiquitous in information and communication technologies. Intensive research efforts have been devoted towards

identifying organic conjugated materials with large third-order NLO responses. Such materials are very desirable as they offer the

potential of greater sensitivity, thus allowing for lower laser intensities to be utilized to generate various NLO processes.

Experimental and theoretical results have allowed for the identification of specific relationships between the molecular structure of the organic molecule or polymer and the magnitude of the third-order nonlinearity it exhibits. Marder and Perry et al. [17] showed that incorporating electron donors or acceptors in the terminal positions of linear conjugated molecules (so-called quadrupolar dyes) could induce intramolecular charge transfer (ICT) upon photoexcitation, resulting in exceptionally large two-photon absorption (2PA) relative to the unsubstituted analogue. The π-conjugated bridge is an important consideration in the design of organic third-order NLO materials. As demonstrated by Brédas et al. [18] and Reinhardt et al. [19], inserting highly polarizable or electron rich π-bridge molecules (such as thiophene or phenylene vinylene) between terminal donor or acceptor units can lead to significant enhancement of the third-order NLO response of an organic material [18].

An increase in third-order nonlinearity is also observed when the π-conjugated bridge is extended, as NLO response is a function of the molecular length [20, 21]. Similar increases in the magnitude of 2PA with length have been reported for quadrupolar molecules [17, 22]. As the charge separation between the terminal groups and the center of the molecule is increased, large changes in the quadrupole moment are observed resulting in larger NLO responses (see Figure 1.2).

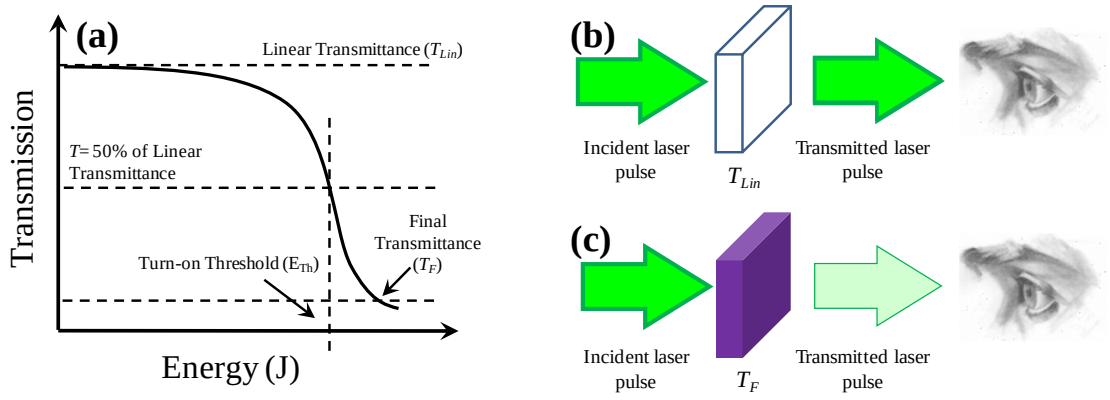

Figure 1.3. (a) Example of energy-dependent transmission curve generated during OPL measurements, along with notation of relavant terms. Illustration of what occurs during the OPL process at T_{Lin} (b) and at T_F (c).

Octupolar or multibranched chromophores are also of interest for third-order NLO applications [23, 24]. These structures generally consist of a central unit on which electron donors or acceptor substituents and/or conjugated segments can be attached in a trigonal arrangement [12]. Photoexcitation of octupolar dyes can result in charge transfer along the three different axes of the chromophore [23]. Although heavily investigated for their second-order

nonlinearities, octupolar dyes show strong 2PA that can be utilized for third-order NLO applications, as well.

1.2. Optical Power Limiting (OPL)

Optical limiters are devices that show high transmission at low fluencies, but strongly attenuate intense laser pulses at high fluencies [16, 25] (see Figure 1.3). These devices are of significant interest for the protection of sensors and of operators of high-power laser systems. While there are a large number of schemes or devices that can perform optical limiting, to do so in a passive or instantaneous manner is accomplished

using NLO materials in which the sensing, processing, and a response due to changes in fluence are all accomplished essentially simultaneously. As opposed active optical limiters, OPL using NLO materials does not require the sending or receiving of electronic signals or the use of a sensor. The OPL response of NLO materials is an intrinsic physical characteristic allowing for such limiters to be effective with short optical pulses. Desired OPL materials exhibit high linear transmission (T_{Lin}) at low fluence, low turn-on energy or fluence threshold (E_{Th} or F_{Th}), and large pulse energy suppression at high fluence over a wide spectral and temporal range.

A number of third-order NLO processes have been demonstrated as effective means for achieving OPL. Instantaneous mechanisms, or processes in which the polarization density resulting from an applied electric field occurs immediately, include nonlinear absorption, nonlinear refraction, and nonlinear scattering [16]. Other methods are characterized as accumulative nonlinearities that develop and/or decay on timescales comparable to or longer than that of the incident laser pulse [25]. Such accumulative OPL methods include excited-state or free-carrier absorption. NLO materials that can give rise to instantaneous and accumulative OPL mechanism are very attractive as their efficacy can extend over a wide range of time domains.

The optical limiting phenomena was first reported in 1967 by Geusic, Singh, Tipping, and Rich at Bell Labs where single crystals of undoped and B- or P-doped silicon exhibited intensity-dependent transmission of nanosecond-laser pulses at 1064 nm [26]. In the 1980s, Van Stryland and coworkers demonstrated OPL using organic materials, wherein CS_2 liquid solutions suppressed ns-laser pulses 1064 nm via self focusing followed by thermal nonlinearities at high fluences [27]. Pioneering work by

Heeger [28], Blau [29], Perry [30-33], Prasad [34-36], and many others have furthered the development of organic conjugated materials for OPL applications. Particularly, research in the Perry group has shown that π-conjugated polymers can exhibit broadband 2PA-based OPL in the near-IR with unprecedented spectral coverage with bandwidths as large as 500 nm [37, 38].

1.2.1. OPL via Reverse Saturable Absorption

During the development of passive mode locking and Q-switching lasers, materials referred to as saturable absorbers were sought that would bleach or show transparency under intense optical irradiation. In 1967, Guiliano and Hess of the Hughes Research Laboratories discovered a process where materials did not bleach but absorbed more strongly as the incident energy increased [39]. The process is referred to as reverse saturable absorption (RSA) or one-photon absorption followed by excited-state absorption (1PA-ESA).

RSA is an accumulative OPL process that generally occurs in a molecular system when the cross section (or probability of absorption) in the excited state is larger than that of the ground state. For example, if we consider a three-level energy diagram (see Figure 1.4a), with σ_{12} being larger than σ_{01} then RSA can occur in the molecule. Organic materials that exhibit RSA have shown to be very effective optical limiters for long pulse durations (>1 ns), but the usable spectral range and linear transmittance are compromised by linear absorption at the excitation wavelength. Nevertheless, the highest figure-of-merit (FOM)[i] values to date have been attained via RSA [30, 31].

[i] For accumulative OPL process, the FOM can be defined as the ratio of the excited-state (σ_{ESA}) and ground-state cross section (σ_{GS}), such that $FOM = \sigma_{ESA} / \sigma_{GS}$. For an instantaneous OPL process, *FOM* =

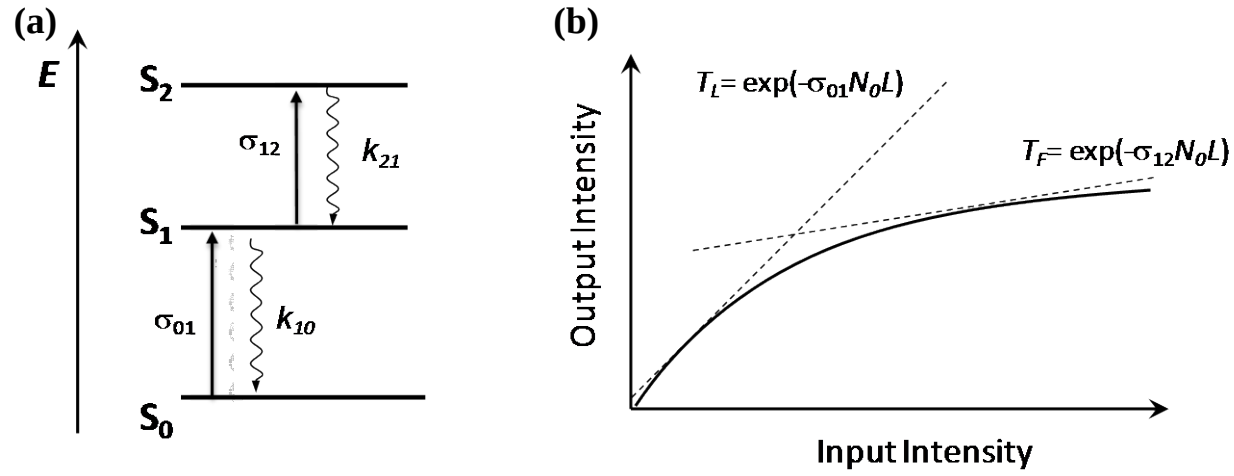

Figure 1.4. (a) Schematic three-level energy diagram and (b) illustration of nonlinear reponse of a reverse saturable absorber.

1.2.1.1. Rates and Responses of RSA Limiters

The simplest case for RSA can be demonstrated using a three-level diagram (see Figure 1.4a). At low pulse energy, the transmission of a material is governed by the ground-state absorption and can be written as

$$T_{Lin} = \exp(-\sigma_{01} N_0 L) \qquad \text{(Eq 1.1)}$$

where σ_{01} is the cross section for the transition between states 0 and 1, N_0 is the initial ground state population, and L is the length of the sample. At high input energy, however, the first excited state becomes sufficiently populated and the transmittance is then governed by the excited-state cross section (σ_{12}):

$$T_F = \exp(-\sigma_{12} N_0 L) \qquad \text{(Eq 1.2)}$$

An illustration of the nonlinear absorption response of a three-level reverse saturable absorber is displayed in Figure 1.4b. As the figure illustrates, to achieve a strong optical limiting response, it is necessary to obtain large σ_{12}/σ_{01} value. Also,

---

T_{Lin}/T_F, where T_{Lin} is the linear transmission and T_F is the final transmission or the transmission just before saturation or damage.

optical limiting via RSA is not truly "limiting" as the transmittance continues to increase with energy; however, it does so more slowly. The three-level RSA model generally involves transitions to the singlet excited states of the molecule which have a decay of 10^{-9}-10^{-12} s; therefore, OPL via a three-electronic state model (or via singlet-singlet ESA) is effective for short pulse durations. OPL via RSA can also be achieved for longer pulse durations (>10^{-9} s) through the ESA of triplet or longer-lived species, such as radical ions. Taking into account additional photophysical processes, such as intersystem crossing, we will now consider a five-electronic state model of a reverse saturable absorber (Figure 1.5).

Initial optical pumping of the molecule can promote an electron from the ground state to the lowest excited singlet state. Subsequent pumping may lead to RSA via singlet-singlet ESA, or if there is intersystem crossing on the time scale of the laser pulse, RSA via triplet-triplet ESA. We can use simple rate equation models in describing the electronic state population for the five-state model:

$$dN_0/dt = -\sigma_{01}N_0\phi + k_{10}N_1 + k_{30}N_3 \quad \text{(Eq 1.3)}$$

$$dN_1/dt = \sigma_{01}N_0\phi - (\sigma_{12}\phi + k_{10} + k_{13})N_1 + k_{21}N_2 \quad \text{(Eq 1.4)}$$

$$dN_2/dt = \sigma_{12}\phi N_1 + k_{21}N_2 \quad \text{(Eq 1.5)}$$

$$dN_3/dt = -(\sigma_{34}\phi + k_{30})N_3 + k_{13}N_1 \quad \text{(Eq 1.6)}$$

$$dN_4/dt = \sigma_{34}\phi N_3 - k_{43}N_4 \quad \text{(Eq 1.7)}$$

$$N_0(0) = N_0(t) + N_1(t) + N_2(t) + N_3(t) + N_4(t) \quad \text{(Eq 1.8)}$$

where ϕ is the photon flux, N is the number density of the subscripted state, and σ_{ij} and k_{ij} is the absorption cross section and rate of decay between the subscripted states i and j.

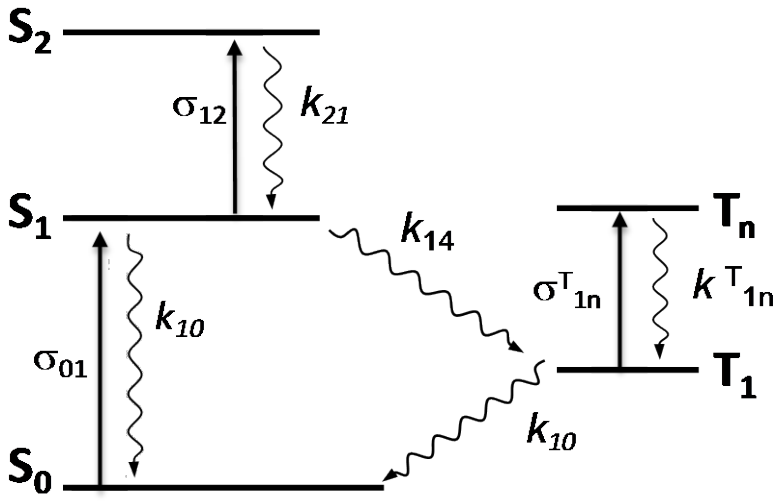

Figure 1.5. Schematic five-level energy diagram and photophysical processes that can occur with a molecule.

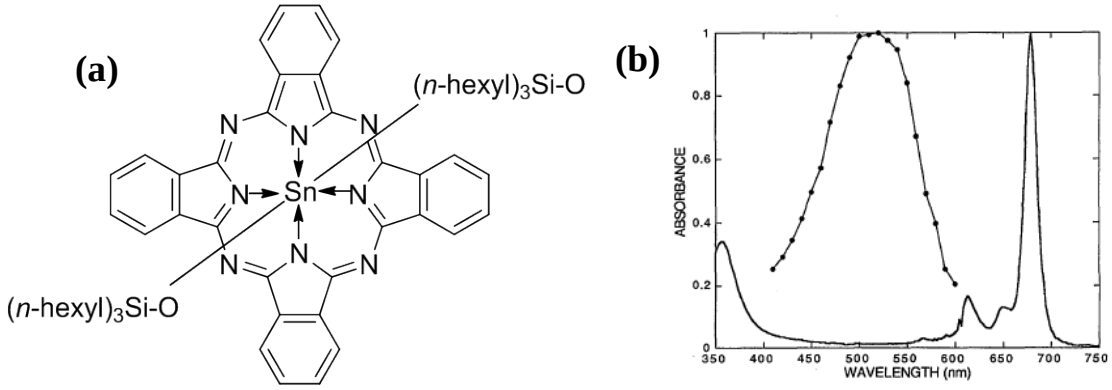

Figure 1.6. (a) Molecular structure of $((hexyl)_3SiO)_2SnPc$ and (b) 1PA (solid line) and triplet-triplet ESA (dotted line) of $((hexyl)_3SiO)_2SnPc$ in toluene. Reprinted with permission from Joseph W. Perry, Kamjou Mansour, Seth R. Marder, Kelly J. Perry, Daniel Alvarez, Ingrid Choong, *Opt. Lett*. 19, 625-627 (1994).

The model equations listed above assumes that no excited states are populated at t=0, such that $N_1(0) = N_2(0) = N_3(0) = N_4(0) = 0$. The propagation equation for a beam as it travels through a five-level RSA material along direction z is:

$$d\phi/dz = -\sigma_{01}N_0\phi - \sigma_{12}N_1\phi - \sigma_{34}N_3\phi \quad \text{(Eq 1.9)}$$

An example of a molecule that performs OPL via RSA processes, including triplet-triplet ESA, is shown in Figure 1.6. Certain assumptions can be made to simplify the Eq. 9. For example, the populations of the high-energy electronic states (S_2 and T_n) are negligible as there is rapid internal conversion from these high-energy states to the lower ones. Further discussion of RSA-OPL processes is provided by Perry [25].

1.2.2. OPL via Two-photon Absorption

2PA is an instantaneous nonlinearity that can be used to construct optical limiters. In contrast with accumulative RSA methods, 2PA involves the simultaneous absorption of two photons to promote an electron from the ground state to the two-photon allowed state of the molecule. The mechanism of 2PA can be thought of in terms of a three-level energy model. The intensity (I) of a laser beam as it traverses a 2PA material is given by:

$$dI/dz = -(\alpha + \beta I)I \quad \text{(Eq 1.10)}$$

where α is the linear absorption coefficient and β is the 2PA coefficient, which is related to the imaginary part of $\chi^{(3)}$ by the following equation

$$\beta = \frac{3\omega}{2\epsilon_0 c^2 n_0^2} Im[\chi^{(3)}] \quad \text{(Eq 1.11)}$$

If we assume there is no linear absorption (α =0) at the wavelength of interest, we can solve for Eq. 1.10 to determine the intensity-dependence equation for a pure two-photon process:

$$I(L) = I_0/(1 + I_0 \beta L) \quad \text{(Eq 1.12)}$$

where I_0 is the input intensity, $I(L)$ is the output intensity, and L is the length of the sample. Eq. 1.12, clearly demonstrates that as the input intensity is increased, output intensity is reduced, hence limiting occurs. We also see that OPL via 2PA is proportional to the input intensity, two-photon coefficient, and length of the sample.

1.3. Issues with the use of NLO organic conjugated materials for OPL applications

Intensive fundamental research over the past thirty years has positioned organic NLO materials to make a technological impact in a variety of photonic applications. Particularly, for third-order NLO phenomena, the knowledge obtained from structure-property studies has resulted in a plethora of discrete molecule and polymer systems that possess strong, third-order NLO responses, as well as the requisite properties for desired applications. Therefore, the question remains as to why organic NLO materials have not played a more central role in photonics, particularly for commercialized photonic devices.

To discuss where the bottlenecks exist for organic NLO materials, we must first consider the desired application. Particularly for OPL, many optical and material properties must be optimized. This is especially true for NLO materials that exploit both instantaneous and accumulative processes for limiting. As previously mentioned, the

effectiveness of accumulative NLO process for OPL depends on the rate of formation and decay of the excited states or free carriers. Should the dynamics of the absorbing states be significantly shorter than the duration of the laser-pulse, OPL will be ineffective. For example, if the excited-state lifetime of an NLO material is ~10^{-12} s, it will not serve as an effective limiter for nanosecond or microsecond laser pulses.

Organic materials offer the possibility of facile solution processing. However, conjugated molecules and polymers are known to exhibit strong intermolecular interactions due to their polarized π-systems, often referred to as π-π stacking [40, 41]. Due to π-π stacking and also due to potential solvation issues [42], many organic materials show a tendency to aggregate at high concentrations. Particularly strong aggregation due to non-covalent forces has been observed in conjugated polymers, resulting in supramolecule polymeric structures [43, 44]. These aggregation effects in conjugated organic systems can result in drastic changes in the linear and nonlinear optical properties of the material as well as and quenching of excited states [45], which may inevitably limit their usage in OPL.

The spectral coverage of limiters is becoming increasingly important as the wavelengths of commercially-available lasers can extend from the ultraviolet to the mid-IR spectral region. Identifying OPL materials with accumulative nonlinearities that show high transparency >50% with broad and strong, excited-state absorption bands is difficult.

It has been deduced that FOMs of 10^3-10^5 [25] are required for the implementation of organic conjugated materials in commercially-viable OPL applications

according to ANSI standards[ii]. These large FOMs have not yet been achieved in single element organic conjugated materials. For accumulative OPL materials, increased FOMs would require significant increases in excited-state absorptivities. For instantaneous OPL materials, increases in the third-order NLO response is needed to achieve such goals.

1.4. Aims and objectives of thesis

It is clear that fundamental physical chemistry work is required to aid in the development of organics for NLO applications. In this regard, we present a body of work that consists of a study of the photophysical and NLO responses of a set of conjugated organic molecules and polymers that are of interest for OPL applications. The objective of this work is to provide knowledge on potential strategies for improving the OPL performance of conjugated organic systems. Specifically, we explore how structural modification and plasmonic effects influence the OPL efficacy of organic conjugated systems. We also examine the optical properties and charge transfer character of $p\pi$-conjugated chromophores, which show potential as optical limiters via 2PA-ESA. While the FOMs obtained in this work are well below those required for commercially-viable OPL applications, the strategies presented here can be considered as a means to surmount some of the bottlenecks associated with organic conjugated materials as optical limiters. It should be noted that the work in this dissertation has not addressed that optimization of OPL devices based on materials with 2PA-ESA absorption properties but has addressed some of the important issues in OPL via 2PA-ESA materials, such as photophysical mechanisms, broad bandwidth optical response and strong nonlinear absorption.

[ii] The American National Standards Institute (ANSI) provides a list of standards and guidance for the use of protective eyewear, and other elements of safe laser use.

In Chapter 3, the spectroscopic effects due to structural modification of conjugated polymers are examined. We seek to determine if the coupling of conjugated side chains (with and without electron donating units) to a phenylene ethynylene (PPE) polymer backbone is an effective means towards yielding the band positions, bandwidths, 2PA and ESA cross sections, and excited state lifetimes suitable for strong, broadband OPL in the visible and near-IR spectral regions. Expanding the understanding of electronic coupling in conjugated polymers with donor/acceptor repeating units, and thus how this coupling affects the linear and nonlinear optical properties of the composite polymeric systems, would provide additional strategies towards the design of organic polymers with strong nonlinearities for photonic applications.

In Chapter 3, the following questions are addressed:

1. How is the 2PA cross section and bandwidth affected when the conjugation is extended in more than one dimension in a conjugated polymeric structure?
2. How are the ESA properties affected when the conjugation is extended in more than one dimension in a conjugated polymeric structure?
3. How does the degree of electronic coupling compare to that of the small molecule analogue?

Chapter 4 serves to improve the understanding of the structural configuration and charge transfer characteristics of $p\pi$-conjugated chromophores that are of interest for photonic applications. To do so, we investigate the spectroscopic changes observed upon extended conjugation in the 1PA, 2PA, fluorescence, and ESA characteristics of a family of donor-acceptor-donor (D-A-D) -type conjugated organoborane oligomers.

Solvatochromic measurements also provide discussion on the conformational changes, changes in radiative and non-radiative decay rates, and the strength of the ICT character experienced by these organoborane chromophores as a function of their local environment. An enhanced understanding of solvent-based changes in the optical behavior of quadrupolar dyes may allow for tuning of the optical band positions, band width, and absorption cross section values of multipolar chromophores without synthetic modification. Furthermore, solvent studies are particularly relevant to 2PA solution-based applications such as two-photon fluorescence imaging [46], two-photon photodynamic therapy [47], or OPL.

In Chapter 4, the following questions regarding the optical properties of borazine oligomers are addressed:

1. How are the linear and nonlinear optical properties of $p\pi$ conjugated systems affected by extending the conjugation length?
2. What is the effect of solvent polarity on the steady-state absorption and emission properties of quadrupolar chromophores?
3. What is the effect of solvent polarity on the ultrafast optical properties of quadrupolar chromophores?

In Chapter 5, we seek to gain a better understanding of the local-field enhancement and subsequent effects on the photophysics and nonlinear behavior of 2PA dyes in the presence of silver nanoparticles (AgNPs) and their aggregates. We also seek to probe whether enhanced nonlinear absorption by plasmonic effects can give rise to enhanced OPL of pulsed laser systems. To do so, we investigate the 1PA, 2PA, ESA and dynamics of two 2PA chromophores with and without the presence of AgNPs. We also

examine and compare the OPL properties of the 2PA dye and dye/AgNP aggregates solutions. Metal nanoparticles are very important in nonlinear optics as they have the ability to act as electric field intensifiers that may enhance the nonlinear behavior in a material. Such effects are of great interest for use in ultrafast optical switching and in OPL applications.

In Chapter 5, the following questions are addressed:

1. How is the 2PA band and cross section of a chromophore impacted due to the presence of AgNP and aggregates?
2. How are the ESA properties impacted due to the presence of AgNP and aggregates?
3. Does the presence of AgNP aggregates result in better OPL response of 2PA chromophores?

A summary of the findings and the conclusions drawn from these investigations are reported in Chapter 6. Ongoing investigations and potential future extensions of this work are included in the discussion.

1.5. References

[1] Kasap, S.O. and Sinha, R.K., *Optoelectronics and Photonics: Principles and Practices*. Vol. 340. 2001: Prentice Hall New Jersey.

[2] Liu, J.-M., *Photonic Devices*. 2005: Cambridge University Press.

[3] Prasad, P.N. and Williams, D.J., *Introduction to Nonlinear Optical Effects in Molecules and Polymers.* 1991, New York: John Wiley & Sons, Inc.

[4] Minoshima, K., Kowalevicz, A., Ippen, E. and Fujimoto, J., *Fabrication of Coupled Mode Photonic Devices in Glass by Nonlinear Femtosecond Laser Materials Processing.* Opt. Express, 2002. **10**(15): p. 645-652.

[5] *Nonlinear Optics of Organic Molecules and Polymers*, ed. H.S. Nalwa and S. Miyata. 1996, Boca Raton, FL: CRC press.

[6] Marder, S.R., *Organic Nonlinear Optical Materials: Where We Have Been and Where We Are Going.* Chem. Commun., 2006(2): p. 131-134.

[7] Brédas, J.L., Adant, C., Tackx, P., Persoons, A. and Pierce, B.M., *Third-Order Nonlinear Optical Response in Organic Materials: Theoretical and Experimental Aspects.* Chem. Rev., 1994. **94**(1): p. 243-278.

[8] Jazbinsek, M., Mutter, L. and Gunter, P., *Photonic Applications with the Organic Nonlinear Optical Crystal Dast.* IEEE J. Sel. Top. Quantum Electron., 2008. **14**(5): p. 1298-1311.

[9] Bosshard, C., Bösch, M., Liakatas, I., Jäger, M. and Günter, P., *Second-Order Nonlinear Optical Organic Materials: Recent Developments*, in *Nonlinear Optical Effects and Materials*, P. Günter, Editor. 2000, Springer Berlin Heidelberg. p. 163-299.

[10] *Organic Thin Films for Waveguiding Nonlinear Optics*, ed. F. Kajzar and J.D. Swalen. Vol. 3. 1996, Amsterdam: Gordon and Breach Publishers.

[11] Göppert-Mayer, M., *Über Elementarakte Mit Zwei Quantensprüngen.* Annalen der Physik, 1931. **401**(3): p. 273-294.

[12] Rumi, M., Barlow, S., Wang, J., Perry, J. and Marder, S., *Two-Photon Absorbing Materials and Two-Photon-Induced Chemistry*, in *Photoresponsive Polymers I*, S. Marder and K.-S. Lee, Editors. 2008, Springer Berlin Heidelberg. p. 1-95.

[13] Gerritsen, H.J., *Nonlinear Effects in Image Formation.* Appl. Phys. Lett., 1967. **10**(9): p. 239-241.

[14] Jones, W.J. and Stoicheff, B.P., *Inverse Raman Spectra: Induced Absorption at Optical Frequencies.* Phys. Rev. Lett., 1964. **13**(22): p. 657-659.

[15] Almeida, V.R., Barrios, C.A., Panepucci, R.R. and Lipson, M., *All-Optical Control of Light on a Silicon Chip.* Nature, 2004. **431**(7012): p. 1081-1084.

[16] Tutt, L.W. and Boggess, T.F., *A Review of Optical Limiting Mechanisms and Devices Using Organics, Fullerenes, Semiconductors and Other Materials.* Prog. Quantum Electron., 1993. **17**(4): p. 299-338.

[17] Albota, M., Beljonne, D., Brédas, J.-L., Ehrlich, J.E., Fu, J.-Y., Heikal, A.A., Hess, S.E., Kogej, T., Levin, M.D., Marder, S.R., McCord-Maughon, D., Perry, J.W., Röckel, H., Rumi, M., Subramaniam, G., Webb, W.W., Wu, X.-L. and Xu, C., *Design of Organic Molecules with Large Two-Photon Absorption Cross Sections.* Science, 1998. **281**(5383): p. 1653-1656.

[18] Shuai, Z. and Brédas, J.L., *Static and Dynamic Optical Nonlinearities in Conjugated Polymers: Third-Harmonic Generation and the Dc Kerr Effect in Polyacetylene, Polyparaphenylene Vinylene, and Polythienylene Vinylene.* Phys. Rev. B., 1992. **46**(8): p. 4395-4404.

[19] Reinhardt, B.A., Brott, L.L., Clarson, S.J., Dillard, A.G., Bhatt, J.C., Kannan, R., Yuan, L., He, G.S. and Prasad, P.N., *Highly Active Two-Photon Dyes: Design, Synthesis, and Characterization toward Application.* Chem. Mater., 1998. **10**(7): p. 1863-1874.

[20] Shuai, Z. and Brédas, J.L., *Static and Dynamic Third-Harmonic Generation in Long Polyacetylene and Polyparaphenylene Vinylene Chains.* Phys. Rev. B, 1991. **44**(11): p. 5962-5965.

[21] Heflin, J.R. and Gartto, A.F., *Electron Correlated States and Third Order Optical Processes in Linear Chains*, in *Nonlinear Optical Materials*, H. Kuhn and J. Robillard, Editors. 1991, CRC Press, Inc.: Boca Raton, FL. p. 13-41.

[22] Rumi, M., Ehrlich, J.E., Heikal, A.A., Perry, J.W., Barlow, S., Hu, Z., McCord-Maughon, D., Parker, T.C., Röckel, H., Thayumanavan, S., Marder, S.R., Beljonne, D. and Bredas, J.-L., *Structure-Property Relationships for Two-Photon Absorbing Chromophores: Bis-Donor Diphenylpolyene and Bis(Styryl)Benzene Derivatives.* J. Am. Chem. Soc., 2000. **122**(39): p. 9500-9510.

[23] Beljonne, D., Wenseleers, W., Zojer, E., Shuai, Z., Vogel, H., Pond, S.J.K., Perry, J.W., Marder, S.R. and Brédas, J.L., *Role of Dimensionality on the Two-Photon Absorption Response of Conjugated Molecules: The Case of Octupolar Compounds.* Adv. Funct. Mater., 2002. **12**(9): p. 631-641.

[24] Makarov, N.S., Mukhopadhyay, S., Yesudas, K., Brédas, J.-L., Perry, J.W., Pron, A., Kivala, M. and Müllen, K., *Impact of Electronic Coupling, Symmetry, and Planarization on One- and Two-Photon Properties of Triarylamines with One, Two, or Three Diarylboryl Acceptors.* J. Phys. Chem. A, 2012. **116**(15): p. 3781-3793.

[25] Perry, J.W., *Organic and Metal-Containing Reverse Saturable Absorbers for Optical Limiting*, in *Nonlinear Optics of Organic Molecules and Polymers*, H.S. Nalwa and S. Miyata, Editors. 1997, CRC press: Boca Raton, FL. p. 813-840.

[26] Geusic, J.E., Singh, S., Tipping, D.W. and Rich, T.C., *Three-Photon Stepwise Optical Limiting in Silicon.* Phys. Rev. Lett., 1967. **19**(19): p. 1126-1128.

[27] Soileau, M.J., Williams, W. and Van Stryland, E.W., *Optical Power Limiter with Picosecond Response Time.* IEEE J. Quantum Electron., 1983. **19**(4): p. 731-735.

[28] Cha, M., Sariciftci, N.S., Heeger, A.J., Hummelen, J.C. and Wudl, F., *Enhanced Nonlinear Absorption and Optical Limiting in Semiconducting Polymer/Methanofullerene Charge Transfer Films.* Appl. Phys. Lett., 1995. **67**(26): p. 3850-3852.

[29] Blau, W., Byrne, H., Dennis, W.M. and Kelly, J.M., *Reverse Saturable Absorption in Tetraphenylporphyrins.* Opt. Commun., 1985. **56**(1): p. 25-29.

[30] Perry, J.W., Mansour, K., Marder, S.R., Perry, K.J., Alvarez, J.D. and Choong, I., *Enhanced Reverse Saturable Absorption and Optical Limiting in Heavy-Atom-Substituted Phthalocyanines.* Opt. Lett., 1994. **19**(9): p. 625-627.

[31] Perry, J.W., Mansour, K., Lee, I.Y.S., Wu, X.L., Bedworth, P.V., Chen, C.T., Ng, D., Marder, S.R., Miles, P., Wada, T., Tian, M. and Sasabe, H., *Organic Optical Limiter with a Strong Nonlinear Absorptive Response.* Science, 1996. **273**(5281): p. 1533-1536.

[32] Ehrlich, J.E., Wu, X.L., Lee, I.Y.S., Hu, Z.Y., Röckel, H., Marder, S.R. and Perry, J.W., *Two-Photon Absorption and Broadband Optical Limiting with Bis-Donor Stilbenes.* Opt. Lett., 1997. **22**(24): p. 1843-1845.

[33] Ehrlich, J.E., Wu, X.L., Lee, I.-Y.S., Heikal, A.A., Hu, Z.-Y., Röckel, H., Marder, S.R. and Perry, J.W., *Two-Photon Absorbing Organic Chromophores for Optical Limiting.* Mat. Res. Soc. Symp. Proc., 1997. **479**: p. 9-15.

[34] He, G.S., Bhawalkar, J.D., Zhao, C.F. and Prasad, P.N., *Optical Limiting Effect in a Two-Photon Absorption Dye Doped Solid Matrix.* Appl. Phys. Lett., 1995. **67**(17): p. 2433-2435.

[35] He, G.S., Xu, G.C., Prasad, P.N., Reinhardt, B.A., Bhatt, J.C. and Dillard, A.G., *Two-Photon Absorption and Optical-Limiting Properties of Novel Organic Compounds.* Opt. Lett., 1995. **20**(5): p. 435-437.

[36] He, G.S., Yuan, L., Bhawalkar, J.D. and Prasad, P.N., *Optical Limiting, Pulse Reshaping, and Stabilization with a Nonlinear Absorptive Fiber System.* Appl. Opt., 1997. **36**(15): p. 3387-3392.

[37] Chi, S.-H., Hales, J.M., Cozzuol, M., Ochoa, C., Fitzpatrick, M. and Perry, J.W., *Conjugated Polymer-Fullerene Blend with Strong Optical Limiting in the near-Infrared.* Opt. Express, 2009. **17**(24): p. 22062-22072.

[38] Hales, J.M., Cozzuol, M., Screen, T.E.O., Anderson, H.L. and Perry, J.W., *Metalloporphyrin Polymer with Temporallyagile, Broadband Nonlinear Absorption Foroptical Limiting in the near Infrared.* Opt. Express, 2009. **17**(21): p. 18478-18488.

[39] Giuliano, C.R. and Hess, L.D., *Nonlinear Absorption of Light: Optical Saturation of Electronic Transitions in Organic Molecules with High Intensity Laser Radiation.* IEEE J. Quantum Electron., 1967. **3**(8): p. 358-367.

[40] Cozzi, F., Ponzini, F., Annunziata, R., Cinquini, M. and Siegel, J.S., *Polar Interactions between Stacked Π Systems in Fluorinated 1,8-Diarylnaphthalenes: Importance of Quadrupole Moments in Molecular Recognition.* Angew. Chem. Int. Ed., 1995. **34**(9): p. 1019-1020.

[41] Martinez, C.R. and Iverson, B.L., *Rethinking the Term "Pi-Stacking".* Chem. Sci., 2012. **3**(7): p. 2191-2201.

[42] Lahiri, S., Thompson, J.L. and Moore, J.S., *Solvophobically Driven Π-Stacking of Phenylene Ethynylene Macrocycles and Oligomers.* J. Am. Chem. Soc., 2000. **122**(46): p. 11315-11319.

[43] Brunsveld, L., Folmer, B.J.B., Meijer, E.W. and Sijbesma, R.P., *Supramolecular Polymers.* Chem. Rev., 2001. **101**(12): p. 4071-4098.

[44] Pu, K.-Y., Qi, X.-Y., Yang, Y.-L., Lu, X.-M., Li, T.-C., Fan, Q.-L., Wang, C., Liu, B., Chan, H.S.O. and Huang, W., *Supramolecule-Regulated Photophysics of Oligo(P-Phenyleneethynylene)-Based Rod–Coil Block Copolymers: Effect of Molecular Architecture.* Chem.-Eur. J., 2008. **14**(4): p. 1205-1215.

[45] Ho, Z.Z., Ju, C.Y. and Hetherington III, W.M., *Third Harmonic Generation in Phthalocyanines.* J. Appl. Phys., 1987. **62**(2): p. 716-718.

[46] Denk, W., Strickler, J. and Webb, W., *Two-Photon Laser Scanning Fluorescence Microscopy.* Science, 1990. **248**(4951): p. 73-76.

[47] Collins, H.A., Khurana, M., Moriyama, E.H., Mariampillai, A., Dahlstedt, E., Balaz, M., Kuimova, M.K., Drobizhev, M., Yang, V.X. and Phillips, D., *Blood-Vessel Closure Using Photosensitizers Engineered for Two-Photon Excitation.* Nature Photon., 2008. **2**(7): p. 420-424.

CHAPTER 2

THIRD-ORDER NONLINEAR OPTICAL RESPONSES AND CHARACTERIZATION TECHNIQUES

2.1. Introduction

As discussed in Chapter 1, organic conjugated molecules and polymers have made large impacts in the field of photonics. Because of their favorable material properties, much effort has gone towards identifying effective design strategies to improve the second- and third-order nonlinear response of organic conjugated materials. To provide additional discussion on the role of organic materials in third-order NLO applications, an understanding of the nonlinearities must be established. In this chapter a qualitative introduction to third-order nonlinear effects and two-photon absorption (2PA) is presented. Additionally, several characterization techniques will be discussed.

2.2. Third-Order Nonlinear Effects

2.2.1. A Microscopic Picture

A molecular medium is generally nonconductive and nonmagnetic, therefore, the electrons in the medium can be thought of as being closely bound to the nuclei. When an atom or a molecule interacts with a low intensity incident electromagnetic field, such as an optical field, it can become polarized. The electron density of the medium is displaced will oscillate harmoniously away from the nuclear core creating a separation of charge, or an induced dipole, μ. This induced polarization is intrinsic to the medium and accounts for an abundance of optical properties exhibited.

The interaction of light with the medium is regarded within the framework of a dielectric interaction with an electric field. Such interactions can be described using the dipole approximation, where the charge distribution in the presence of the field is readily approximated by that of an induced dipole with a moment, $\boldsymbol{\mu}$:

$$\boldsymbol{\mu} = \alpha \mathbf{E} \qquad \text{(Eq. 2.1)}$$

where α is the linear polarizability which consists of an in-phase component, α', and an out-of-phase component, α'', such that $\alpha = \alpha' + i\,\alpha''$. **E** is the electric or optical field. Both $\boldsymbol{\mu}$ and **E** are vectors with direction and magnitude.

Although fairly accurate, Eq. 2.1 neglects some effects of the inherent properties of organic molecules. As discussed in Chapter 1, the π-conjugated network of organic materials allow for fast changes in electron density and thusly fast structural reorganization upon the lifetime of excitation (10^{-15}-10^{-6} s). Therefore significant structural changes between electronic states are observed during excitation, resulting in heating effects due to structural reorientation (or nonradiative decay) from higher-lying electronic states to lower-lying ones. These heating effects are dependent on frequency of the optical field. Additionally, the polarization of a medium may not be the same for all directions, so the anisotropic nature of polarizability must be considered. Taking into account the above discussion, Eq. 2.1 can be rewritten as

$$\boldsymbol{\mu}_i(\omega) = \sum_j \alpha_{ij}(\omega)\, \mathbf{E}_j(\omega) \qquad \text{(Eq. 2.2)}$$

where the linear polarizability, α_{ij} (ω), is represented as a tensor that is sensitive to direction and the frequency of the field.

Many areas of interest in optics involve nonlinear interactions that occur when the electromagnetic interaction becomes too large for the medium to continue to respond linearly. This causes the electron to oscillate anharmonically in response to the applied field. Therefore, when a molecule experiences a high intensity optical field, its induced polarization responds in a manner which is nonlinear with respect to the field strength. An exact solution for the functional form of $\boldsymbol{\mu}$ is no longer valid and it is therefore quite common to express the total dipole as a Taylor series expansion in **E** [19]:

$$\boldsymbol{\mu}_i = \mu_0 + \alpha_{ij}\,\mathbf{E}_j + \beta_{ijk}/2\,\mathbf{E}_j\,\mathbf{E}_k + \gamma_{ijkl}/6\,\mathbf{E}_j\,\mathbf{E}_k\,\mathbf{E}_l + \ldots \qquad \text{(Eq. 2.3)}$$

The terms beyond $\alpha\mathbf{E}$ show a nonlinear dependence on **E**, and are what gives rise to nonlinear optical effects described in Chapter 1. The terms β and γ are the first- and second-order hyperpolarizabilities, respectively. It can be inferred from Eq 2.3, that the nonlinear polarizability terms become more important with increasing field strength.

2.2.2. A Macroscopic Picture

NLO device applications are based on bulk materials, rather than individual molecules. Therefore, it is necessary to understand nonlinear effects at the bulk, macroscopic level. The bulk properties of a material can be described in a similar fashion as what was presented above. In bulk materials, the linear polarization, **P**, is given by

$$\mathbf{P}_i(\omega) = \sum_j \chi_{ij}(\omega)\,\mathbf{E}_j(\omega) \qquad \text{(Eq. 2.4)}$$

where $\chi_{ij}(\omega)$ is the linear susceptibility of a material. As in the case of α, χ is a tensor product and contains and in-phase and out-of-phase component. To relate Eq. 2.4 to observable properties, the $\mathrm{Im}\{\chi_{ij}(\omega)\}$ is proportional to the dielectric constant, ϵ, and the $\mathrm{Re}\{\chi_{ij}(\omega)\}$ is proportional to the refractive index of a material, n.

Under an intense optical field, we can again use a Taylor series expansion to describe the relationship of the material polarization to the incident field:

$$\mathbf{P} = \mathbf{P}_0 + \chi^{(1)} \cdot \mathbf{E} + \chi^{(2)} \cdot \mathbf{E}\cdot\mathbf{E} + \chi^{(2)} \cdot \mathbf{E}\cdot\mathbf{E}\cdot\mathbf{E} + \ldots \qquad \text{(Eq. 2.5)}$$

where $\mathbf{P}_0$ is the static polarization of the material. In Eq. 2.5, the linear susceptibility is represented as $\chi^{(1)}$. The higher-order terms are the second- and third-order susceptibility, respectively. As this study concerns the third-order NLO processes, the term of particular importance for this work is $\chi^{(3)}$. Again, the $\mathrm{Re}\{\chi^{(3)}\}$is proportional to the nonlinear refractive index, n_2, and the $\mathrm{Im}\{\chi^{(3)}\}$is proportional to the two-photon absorption coefficient, β, that lead to the phenomena of nonlinear refraction (NLR) and two-photon absorption (2PA), respectively. For the purposes of this work, only β and 2PA will be discussed. Other third-order NLO processes will be ignored.

2.3. Two-photon Absorption

In 1931 the pioneering work of Maria Göppert Mayer was published in her doctoral dissertation [1], wherein the author theoretically describes the process of two-photon absorption: the "simultaneous" absorption of two photons (of energy E_1 and E_2) by a material system. Unfortunately, it was not until thirty-years later, with the advent of the laser, that the experimental evidence of 2PA processes could be observed.

As discussed in the previous section, 2PA is a third-order nonlinear process. During 2PA, one photon is absorbed and promoted to a temporary or virtual state of E_1 above the ground state for a short time interval of τ_v (see Figure 2.1). If a second photon (E_2) interacts with the molecule

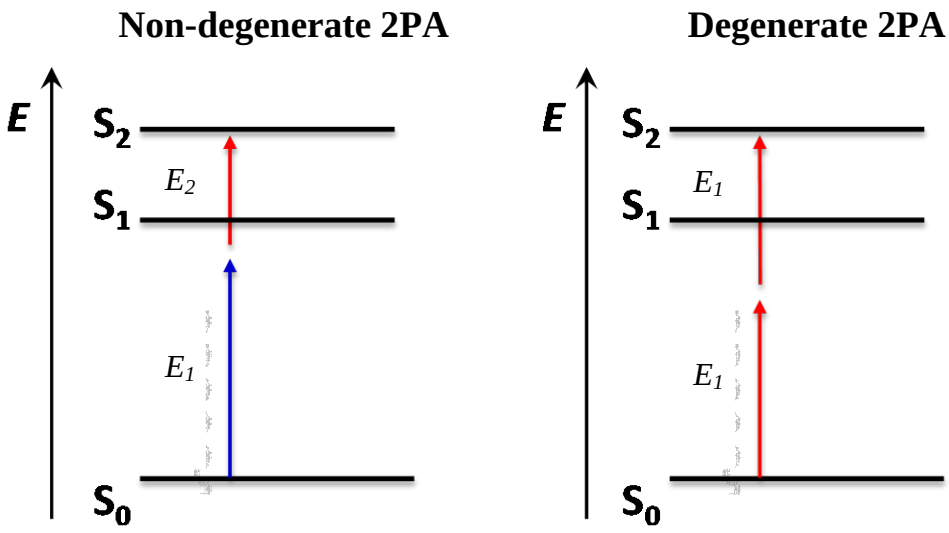

Figure 2.1. Schematic energy level diagram showing the non-degenerate and degenerate two-photon excitation of a molecule from its ground state (S_0) to its two-photon allowed state (S_2)

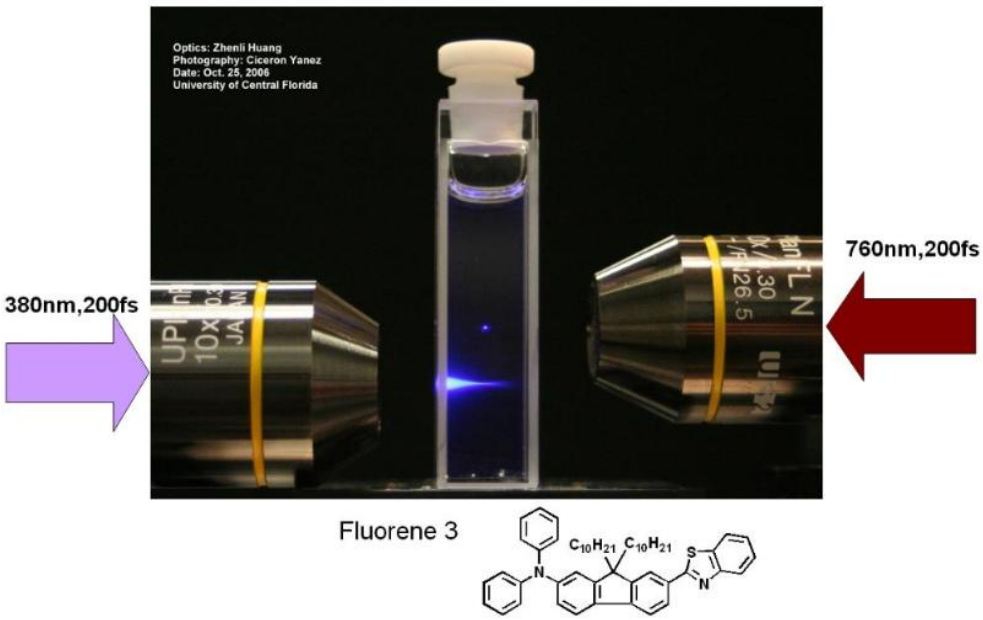

Figure 2.2. Picture demonstration of the spatial selectivity of 1PA (left at 380 nm) vs.2PA (right at 760 nm) in a solution containing Fluorene3.

during τ_v, the electron can be promoted to a two-photon allowed state, as determine by the symmetry of the molecule or bulk material. Unlike one photon absorption (1PA) whose probability is linearly proportional to the incident intensity, 2PA depends on the spatial and temporal overlap of the photons and is proportional to the intensity squared times the number of molecules in the cross section of the laser beam. The absorption rate therefore scales inversely with the area, resulting in highly localized photoexcitation with a focused laser beam (Figure 2.2).

The strength or magnitude of the 2PA of a material can be described by the 2PA coefficient (β) a macroscopic term, or by the 2PA cross section (δ), a microscopic term.

$$\beta = \frac{3\omega}{2\varepsilon_0 n_0(\omega)^2 c^2} \mathrm{Im}[\chi^{(3)}(-\omega;\omega,-\omega,\omega)] \qquad \text{(Eq. 2.6)}$$

β is measured in units of m/W. For δ, the microscopic 2PA term is related to the second-order hyperpolarizability,γ, such that

$$\delta = \frac{4\pi^2 3h\omega^2}{n^2 c^2} L^4 \, \mathrm{Im}[(-\omega;\omega,-\omega,\omega)] \qquad \text{(Eq. 2.7)}$$

where *n* is the refractive index, *c* is the speed of light, and *L* is the local field factor. The units for δ are $m^4 \cdot s \cdot photon^{-1}$. We can relate the macroscopic and microscopic 2PA terms by the following equation:

$$\delta = \beta E_{ph}/N \qquad \text{(Eq. 2.8)}$$

where E_{ph} is the energy of the photon and N is the number of molecules.

2.4. Characterization Techniques

In this dissertation, steady-state and ultrafast spectroscopic techniques were used to characterize the linear and nonlinear optical response of several conjugated organic molecules and polymers. Pump-probe transient absorption spectroscopy via femtosecond- and nanosecond-pulsed laser excitation was used to characterize the excited-state absorption and ultrafast dynamics of the organic materials considered in this study. Time-resolved fluorescence measurements were performed in order to obtaine the lifetime of the fluorescence decay, and to estimate the rate constants for the radiative and nonradiative decays of organic fluorophores. To investigate the two-photon absorptivities of the organic material considered in this work, two-photon excited fluorescence (2PEF) measurements were performed. Finally, power-dependent nonlinear transmission (NLT) or optical power limiting (OPL) measurements were used to test the performance of potential materials for OPL applications. In the following section we will review various spectroscopic techniques in detail.

2.4.1. Steady-state Absorption Characterization Methods

2.4.1.1. UV-VIS Absorption Measurements and Linear Absorption Parameters

Steady-state absorption measurements were performed using a UV-Vis-NIR scanning spectrophotometer (UV-3101PC, Shimadzu), and were used to determine various linear parameters. Molar extinction coefficients (ε) were obtained from a linear regression analysis of absorbance versus concentration using the Beer-Lambert equation

$$A(\lambda)=\varepsilon(\lambda)\ell C \qquad \text{(Eq. 2.9)}$$

where A(λ) and ε(λ) are the absorbance and molar extinction coefficient, respectively, that vary with wavelength λ, ℓ is the length of the cell, and C is the concentration of the material.

Steady-state absorption measurements were also used to determine the ground-state cross section (σ_{01}) of the materials using the following equation:

$$T_{Lin}=\exp(-\sigma_{01}N_0L) \qquad \text{(Eq. 2.10)}$$

where σ_{01} is the cross section for the transition between states 0 and 1, N_0 is the initial ground state population, and L is the length of the sample (see section 1.2.1.1).

Finally, the transition dipole moment (M_{ge}) can be calculated as the integrated strength of the $1A_g \rightarrow 1B_u$ band according to [2-4]

$$M_{ge} = \left[\frac{1500(\hbar c)^2 \ln 10}{\pi N_A E_{ge}} \int \varepsilon_{ge}(\nu)\, d\nu\right]^{1/2} \qquad \text{(Eq. 2.11)}$$

where N_A is Avagadro's number, $\varepsilon_{ge(}\nu)$ is the molar extinction coefficient at the wavenumber, ν, and the integral is performed over the 1PA band.

2.3.1.2. Fluorescence Measurements and Fluorescence Parameters

A spectrofluorometer (Fluorolog-2, Spex) was used for the measurement of steady-state fluorescence of all molecules considered in this study. All spectra were corrected via subtraction of the scattering response from the solvent and the spectral response of the instrument. Low concentration solutions (10^{-6} M) were used for all steady-state fluorescence measurements to minimize inner filter effects.

The fluorescence quantum yield (Φ_{Fl}) is an important parameter that describes the ratio of photons absorbed to photons emitted through fluorescence. This parameter is extremely informative as it provides the probability of the excited state being deactivated by emission rather than a non-radiative decay process, such as internal conversion, intersystem crossing, or energy or electron transfer [5]. Fluorescence quantum yields were determined using comparative methods [6] which involves the use of well-characterized fluorescence standards with known Φ_{Fl} values. The unknown Φ_{Fl} values were determined using the following equation:

$$\Phi_u = \frac{F_u A_r n_u^2}{F_r A_u n_r^2} \Phi_r \qquad \text{(Eq. 2.12)}$$

where Φ is the fluorescence quantum yield of the unknown, F is the integrated fluorescence, A is the absorption at the excitation wavelength, and n is the refractive index of the solvent. The subscripts u and r denote the parameter for the unknown and the reference sample, respectively

2.4.2. Ultrafast Characterization Techniques

2.4.2.1. Pump-Probe Transient Absorption Spectroscopy

Transient absorption (TA) spectroscopy, or flash photolysis, has developed from a niche tool into a commercialized instrument that is ubiquitous among all science and technology disciplines [7].

In TA spectroscopy, a fraction of molecules in the sample is promoted from the ground state to an excited state by means of optical pumping (pump pulse). A probe pulse is then sent through the sample with a delay τ with respect to the pump pulse. The intensity of the probe pulse is low, such that that multiphoton processes are avoided during probing. A transient optical density difference (ΔOD) or absorption spectrum is then determined, which is the optical density of the excited sample (OD_{ES}) minus the optical density of the sample in the ground state (OD_{GS}), hence $\Delta OD = OD_{ES} - OD_{GS}$. By adjusting the time delay by τ with respect to the pump pulse, the spectral and temporal evolution of the TA features can be obtained. Kinetic decays at select wavelengths can also be obtained. In this work, TA measurements were performed using femtosecond- and nanosecond-pulsewidths to allow for the monitoring of various photophysical processes in different temporal regimes.

Femtosecond Pump-Probe TA Experimental Methods

Femtosecond TA spectra and kinetic traces were measured with a commercially available broadband pump-probe spectrometer (HELIOS, Ultrafast Systems LLC) using a

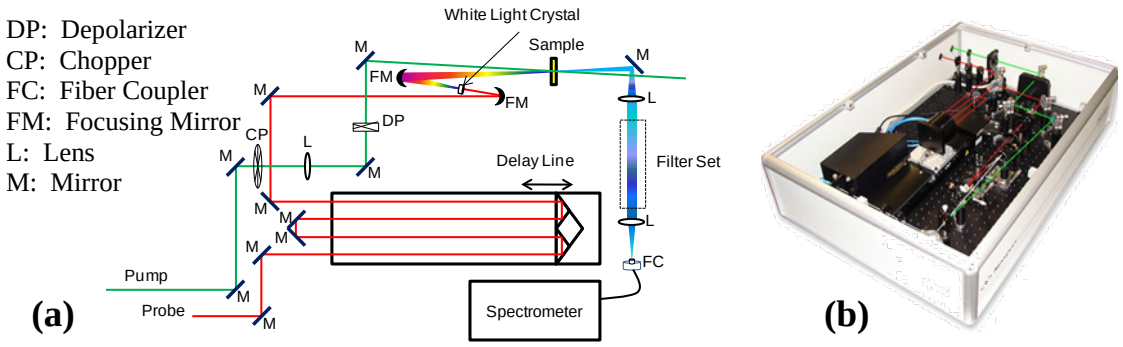

Figure 2.3. (a) the optical layout and (b) photo of the HELIOS femtosecond TA spectrometer. Adapted with permission from Chi, S-H., *Third-order Nonlinear Optical Properties of Conjugated Polymers and Blends*, Ph.D. Thesis, The Georgia Institute of Technology, December 2009. Copyright 2009 © Georgia Institute of Technology.

femtosecond Ti:Sapphire regenerative amplifier laser source (Spitfire, Spectra-Physics). The optical layout and image of the spectrometer is shown in Figure 2.3. The probe beam was produced by splitting a portion (~5%) of the laser source (800 nm, 1 kHz repetition rate) and focusing into a sapphire crystal in order to generate a white-light continuum (WLC; 400-950 nm). A tunable pump beam was generated by directing the remainder from the laser source to an optical parametric amplifier (OPA; TOPAS, Spectra-Physics) that produces tunable laser pulses over the range of 190 nm-2600 nm. The pump beam was chopped at 500 Hz to allow for the collection of a pumped (WLC plus pump) and a non-pumped (WLC only) sample spectrum, which were used to generate a transient ΔOD spectrum of the sample. The transmitted probe signal was collected using a fiber optic cable that was coupled to a multichannel spectrometer with a silicon CCD detector. Spectra at each time delay were averaged for 2-5 seconds. The linear and excited state spectra of the samples were monitored after every measurement to ensure that no

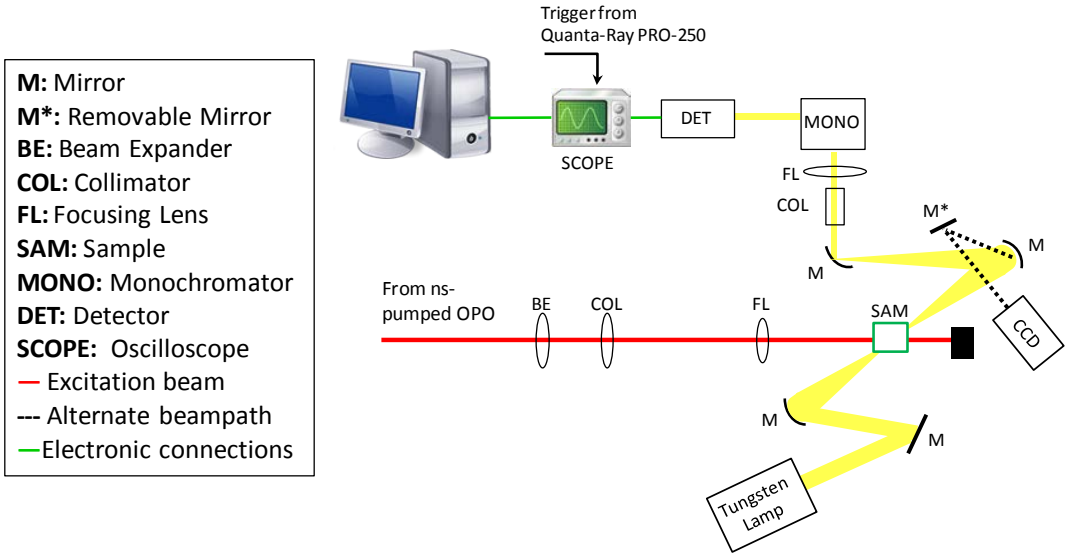

Figure 2.4. Schematic of the optical layout of the nanosecond TA experiment.

photodegradation had occurred during the experiment. To correct for temporal dispersion of the probe light, a chirp correction function was obtained using spectrophotometric grade solvents and was applied to all spectra. All samples were prepared at moderate concentrations at ~10^{-4} M and were stirred continuously during measurements in 2 mm path-length fused silica cuvettes.

Nanosecond Pump-Probe TA Experimental Methods

For nanosecond TA measurements, two different ns-pumped optical parametric oscillator (OPO) lasers were used as the excitation sources: MOPO 730, Quanta-Ray OPO and a premiScan-ULD, GWU OPO. The excitation source has been listed in the experimental section of each chapter. The white-light probe beam was produced by a 250 W tungsten-halogen lamp (300 W radiometric power supply, model Oriel 69931, Newport). The pump and probe were overlapped at a slight angle as they passed through

the sample. For nanosecond transient kinetic measurements, the white light was focused onto the slit of a monochromator (Acton SpectraPro 2150i monochromator, Princeton Instruments) set to the selected probe wavelength and was detected using a high-speed InGaAs PIN photodiode (HCA-S-200M-Si, Femto). The temporal responses of oxygenated and deoxygenated samples (accomplished via purging with nitrogen gas) were compared in order to test for the presence of triplet species. To acquire nanosecond TA spectra, the transmitted white light probe beam was directed into a spectrometer (320PI, Acton) equipped with a gated-intensified CCD camera (ST-133, Princeton Instruments). A pulse delay generator (model 575, Berkeley Nucleonics) was used to control the time delay of the CCD gate relative to the pump pulse. The solutions used in these experiments were prepared at concentrations of ~10^{-5} M and contained in 1 cm cuvettes while stirring continuously. The optical layout of the ns-TA experimental design is shown in Figure 2.4.

2.4.2.2. Time-Correlated Single Photon Counting (TCSPC)

Time-resolved measurements are widely used in fluorescence spectroscopy and can provide information not available from the steady-state data. For example, one can distinguish between static and dynamic quenching, determine radiative and nonradiative decay rates, or observe resonant energy transfer processes using time-resolved fluorescence spectroscopy.

Time-resolved fluorescence can be obtained either in the time-domain or frequency-domain. In the work presented here time-resolved fluorescence was obtained in the time-domain using time-correlated single photon counting (TCSPC) methods.

During TCSPC, the sample is excited with short pulsed excitation at a high repetition rate in such a manner that less than one photon is detected per laser pulse. The TCSPC method makes use of the fact that under low energy, high repetition rate excitation the probability of detecting one photon in one signal period is <<1. When a photon is detected, the time of the pulse is measured, allowing for a build-up of a histogram of the detection times. The time-dependent intensity of photon measured following the excitation is shown as a waveform and the fluorescence decay of the sample is then determined.

Two TCSPC methods were used to determine the fluorescence decay of molecules and polymers mentioned in this work. The first method utilized a femtosecond mode-locked Ti:Sapphire laser (Mai Tai HP, Spectra-Physics) operating at 80 MHz with tunable wavelength range of 690-1040 nm as an excitation source. The output of laser was frequency doubled by a BBO crystal and was used to excite fluorescence from the molecules under study via one-photon excitation. The details of the experimental setup and the method of analysis have been previously described [8]. All samples were prepared in toluene at low concentration (~10^{-6} M) and were stirred continuously during measurements in 1 cm path-length fused silica cuvettes.

In the second method, fluorescence lifetimes were measured using a LifeSpec II (Edinburgh Instruments) TCSPC system. In this measurement, a picosecond-pulsed diode laser (PicoQuant, LDH-P-C-375) with an excitation wavelength of 375 nm was used as an excitation light source. The detection system consisted of a high speed MicroChannel

Plate PhotoMultiplier Tube (MCP-PMT, Hamamatsu R3809U-50) and TCSPC electronics.

2.4.3. Two-photon Characterization Techniques

2.4.3.1. Two-photon Excited Fluorescence (2PEF) Measurements

Two-photon excited fluorescence (2PEF) is an indirect approach to determining the 2PA cross sections and spectra of a sample. During a 2PEF measurement, a sample is excited by a laser beam in a spectral region far from its one-photon absorption band. For 2PA dyes, the excitation is confined to a small volume around the focus of the beam. 2PA dyes that are in this excitation volume will be excited to their two-photon allowed excited state and will relax quickly to their lowest singlet excited state where they, in turn, will return to the ground state via radiative (fluorescence) and non-radiative decay processes [9]. By monitoring the intensity of the fluorescence signal, it is possible to determine the relative 2PA spectra of a sample. Absolute 2PA cross sections can be determined by using a reference compound with well-characterized 2PA spectra. This method of characterization can be viewed as the nonlinear equivalent to a fluorescence excitation experiment. For materials with large intersystem crossing rates, a comparative method in which the two-photon-induced phosphorescence is measured can also provide information on the 2PA properties of a material [10, 11].

The benefit to 2PEF method over direct 2PA methods, such as Z-scan [12, 13] or nonlinear transmission [12, 14], is the broadband nature of the measurement. Originally used for two-photon microscopy [15], Webb and co-workers demonstrated that by sweeping the excitation wavelength, broadband 2PA spectra in the spectral range of 690-

1050 nm can be obtained for commercial dyes via 2PEF measurements [16]. Makarov et. al. extended the range of the 2PEF experimental technique to 550-1600 nm, demonstrating the efficacy of 2PEF methods for broadband 2PA characterization [17, 18].

Indirect 2PA characterization methods, such as 2PEF, are also highly selective for measuring only the 2PA contribution in a material. Because the de-excitation process (fluorescence) is monitored, higher-order absorption and scattering processes (such as ESA) do not affect the δ values or 2PA spectra experimentally determined, regardless of the pulse duration. Thus, 2PEF measurements obtained via femtosecond- and nanosecond-pulsed or CW excitation show good agreement [16].

Theory of Two-photon Excited Fluorescence Method

Referring to Eq 1.10, for the case in which the linear absorption is negligible (α=0), the attenuation of a laser beam as it traverses a 2PA material is given by

$$dI / dz = -\beta I^2 \qquad \text{(Eq. 2.13)}$$

where I is the intensity of the beam of frequency ν, z is the direction of propagation, and β is the 2PA coefficient. Eq 2.5 can also be written in terms of photon flux (F) where $F=I/h\nu$, such that

$$dF / dz = -\beta h\nu F^2 \qquad \text{(Eq. 2.14)}$$

In the absence of saturation or any subsequent photochemical processes, the number of photons absorbed ($N_{Abs}^{(2)}$) per unit time and volume for a 2PA process is given by

$$N_{Abs}^{(2)} = dF / dz \qquad \text{(Eq. 2.15)}$$

The 2PA cross section (δ) of a material can be defined as $\delta = h\nu\beta/C$, where C is the number density of molecules in the sample. Thus, Eq 2.7 becomes

$$N_{Abs}^{(2)} = F^2 \delta \; C \qquad \text{(Eq. 2.16)}$$

For a 2PA process, the number of excited molecules is given by $\frac{1}{2} N_{Abs}^{(2)}$, where the factor 1/2 reflects the fact that two photons are needed to excite the molecule. Assuming there is no stimulated emission or self-quenching of fluorescence, the molecules excited via two-photon excitation may return to their lowest singlet excited state where emission can occur. The number of photons emitted due to 2PA ($N_{Fl}^{(2)}$) is given by

$$N_{Fl}^{(2)} = \tfrac{1}{2}\eta N_{Abs}^{(2)} = \tfrac{1}{2}\eta F^2 \delta \; C \qquad \text{(Eq. 2.17)}$$

where η is the fluorescence quantum yield.

As a matter of practice, the intensity of the signal collected by a detector used in a 2PEF measurement is $S = \Phi\left\langle N_{Fl}^{(2)} \right\rangle$, where Φ is the fluorescence collection efficiency of the measurement, which depends on the geometry of the experimental setup, the transmission and wavelength dependence of the optics in the path of the detector, and the quantum efficiency of the detector. Considering the second-order temporal coherence term of the excitation source, $g^{(2)} = \left\langle F^2(t) \right\rangle / \left\langle F(t) \right\rangle^2$, S can be expressed as

$$S = \tfrac{1}{2}\eta\Phi g^{(2)} \left\langle F \right\rangle^2 \delta \; C \qquad \text{(Eq. 2.18)}$$

It is observed from Eq 2.10, that a number of experimentally determined parameters must be obtained to determine the δ for a sample. While absolute methods can

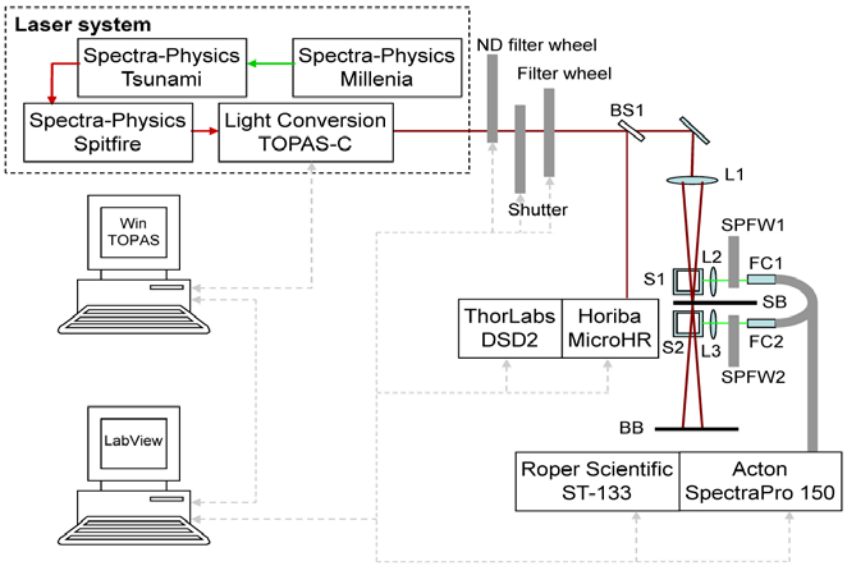

Figure 2.5. Schematic of the femtosecond 2PEF experimental setup used in this work. Reprinted with permission from Nikolay S. Makarov, Jochen Campo, Joel M. Hales, and Joseph W. Perry. Opt. Mater. Express, 2011, 1(4), 551-563. DOI: 10.1364/OME.1.000551 Copyright © 2011 Optical Society.

be used, a more common approach is to use a 2PEF referential technique during which fluorescent materials with known two-photon absorptivities are used as references. In most cases, for a 2PEF referential technique the value of δ for a sample is obtained by the equation

$$\delta_s = \frac{S_s}{S_r}\frac{\eta_r \Phi_r C_r}{\eta_s \Phi_s C_s}\delta_r \qquad \text{(Eq. 2.19)}$$

where the subscripts s and r refer to the sample and reference material, respectively. The fluorescence collection efficiency will vary with experimental design. Eq 2.11 provides an example equation for the determination of δ using a two-arm 2PEF setup.

Femtosecond Two-photon Excited Fluorescence Experimental Methods

2PA cross sections (δ) were determined using 2PEF experimental methods with a femtosecond excitation source. A one-arm, dual-channel referential 2PEF technique was

utilized [18]. The excitation source was an optical parametric amplifier (OPA; TOPAS, Spectra-Physics) that produces tunable laser pulses over the range of 190 nm-2600 nm. The OPA was pumped by a Ti:Sapphire regenerative amplifier (Spitfire, Spectra-Physics) operating at a 1 kHz repetition rate. The output of the OPA was used to excite the two-photon absorbing compounds under study and was weakly focused between two cuvettes in series containing the reference dye (*r*) whose 2PA properties have been well characterized and the sample of interest (*s*). Measurements were repeated with the sample and reference positions exchanged. At each wavelength (λ_0), δ for the sample of interest was determined using the following equation:

$$\delta_2^s(\lambda_0) = \delta_2^r(\lambda_0)\frac{C^r}{C^s}\sqrt{\frac{S_1^s(\lambda_0)S_2^s(\lambda_0)}{S_1^r(\lambda_0)S_2^r(\lambda_0)}}\frac{\varphi^r(\lambda')}{\varphi^r(\lambda')} \qquad \text{(Eq. 2.20)}$$

where *C* is the concentration, *S* is the detected 2PEF signal, φ is the differential fluorescence quantum yield at a common emission wavelength (λ') for the sample and reference, superscripts *r* and *s* signify reference and sample of interest, respectively, and subscripts 1 and 2 indicate channel positions one and two. All samples were prepared at a concentration of ~10^{-5} M and contained in 1 cm path-length fused silica cuvettes.

Nanosecond Two-photon Excited Fluorescence Experimental Methods

A 2PEF characterization technique utilized a dual-arm system [16] excited using nanosecond laser pulses from a Q-switched Nd:YAG (Pro250, Quanta-Ray, ~5 ns pulse duration, 10 Hz repetition rate) pumped optical parametric oscillator (OPO) laser (MOPO 730, Quanta-Ray), with a tunable wavelength range of 430-2000 nm. Solutions with a concentration of ~10^{-5} M were prepared and contained in a 1 cm path-length cuvettes.

Fluorophores whose 2PA cross sections and fluorescence quantum yields have been well characterized (such as 1,4-bis(2-methylstyryl)benzene in cyclohexane [16, 19] and fluorescein in water at pH=11 [16]) were used as reference standards in these measurements. At each wavelength, δ for a sample was calculated using Eq. 2.11 . The experimental setup and method of analysis for both 2PEF experimental techniques used have been previously described elsewhere [18, 20].

2.4.3.2. Power-dependent Nonlinear Transmission Measurements

Nonlinear transmission (NLT) is a direct method to measure the effective 2PA response in a nonlinear medium. During a NLT experiment, a sample is placed in a stationary position in the path of the excitation beam. The energy of the incident beam is varied over a range of pulse energies while the beam attenuation after it traverses the sample is measured. Because the transmission (or output intensity) of a NLO materials is energy dependent (Eq 1.12), NLT measurements can provide information regarding the magnitude of nonlinear absorption in a medium [12, 14]. NLT measurements using both fs- and ns-pulsed laser excitation were used to determine the efficacy of potential OPL materials by providing the change in transmission with respect to the incident energy of the pulsed laser.

Femtosecond NLT Experimental Methods

For fs OPL, samples were prepared at relatively high concentrations (~10^{-3} M) and contained in 1 mm path-length fused-silica cuvettes. The fs-OPA mentioned previously was used as an excitation source and the repetition rate was reduced to 50 Hz to minimize potential contributions from thermal nonlinearities. The excitation beam was

focused using a 50 mm focal length lens (f/20 geometry) with the focus placed in the middle of the 1 mm cuvette. The transmitted excitation beam as well as a reference beam (used to minimize pulse-to-pulse energy fluctuations) were detected using large area visible photoreceivers (model 2031, New Focus, Inc.) and integrated using Boxcar integrators (SR250, Stanford Research Systems). A scanning knife-edge method was used to determine the beam waist of the excitation laser pulse. The energies at the sample were measured using a power meter (PD300-UV-SH, Ophir) and were varied using a computer-controlled half-waveplate rotator (ESP300, Newport) in conjunction with a Glan-laser polarizer. Energy-dependent reference and excitation signals were acquired using a Labview-based data acquisition program.

Nanosecond NLT Experimental Methods

Nanosecond NLT measurements were performed similarly to the femtosecond measurements, using the ns-OPO as the excitation source described previously. The optical geometry was more tightly focused (f/5) than for the fs measurements. Sample solutions (~10^{-3} M) used in nanosecond OPL measurements were deoxygenated and contained in 1 cm quartz cuvettes which were stirred continuously. Z-scan measurements were used to place the focused beam in the center of the sample cell (Figure 2.6a). The beam profile of the ns laser pulses was obtained for numerical simulations using a 5 μm pinhole. An example of the profile of the ns laser pulses used in the NLT experiments is shown in Figure 2.6b. The optical setup for ns-pulsed NLT measurements is displayed in Figure 2.7.

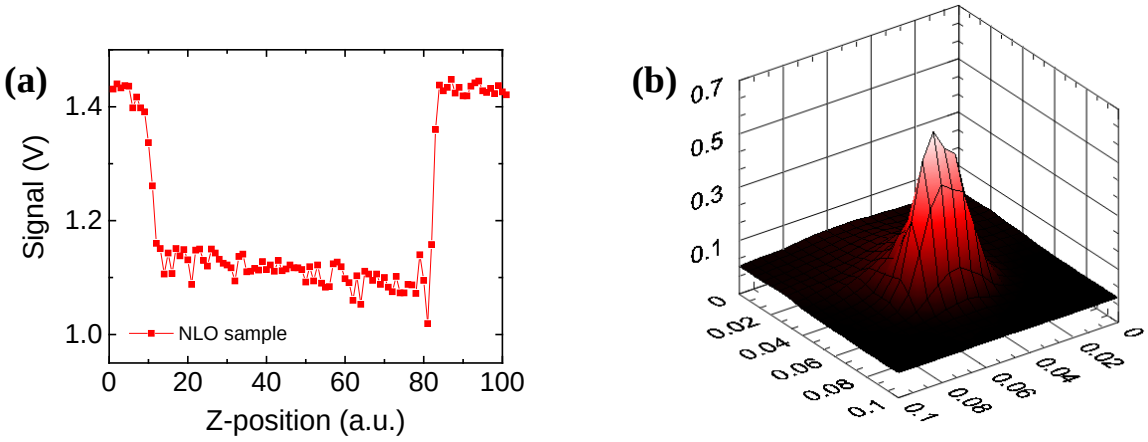

Figure 2.6. (a) Typical Z-scan response acquired from a OPL sample in a 1 cm cell. (b) Example of a ns-pulsed laser beam profile used for NLT measurements. The axes are in microns.

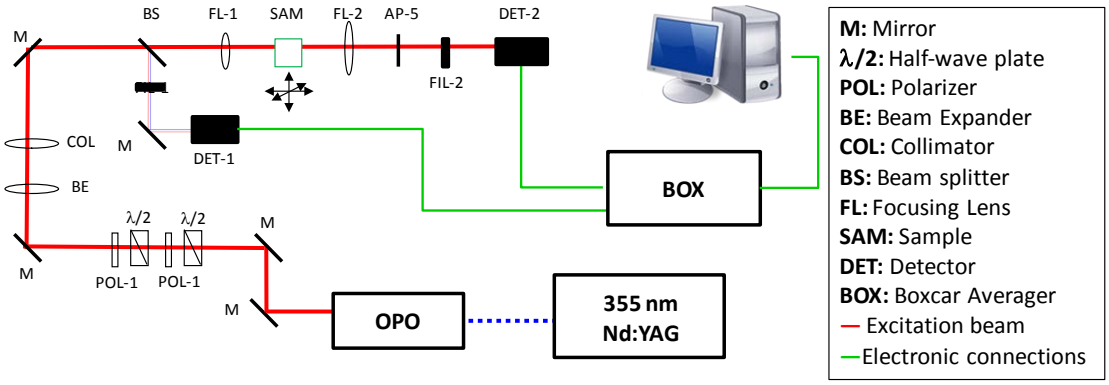

Figure 2.7. Schematic for the ns-pulsed NLT experiment.

2.5. References

[1] Göppert-Mayer, M., *Über Elementarakte mit zwei Quantensprüngen.* Annalen der Physik, 1931. **401**(3): p. 273-294.

[2] Kliger, D., *Ultrasensitive laser spectroscopy*. 1983: Elsevier.

[3] Herzberg, G., *Molecular spectra and molecular structure. I. Spectra of diatomic molecules.* American Journal of Physics, 1951. **19**: p. 390-391.

[4] Mulliken, R.S., *Intensities of Electronic Transitions in Molecular Spectra I. Introduction.* The Journal of Chemical Physics, 1939. **7**(1): p. 14-20.

[5] Lakowicz, J.R., *Principles of fluorescence spectroscopy*. 2007: Springer.

[6] Williams, A.T.R., Winfield, S.A. and Miller, J.N., *Relative fluorescence quantum yields using a computer-controlled luminescence spectrometer.* Analyst, 1983. **108**(1290): p. 1067-1071.

[7] Berera, R., van Grondelle, R. and Kennis, J.T., *Ultrafast transient absorption spectroscopy: principles and application to photosynthetic systems.* Photosynthesis research, 2009. **101**(2-3): p. 105-118.

[8] Malicki, M., Hales, J.M., Rumi, M., Barlow, S., McClary, L., Marder, S.R. and Perry, J.W., *Excited-state dynamics and dye-dye interactions in dye-coated gold nanoparticles with varying alkyl spacer lengths.* Physical Chemistry Chemical Physics, 2010. **12**(23): p. 6267-6277.

[9] Kasha, M., *Characterization of electronic transitions in complex molecules.* Discussions of the Faraday Society, 1950. **9**(0): p. 14-19.

[10] Esherick, P., Zinsli, P. and El-Sayed, M.A., *The low energy two-photon spectrum of pyrazine using the phosphorescence photoexcitation method.* Chemical Physics, 1975. **10**(2–3): p. 415-432.

[11] Singer, L., Baram, Z., Ron, A. and Kimel, S., *The two-photon phosphorescence excitation spectrum of triphenylene.* Chemical Physics Letters, 1977. **47**(2): p. 372-376.

[12] Sutherland, R.L., *Handbook of nonlinear optics*. 2003: CRC press.

[13] Sheik-Bahae, M., Said, A.A., Wei, T.H., Hagan, D.J. and Van Stryland, E.W., *Sensitive measurement of optical nonlinearities using a single beam.* Quantum Electronics, IEEE Journal of, 1990. **26**(4): p. 760-769.

[14] Tutt, L.W. and Boggess, T.F., *A review of optical limiting mechanisms and devices using organics, fullerenes, semiconductors and other materials.* Progress in Quantum Electronics, 1993. **17**(4): p. 299-338.

[15] Denk, W., Strickler, J. and Webb, W., *Two-photon laser scanning fluorescence microscopy.* Science, 1990. **248**(4951): p. 73-76.

[16] Xu, C. and Webb, W.W., *Measurement of two-photon excitation cross sections of molecular fluorophores with data from 690 to 1050 nm.* J. Opt. Soc. Am. B, 1996. **13**(3): p. 481-491.

[17] Makarov, N.S., Drobizhev, M. and Rebane, A., *Two-photon absorption standards in the 550-1600 nmexcitation wavelength range.* Opt. Express, 2008. **16**(6): p. 4029-4047.

[18] Makarov, N.S., Campo, J., Haley, M.M. and Perry, J.W., *Rapid, broadband two-photon-excited fluorescence spectroscopy and its application to red-emitting reference compounds.* Opt. Express, 2011. **1**(4): p. 551-563.

[19] Kennedy, S.M. and Lytle, F.E., *p-Bis(o-methylstyryl)benzene as a power-squared sensor for two-photon absorption measurements between 537 and 694 nm.* Analytical Chemistry, 1986. **58**(13): p. 2643-2647.

[20] Rumi, M., Ehrlich, J.E., Heikal, A.A., Perry, J.W., Barlow, S., Hu, Z., McCord-Maughon, D., Parker, T.C., Röckel, H., Thayumanavan, S., Marder, S.R., Beljonne, D. and Bredas, J.-L., *Structure-Property Relationships for Two-Photon Absorbing Chromophores: Bis-Donor Diphenylpolyene and Bis(styryl)benzene Derivatives.* J. Am. Chem. Soc., 2000. **122**(39): p. 9500-9510.

CHAPTER 3

SUBSTITUTED PHENYLENE ETHYNYLENE-BASED CO-POLYMERS WITH ENHANCED BROADBAND NONLINEAR ABSORPTION FOR OPTICAL POWER LIMITING

3.1. Introduction

Materials exhibiting strong nonlinear absorption (NLA) are of considerable interest for their use in photonic applications, such as dynamic range compression of optical pulse trains [1], loss-based optical switching [2], and optical power limiting (OPL) of intense laser pulses for the protection of optical sensors and human eyes [3-6]. The visible and near-IR spectral regions are particularly important for OPL given the ubiquitous nature of high-powered, frequency-agile pulsed laser systems. Materials for OPL applications should exhibit high optical transparency in the region of interest below a threshold power or energy, but above this threshold should show strong induced absorption over a large spectral and temporal range.

Early work on organic OPL materials mainly focused on small molecular systems whose nonlinear absorption properties arise from one-photon absorption (1PA) followed by excited state absorption (1PA-ESA), also known as reverse saturable absorption (RSA) [5, 7, 8]. OPL via RSA can be effective for long pulse durations (>1 ns), but the usable spectral range and linear transmittance (T_L) are compromised by linear absorption at the excitation wavelength. Two-photon absorption induced excited state absorption (2PA-ESA) is an attractive alternative to achieve very high linear transmittance as the excitation wavelength for 2PA can be well below the 1PA edge, resulting in high

transparency over a larger spectral range. To achieve effective OPL through 2PA-ESA, however, several conditions must be met: 1) the positions, in terms of photon wavelength, for the 2PA and ESA bands must show significant spectral overlap with sizable two-photon and ESA cross sections, 2) 2PA and ESA bands should have relatively broad spectral widths, and 3) for limiting of femtosecond to nanosecond laser pulses, excited states must be formed rapidly, and the lifetime of the absorbing excited-state species should be long-lived relative to the pulse duration (i.e. long-lived singlet or triplet excited states).

Materials examined previously for 2PA-ESA based OPL in the visible region have focused mainly on either fluid solutions or polymer and sol-gel solid matrices doped with discrete organic molecules [9-12]. While large suppression values have been realized, relatively few materials have demonstrated effective broad bandwidth OPL [13, 14]. Broader bandwidth response has been reported using either a tandem cell arrangement or a multi-component nonlinear absorber system, which may have issues associated with quenching, compatibility, and solubility [15, 16]. To address these issues, researchers have investigated the development of π-conjugated polymers with strong nonlinear absorption for OPL applications [17-22]. As opposed to discrete molecules, which generally show narrowband ESA spectra, π-conjugated polymers provide a large density of excited states and can display broadband ESA due, in part, to conformational heterogeneity within the polymer structure [23]. This, in turn, may result in broader spectral ranges for effective OPL than those observed in small molecule systems. Previous research in the Perry group has shown that π-conjugated polymers can exhibit

broadband 2PA-based OPL in the near-IR with unprecedented spectral coverage with a bandwidth as large as 500 nm [18, 19].

Poly(*p*-phenyleneethynylene) (PPEs) and poly(aryleneethynylene) (PAEs) derivatives have also been used to demonstrate OPL of nanosecond pulses at single wavelengths in the visible region via 2PA-based mechanisms [24, 25]. Broadband OPL within this family of polymers has not yet been demonstrated to date. This is likely due to a combination of narrow 2PA bandwidths with relatively low 2PA cross sections (δ), and rather short excited-state lifetimes. Previous studies of the two-photon spectroscopy of cruciform structures based on centrosymmetric and noncentrosymmetric oligo(phenylene vinylene)s [26, 27], oligo(phenylene ethynylene)s [28, 29], and phenylene vinylene / phenylene ethynylene co-oligomers [30-33] have shown that addition of electron donor and acceptor groups to the arms of cruciform structures can give rise to significant electronic coupling of the arms. This coupling impacts on the 1PA and 2PA band positions, strengths, and bandwidths [26, 33].

In this chapter, we address the question of whether the coupling of conjugated side chains to a PPE polymer backbone can yield the band positions, bandwidths, 2PA and excited state absorption cross sections and excited state lifetimes suitable for enable strong, broadband OPL in the visible and near-IR spectral regions. Specifically, we report on the 1PA and 2PA spectroscopy, transient absorption spectroscopy and the OPL properties of two phenylene ethynylene (PPE)-based copolymers with conjugated side arms that result in a repeating cruciform-like structure in the polymer main chain: one PPE polymer (see Figure 3.1) has a bis-(4,4'-isopropylstyryl)benzene group and the second bears a bis-(4,4'-alkylaminostyryl)benzene in the main chain of the PPE. The

incorporation of a donor- π conjugated bridge-donor (D-π-D) group in the latter should impart a reasonably large 2PA cross section, due to the symmetric intramolecular charge transfer (ICT) upon excitation of the D-π-D system [34-36].

3.2. Background

Since the ground-breaking discoveries[i] of Alan Heeger, Alan MacDiarmid, and Hideki Shirakawa [37], conjugated polymers have revolutionized the field of photonic and optoelectronic devices. Conjugated polymers are organic semiconductors that have charge transport properties similar to their inorganic counterparts, but also offer the potential for mass production of devices via low-cost, wet processing methods, such as spin-casting or ink-jet printing. Furthermore, conjugated polymers provide a seemingly endless possibility for tailoring of properties due to the interplay of their geometric and π-electronic structure. Consequently, conjugated polymers have transformed organic photonics and optoelectronics into a dynamic field of research and development [38, 39].

PPEs and PAEs are a class of conjugated polymers that have garnered recent attention. Due in part to the rigidity of their polymer structure, PPEs posses interesting emissive properties, high photoluminescence efficiencies, and have shown their usefulness in detection of explosives [40], light-emitting diodes (LEDs) [41, 42], molecular wires [43], and as polarizers for liquid crystal displays [44]. This family of polymers also shows charge carrier mobility and has been incorporated into polymer field-effect transistor (PFETs) [45] and polymer solar cell devices [46]. The charge carrier mobility of PPE polymers has also been demonstrated. Furthermore, PPEs reportedly show better photostability than the more popular poly(*p*-phenylene vinylene) (PPV) [47].

[i] The Nobel Prize in Chemistry in 2000 was awarded to Alan J. Heeger, Alan G. MacDiarmid and Hideki Shirakawa "for the discovery and development of conductive polymers".

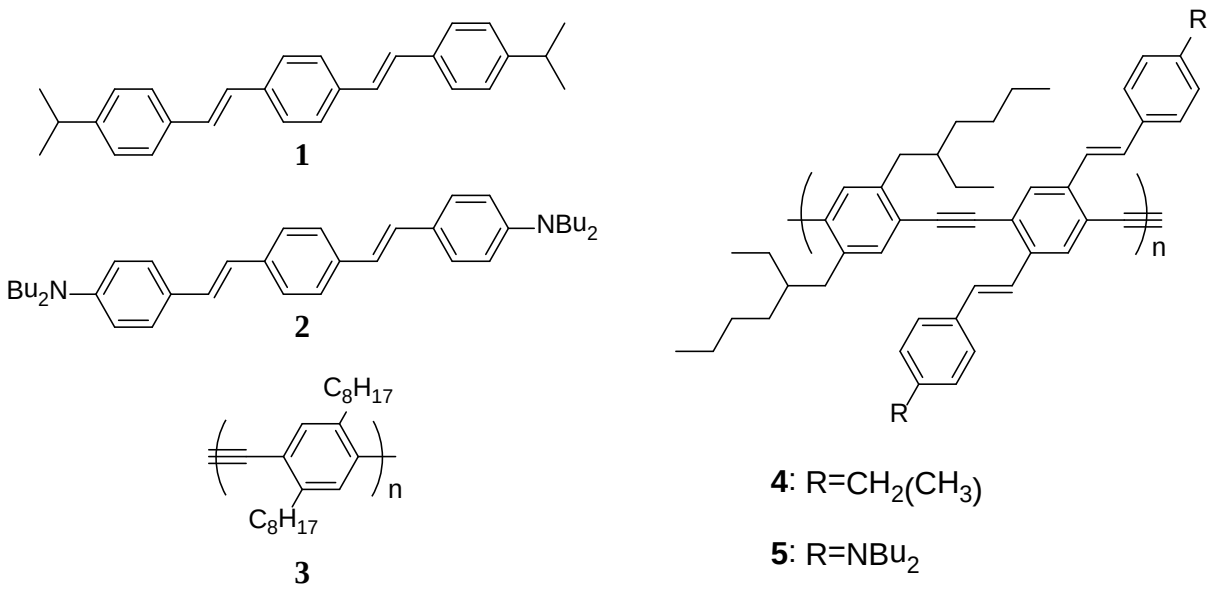

Figure 3.1. Molecular structure of linear and cross-shaped chromophores and polymers considered in this work.

The nonlinear optical properties of PPEs have also been investigated. Prasad and coworkers reported a large 2PA section (δ = 196 x 10^{-48} cm^4·s or 19,600 GM) for a poly(2,5-dialkoxy-*p*-phenylen ethynylene) derivative, and demonstrated OPL at 810 nm with a figure-of-merit (FOM)[ii] of 3.3 [25]. Additionally, laser action in has been reported for PPE derivatives[48].

Despite the large δ values reported by Prasad and potential applications in polymer laser devices, the usage of PPEs in nonlinear optical applications has received little attention relative to other conjugated polymers, such as PPVs. Further investigation of the nonlinear optical properties of PPEs and their derivatives would provide additional insight towards effective design strategies for conjugated polymers for 2PA applications.

[ii] Figure-of-merit (*FOM*) defined as T_{Lin}/T_F where T_{Lin} is the linear transmittance and T_F is the transmittance just prior to optical breakdown or nonlinear scattering.

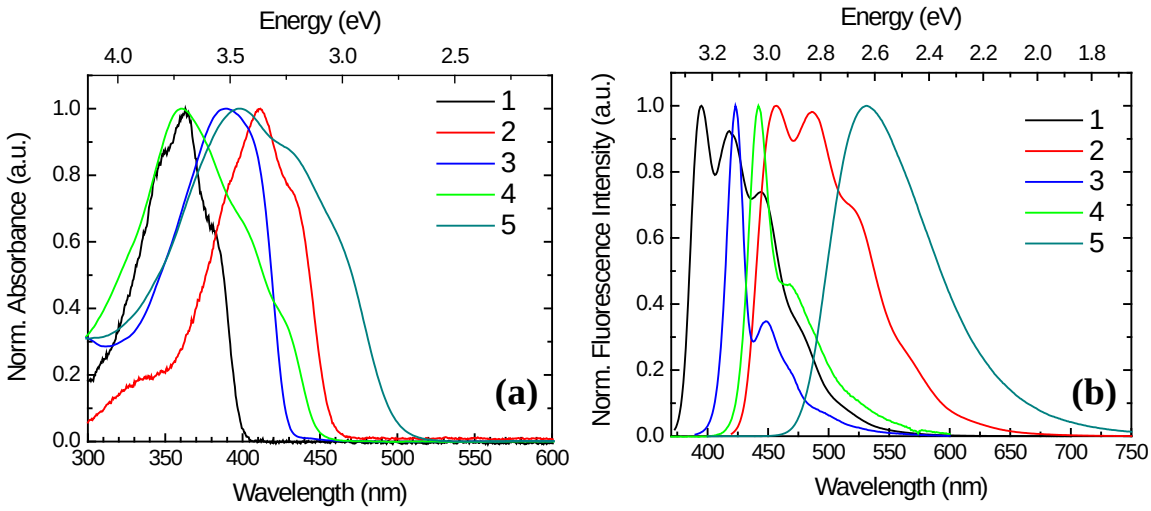

Figure 3.2. Normalized linear absorption (a) and fluorescence (b) spectra of **1**-**5** in toluene. Excitation wavelengths of $\lambda_{abs}^{(1)}$ of each molecule were used to receive fluorescence spectra.

Specifically, furthering the understanding of the 2PA behavior of PPEs may increase their usefulness for optical limiting and two-photon fluorescence imaging applications.

3.3. Photophysical characterization of PPE-based co-polymers

Figure 3.1. depicts the molecular structure of the molecules and polymers considered in this study. The photophysical characterization of **1**-**5** is described below. The experimental details are listed in section 3.6.

3.3.1. Steady-state absorption and fluorescence measurements

The one- photon absorption and fluorescence for molecules **1**-**5** are displayed in Figure 3.2., along with the corresponding spectroscopic parameters listed in Table 3.1. Excitation spectra of **3**, **4**, and **5** were also obtained and are displayed in Figure 3.3.

Chromophores **1** and **2** show one-photon absorption wavelength maxima ($\lambda_{abs}^{(1)}$) at 363 nm and 411 nm, respectively, with one prominent electronic absorption band that displays vibronic structure. The peak molar extinction coefficients (ε_{max}) of **1** and **2** are

Table 3.1. One-Photon Spectroscopic Parameters for **1-5** (Solvent: Toluene)

	1	2	3	4	5
$\lambda_{abs}^{(1)}$ (nm)[a]	363	408	390	362	398
ε_{max} (10^4 M^{-1} cm^{-1})[a]	5.7	7.6	1.5	4.0	3.9
M_{ge} (D)[b]	9.3	11.4	5.8	9.8	10.9
$\lambda_{fl}^{(1)}$ (nm)[c]	396	455	423	442	530
η[c]	0.93 ± .04	0.88 ± .02	0.79 ± .06	0.46 ± .03	0.34 ± .03

[a] One-photon absorption maximum ($\lambda_{abs}^{(1)}$) and peak molar extinction coefficient (ε_{max}). [b] Transition dipole moment shown in Debye (1 D = 1 x 10^{-18} esu cm) was obtained as in ref 35; $M_{ge}=(\{750\ \hbar c(\ln 10)/\pi^2 N_A\}\int\{\varepsilon(\nu)/\nu\}\ d\nu)^{1/2}$, where $\varepsilon(\nu)$ is the molar extinction coefficient ($M^{-1}cm^{-1}$) as a function of wavenumbers ν (cm^{-1}), N_A is Avagadro's number, and $\hbar$ and c are in cgs units. [c] One-photon fluorescence maximum ($\lambda_{fl}^{(1)}$) and fluorescence quantum yield, η. The error reported is the standard deviation of the fluorescence quantum yields at different concentrations.

relatively large (see Table 3.1.). Both chromophores are highly fluorescent ($\eta > 0.8$) with spectra that exhibit vibronic structure with a progression of several peaks, all of which suggest a relatively planar conformation of the lowest singlet excited state of distyrylbenzene (DSB) chromophores in toluene. The dialkyl-substituted *p*-PPE polymer, **3** shows a broad, featureless absorption band ($\lambda_{abs}^{(1)}$ =390 nm), and characteristic PPE emission, with a strong 0-0 vibronic transition and a well-resolved shoulder. In contrast to the DSB chromophores, which display planar geometries in both the ground and excited states, PPEs can experience a large degree of torsion in the ground state due to rotation between adjacent phenylene ethynylene units within the polymer, resulting in a broad ground-state absorption band. In the excited state, however, the amount of rotation is greatly reduced as the polymer undergoes planarization, likely through the contribution

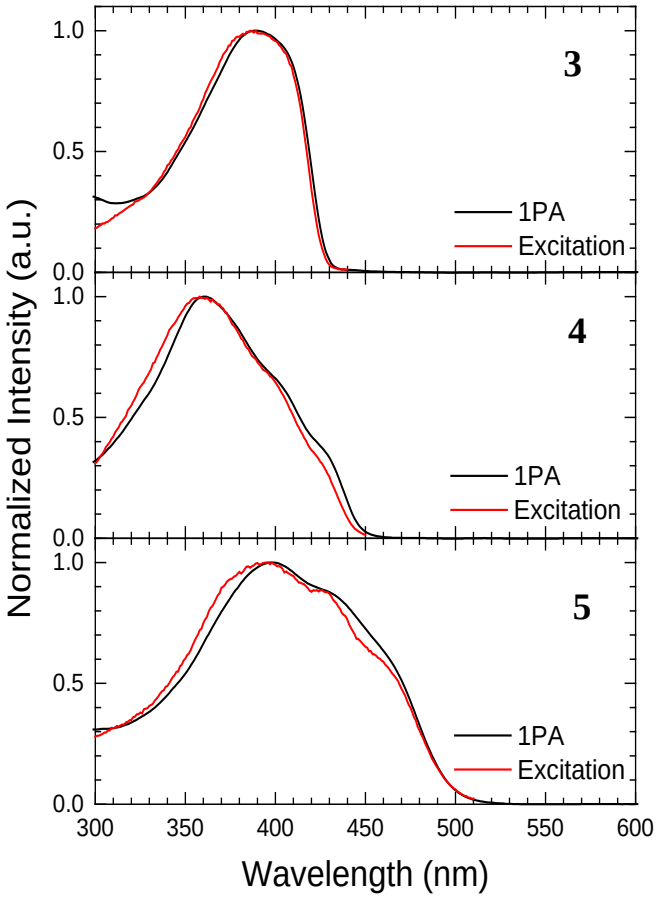

Figure 3.3. Normalized 1PA and fluorescence excitation spectra of polymer **3** (top) and co-polymers **4** (middle) and **5** (bottom) in toluene. The excitation spectra were recorded at a fixed emission wavelength of 470 nm, 480 nm, and 540 nm for **3**, **4**, and **5**, respectively.

of quinoidal resonance structures, resulting in narrow emission bands as seen in Figure 3.2 [49, 50].

The one-photon absorption spectra of polymers **4** and **5** exhibit noticeable differences relative to the spectra of model compounds **1** and **2** and polymer **3,** as a result of the incorporation of 2,5-bis-isopropylstyrylphenylene or 2,5-bis-diethylaminostyrylphenylene as polymer side chains. For example, the low energy portion of the 1PA band of co-polymer **4** is red-shifted in comparison to the PPE polymer, **3**, and shows two shoulders at 405 and 420-430 nm, while the $\lambda_{abs}^{(1)}$ of **4** is slightly blue-shifted (<100 cm^{-1}) from the position of the 1PA band of the DSB model compound, **1**. Similar shifts and splitting of electronic absorption bands have been observed for noncentrosymmetric benzene-centered cruciforms, where the significant overlap of the $\pi\pi^*$ electronic absorption bands of the chromophoric arms results in moderate mixing of the lowest excited states of the components [26, 29, 51]. These cruciforms may also be described as oblique excitons [52] formed by two nonequivalent chromophoric units connected through a central aromatic ring. Such systems show one-photon allowed transitions to both excitonic levels of the coupled system, so that the higher energy absorption band has a larger contribution from the higher energy chromophoric unit and vice versa. In the case of **4**, the 1PA spectrum of the co-polymer suggests that the higher energy peak is largely associated with the DSB absorption and the lower energy features are mainly associated with the PPE polymer spectrum. It should be noted that the molar extinction coefficient of the DSB group is significantly larger than that of polymer **3**. As a result, the peak at 360 nm is

significantly stronger than that of the lower energy shoulder we attribute to the PPE backbone absorption.

The description above is additionally supported by the emission properties of **4**: the emission of the co-polymer strongly resembles that of the lower-energy PPE unit irrespective of excitation wavelength (see Figure 3.3). This result indicates rapid internal conversion (IC) from the DSB dominated exciton state to the lower energy PPE excitonic state. Indeed, the fluorescence spectrum of **4** is very similar in shape to **3**, but shows a small red-shift (~20 nm) of the wavelength of maximum fluorescence ($\lambda_{fl}^{(1)}$) indicating a stabilization of the lowest excited singlet state, possibly due to the effects of geometry changes and/or the electronic coupling of the DSB arms and the PPE backbone. **4** also shows a significant reduction of the fluorescence quantum yield (η) compared to each of the components, indicating that the addition of distyryl arms to the PPE polymer facilitates relaxation via nonradiative pathways.

Somewhat different spectral changes were observed in the absorption spectrum of **5** where, in contrast to **4**, the electronic transition of the PPE polymer is at higher energy and the donor-substituted DSB chromophore is at lower energy. The 1PA of **5** shows a $\lambda_{abs}^{(1)}$ at 398 nm, which is close to the position of the PPE polymer, along with two weak shoulders at 430 nm and 450-460 nm that can be attributed to the vibronic features characteristic of **2**. In addition, there is a significant red-shift of the absorption band-edge (~2200 cm^{-1}) with respect to **2**. These features can be rationalized in terms of excitonic coupling of the distinct units, as previously mentioned. The sizeable red shift of the bandedge of **5** relative to that of **2** is likely due to both an overall stabilization (diagonal shift) and an electronic coupling of the units (off-diagonal shift). The small shift of $\lambda_{abs}^{(1)}$

of the high-energy band observed for **5** with respect to **3**, can be attributed to an offsetting of the excitonic splitting by the diagonal shift. It is possible that intramolecular charge transfer (ICT) between the donor distyryl arms and the polymer chain, may contribute to the magnitude of the exitonic coupling as well. Bunz and coworkers have reported that ICT transitions occur between largely spatially separated HOMO and LUMO frontier orbitals of the D/A-substituted arms of benzene-centered ethynyl/vinyl cruciform [30-32].

The above interpretation is further supported by through the emission properties of **5**. As observed in **4**, the emission spectrum of co-polymer **5** strongly resembles that of the arm with the lower transition-energy, irrespective of excitation wavelength (see Figure 3.3), suggesting that IC from the PPE excitonic state to the lower-energy, DSB-dominated exciton state occurs. The $\lambda_{fl}^{(1)}$ of **5** is, however, substantially red-shifted (~75 nm) with respect to **2**, and the vibronic features seen in the DSB analogue are not preserved, suggesting partial ICT and/or torsional process in the co-polymer. Compound **5** also shows a significant reduction of η (0.34) compared to **2** and **3**. Furthermore, **5** shows a large Stokes shift in toluene (~2870 cm^{-1}) that is comparable to those observed in related dipolar molecules (specifically, the Stokes shift of (dimethylamino)stilbene in *n*-hexane is ~2400 cm^{-1}) [53].

3.3.2. Solvatochromic shifts of absorption and fluorescence spectra

The observations of the 1PA and fluorescence spectra of **4** and **5** suggest that ICT between the distyryl arm and the polymer chain may contribute to the excitonic coupling and 2PA properties of these substituted PPE co-polymers. To add further discussion on the conformation and CT character of cruciform-like PPE co-polymers, the 1PA and

emission characteristics were obtained in solvents with different polarizability values. The steady-state spectra of **3**, **4**, and **5** in various solvents are shown in Figure 3.4.

Solvatochromic effects are observed in the 1PA spectra of **3**. As shown in Figure 3.4a, a slight hypsochromic shift of $\lambda_{abs}^{(1)}$ and slight narrowing of the 1PA band occurs as the solvent polarity is increased. In contrast to **3**, very little solvent-based changes are observed in the 1PA band position of **4** and **5**. Subtle changes are observed in the absorption tail of both co-polymers, which can be attributed to slight aggregation in the more polar solvents.

Polymer **3** shows significant solvent-based changes in its emission spectra, including the broadening of the 0-0 transition and an increase in the 0-1 vibronic band with increased solvent polarity. Similar changes in the emission spectrum of dialkyl-PPEs have been reported when these polymers (or long-chain oligomers) are placed in a films [54] or viscous solvents [49, 55], or when fluorescence measurements are performed at low temperatures [49]. Under conditions of a confining medium or low temperatures, smaller structural changes occur directly after excitation. The planarization of the polymer is thus hampered and is on the time scale of the fluorescence lifetime; therefore, PPE emission in highly viscous media and at low temperatures may take place from an excited-state population that is torsionally disordered as opposed to the preferred quinodial/cumulenic configuration of the S_1 state. Although the solvents used in the solvatochromic measurements are not viscous, similar effects in emission are observed suggesting that the polarity of the solvent allows for an increase in emission from the nonplanar configuration of the lowest excited state.

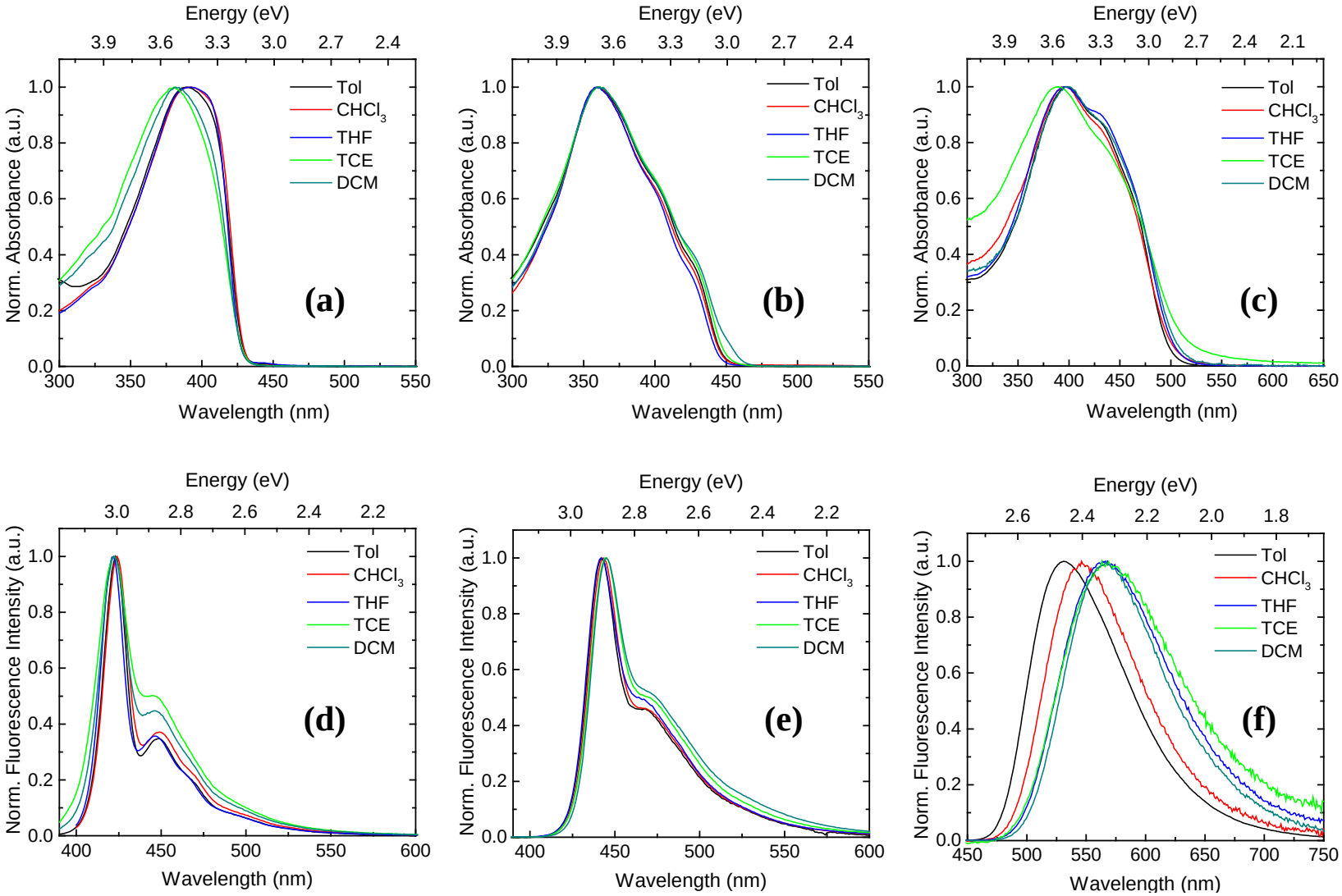

Figure 3.4. 1PA and fluorescence spectra of PPE polymers **3** (a and d), **4** (b and e) and **5** (c and f) in solvents of different polarity: toluene (Tol), $CHCl_3$, tetrahydrofuran (THF), 1,1,1-trichlororethane (TCE), and dichloromethane (DCM). Fluorescence spectra were obtained by exciting at $\lambda_{abs}^{(1)}$ for all polymers.

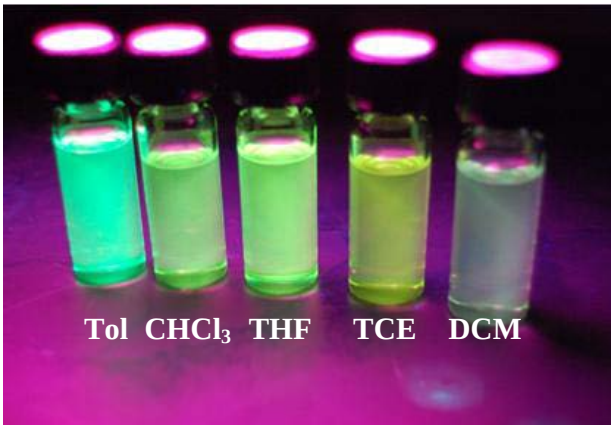

Figure 3.5. Photograph showing fluorescence emission of **5** in various solvents under UV radiation.

Solvent effects are also observed in the emission spectra of **4** and **5**. Similar to **3,** the emission of **4** shows an increase in the 0-2 vibronic band along with broadening and a slight red-shift of $\lambda_{fl}^{(1)}$ (~3 nm) with increased polarity reflecting a greater change in geometry. Positive solvatochromism is clearly observed in the fluorescence of the co-polymer **5** (see Figure 3.5). For example, a ~30 nm bathochromic shift of $\lambda_{fl}^{(1)}$ and slight broadening of the emission band can be seen in Figure 3.4f. Solvent-induced spectral changes in the emission of the co-polymers would suggest that, as in the case of dialkyl-PPEs, **4** and **5** experience increased conformational disorder in more polar media; however, the relatively large shifts in $\lambda_{fl}^{(1)}$ observed in **5** (and not **4**) indicate that only the donor-substituted co-polymer possesses moderate charge transfer character.

3.3.3. Time-resolved fluorescence spectroscopy

As mentioned above, the substitution of PPE polymers by distyryl units has a pronounced effect on the fluorescence quantum yield of these chromophores. Time-resolved fluorescence measurements were conducted in order to investigate the effect of

Table 3.2. Fluorescence Lifetime (τ_{FL}) and Rate Constants for the Radiative (k_r) and Non-radiative (k_{nr}) Decay Rates for **1-5** (Solvent: Toluene)

	1	**2**	**3**	**4**	**5**
τ_{FL} (ns)[a]	1.25	1.44	0.360	1.32	2.58
k_r (10^8 s^{-1})	7.6	6.12	21.9	3.48	1.32
k_{nr} (10^8 s^{-1})	0.400	0.834	5.83	4.09	2.56

[a] Lifetime of S_1 state after one-photon excitation at 376 nm. Fluorescence was monitored at λ_{fl} for each molecule. Concentration of samples were 10^{-6} M.

the substitution on the fluorescence lifetime (τ_{FL}) of these polymers. The fluorescence decay of **1-5** are listed in Table 3.2.

The fluorescence lifetimes of **1** and **2** are slightly longer than 1 ns and are similar to those reported for 1,4-distyrylbenzene (measured in toluene) [56] and bis-(4,4'-alkylaminostyryl)benzene (measured in acetonitrile) [35], respectively. Polymer **3** posses a significantly shorter fluorescence lifetime of 364 ps. In contrast to **3**, the τ_{FL} for the cruciform-like co-polymers are 1.3 ns and 2.6 ns for **4** and **5**, respectively. The fluorescence lifetimes of **4** and **5** are similar to those reported for cruciform small molecule analogs [31].

From the fluorescence quantum yield, η, and τ_{Fl}, the rate constants for the radiative (k_r) and nonradiative decay (k_{nr}) of the molecules can be determined using the following equation given by [57]

$$\eta = \frac{k_r}{(k_r + k_{nr})} \quad \text{(Eq 3.1)}$$

$$\tau_{FL} = (k_r + k_{nr})^{-1} \quad \text{(Eq 3.2)}$$

The k_r and k_{nr} values are listed in Table 3.2. The DSB molecules show similar k_r and k_{nr} values, suggesting that the substitution of the terminal amine groups results in very little

change in the decay pathways of DSB molecules. Polymer **3** shows relatively large k_r and k_{nr} values, indicating that the polymer experiences a very fast and efficient decay from S_1. There is a large reduction of k_r when comparing **4** and **5** to the linear models. Furthermore, the k_{nr} of the co-polymers increases significantly relative to the DSB model chromophores.

The reduction of η and k_r, along with the increase in k_{nr} observed in **4** and **5** may be explained by torsional fluctuations that lead to nonradiative decay associated with vibronic coupling due to the substitution distyryl units on the PPE main chain. Similar observations have been reported for PPE oligomers and polymers in viscous media or at low temperatures, where an increase in torsional motion increases the rate of nonradiative decay from the excited state [55]. The cruciform-like structure of the co-polymers provides for more torsional freedom than that available, and thus, the number of nonradiative decay pathways available to the co-polymer is increased.

3.3.4. Two-Photon Spectroscopy

In order to understand the 2PA properties of the cruciform-like polymers and to assess the potential spectral regions in which OPL via 2PA-ESA may be feasible, we have characterized the relevant nonlinear absorption properties of the cruciform-like co-polymers. We have obtained the 2PA spectra and 2PA cross sections (δ) of **1**-**5** via 2PEF using femtosecond pulses. 2PEF results are displayed in Figure 3.6 and Table 3.3.

As shown in Figure 3.6, **1** has a 2PA band in the visible spectral region with a maximum 2PA cross section (δ_{max}) of ~350 GM (1 GM ≡ 1 x 10^{-50} cm^4·s/photon-

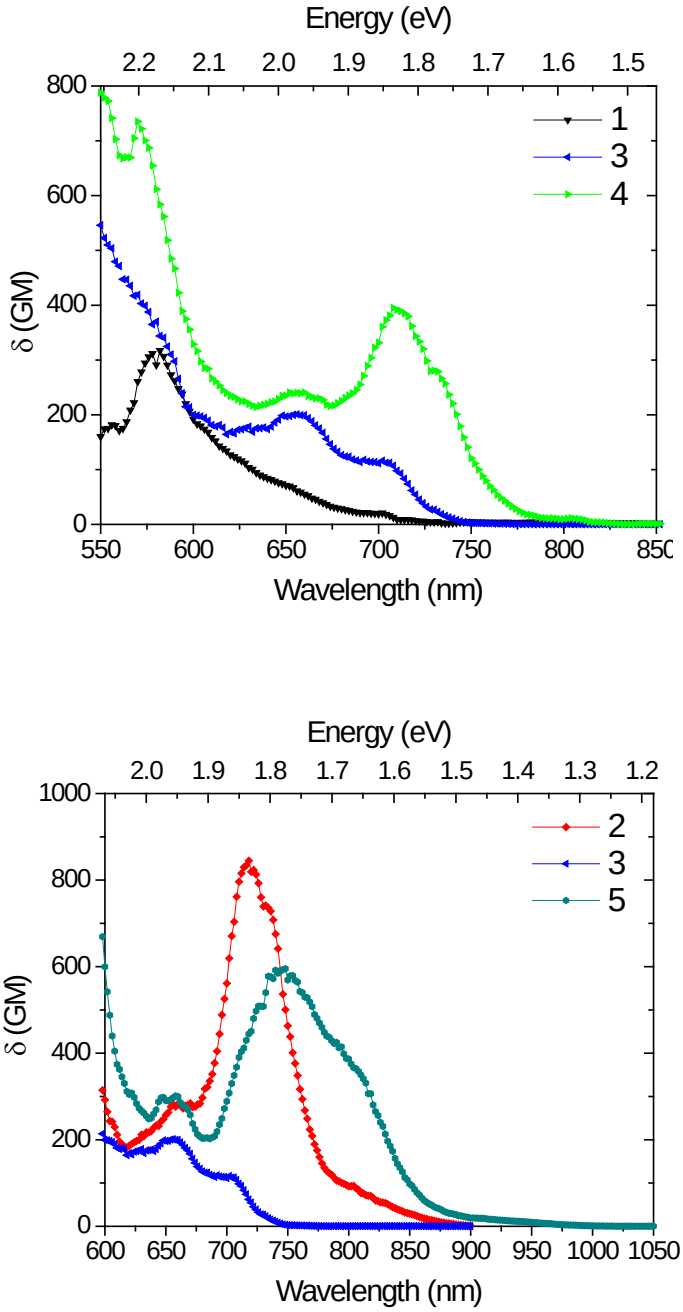

Figure 3.6. 2PEF spectra of molecules **1**-**5** in toluene obtained via femtosecond laser pulse excitation.

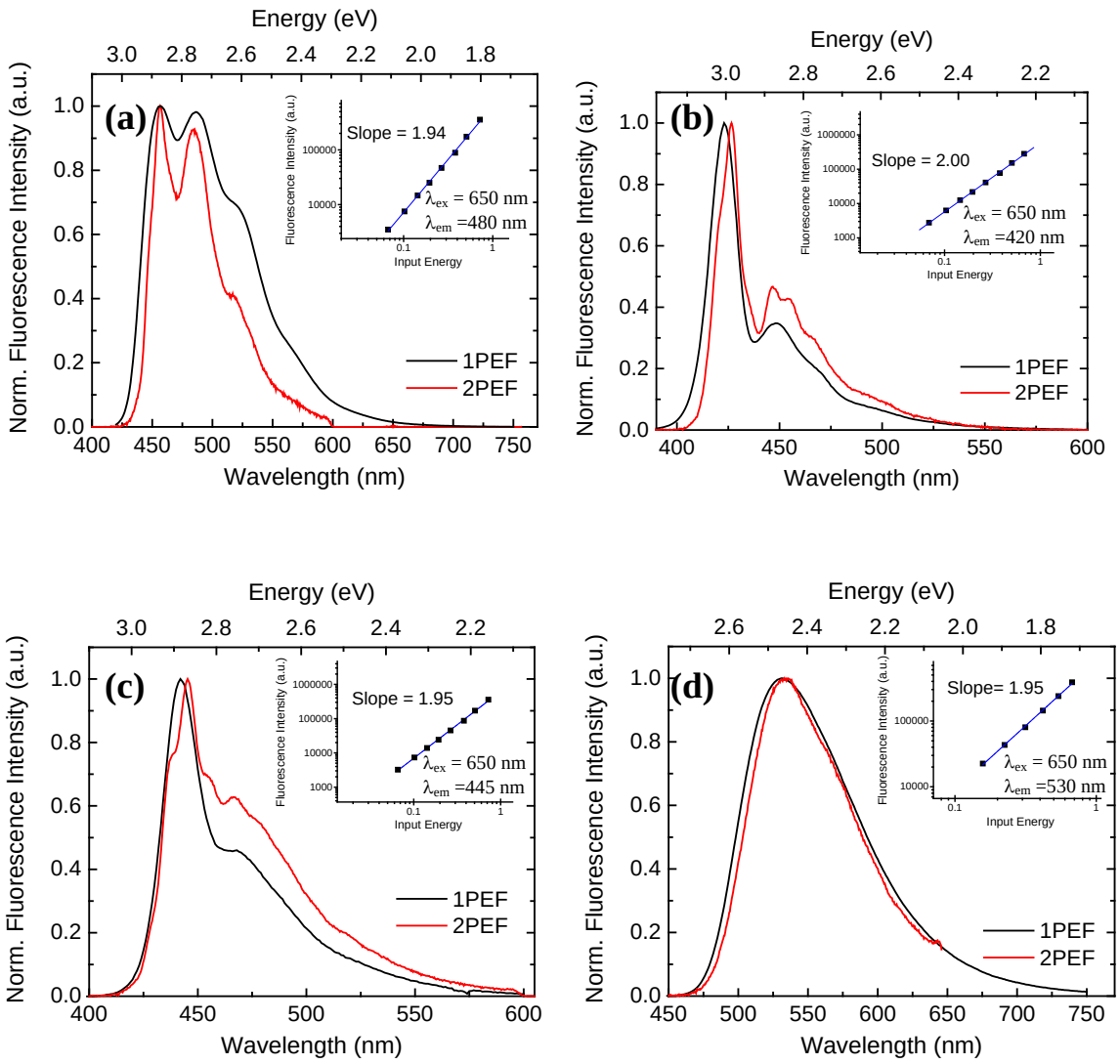

Figure 3.7. Normalized one-photon excited fluorescence (1PEF) and fs 2PEF of **2**(a), **3**(b), **4**(c), and **5**(d). Inset show a logarithmic plot of the dependence of the relative 2PEF signal (■) on the pulse intensity for each molecule along with a linear fit (—) and the slope of the results. The excitation wavelengths (λ_{ex}) and emission wavelengths (λ_{em}) of each chromophore are listed in the plots. All samples were prepared in toluene. 2PEF measurements were carried out with samples at a concentration of 10^{-5} M.

Table 3.3. Two-Photon Spectroscopic Parameters for **1-5** (Solvent: Toluene)

	1	**2**	**3**	**4**	**5**
$\lambda_{abs}^{(2)}$ (nm)[a]	580	718	656	708	748
δ_{max} (GM)[a]	317	844	200	395	595
band area [b] (GM cm^{-1})	5.7×10^5	1.2×10^6	1.0×10^6	1.8×10^6	1.8×10^6

[a] Maximum of the two-photon fluorescence excitation spectrum ($\lambda_{abs}^{(2)}$) and peak two-photon absorption cross-section (δ_{max}). The maximum values were determined considering only areas absent of preresonance enhancement. [b] Band area obtained by integrating the cross section over the two-photon band absent of preresonance enhancement.

molecule) at its 2PA maximum wavelength ($\lambda_{abs}^{(2)}$) of 580 nm. These values are of the same order as those of 1,4-bis(2-methylstyryl)benzene in cyclohexane (160 GM) whose 2PA properties have been well characterized [58, 59]. In the case of **2**, the addition of terminal dibutylamine donors and thus the introduction of a "quadrupolar" geometry to the DSB structure results in a red-shift of $\lambda_{abs}^{(2)}$ (580 vs 720 nm) and an enhancement of δ, compared to **1**. There is a large increase in δ in the 550-600 nm region which can be attributed to preresonance enhancement due to the proximity to the bandedge of the lowest one-photon transition [60, 61]. The donor-substituted DSB also shows a change in 2PA band shape, exhibiting vibronic structure, along with a weak shoulder to the red of 780 nm corresponding to the $S_0 \rightarrow S_1$ absorption band of **2**. The enhancement of δ along with 2PA spectral changes observed in **2** vs. **1** are a due to photoinduced ICT from the terminal amine donor groups to the center phenylene ring, as previously demonstrated by Perry and coworkers [34].

Polymer **3** shows marginal 2PA ($\delta_{max} \approx 200$ GM) in the visible spectral region with $\lambda_{abs}^{(2)}$ at ~660 nm, a low energy shoulder at 702 nm, and preresonance enhancement

at shorter wavelengths. The δ values reported here are substantially lower than those from Prasad and coworkers[25] who report of a poly(2,5-dialkoxy-*p*-phenylene ethynylene) derivative with $\delta = 196 \times 10^{-48}$ $cm^4 \cdot s$ or 19,600 GM at 810 nm determined via nonlinear transmission (NLT) methods [62] using ~7 ns laser pulses. It has been shown that, under certain conditions, direct measurements such as NLT are not specific for 2PA and can contain contributions from higher order absorption and scattering processes which can occur at the high input intensities required for the measurement [16, 63, 64]. Additionally, δ values determined by using NLT methods have been known to significantly vary with laser pulse duration where substantially larger δ values are obtained with longer laser pulses, primarily as a result of 2PA-ESA, which leads to a larger excited state population [16, 65]. Polymer **3** shows sizeable ESA at 810 nm (*vide infra*); therefore, we attribute the aforementioned δ values to be an overestimation due to 2PA-ESA, and suggest our δ values are a more accurate representation of the nonlinear absorption properties of dialkyl-substituted *p*-PPE polymers. Furthermore, we have demonstrated a quadratic dependence of the output fluorescence intensity of **1**-**5** on the input laser power, which verified that the δ values we report are solely due to 2PA (see Figure 3.7).

Considerable changes in both band positions and δ values were observed when comparing the 2PA spectra of the distyryl-substituted PPE co-polymers to that of the linear models. The 2PA band shape of **4** and **5** are quite similar and are characterized by preresonance enhancement at shorter wavelengths along with a prominent transition at ~710 nm and ~748 nm, respectively, followed by a lower energy shoulder. Both co-polymers display an overall red-shift of 2PA band position with respect to the linear

analogues, resulting in sizable 2PA in the near-IR spectral region. Specifically, **4** and **5** show red shifts in 2PA band-edge position of ~30 nm and ~150 nm, respectively, compared to polymer **3**. Similar to what was discussed in the previous section, multiple states appear to contribute to the 2PA of co-polymers **4** and **5**. For example, the 2PA of **4** shows features at 570 nm and 650 nm that coincide with the $\lambda_{abs}^{(2)}$ of **1** and **3**, respectively. The PPE-dominated transition at 650 nm is also observed for **5** along with a $\lambda_{abs}^{(2)}$ that is slightly red-shifted (~30 nm) from that of **2**. The interpretation of these findings will be discussed later (see section 3.4).

A considerable increase in δ values was observed when comparing the PPE polymer to those with conjugated side chains. Co-polymers **4** and **5** show δ_{max} values that are 2- and 3-fold larger than that of **3**, respectively. An increase in δ_{max} was also observed when comparing **4** to **1**; however, a slight decrease in δ_{max} was observed in **5** in comparison to **2**. This is likely due to the slight reduction in the ground to lowest excited state transition dipole moment in the co-polymer compared to **2** (10.9 D vs 11.4 D).

3.3.5. Excited-state absorption and transient kinetics

In order to determine the strength of the ESA and dynamics of the PPE co-polymers, transient absorption (TA) spectroscopy was performed following excitation into the lowest lying one-photon allowed state of all molecules and polymers considered in this study. Representative TA spectra and kinetics of **1**-**5** obtained via femtosecond excitation are displayed in Figure 3.8 and Figure 3.10, with relevant kinetic information displayed in Figure 3.9.

As shown in Figure 3.8, the DSB model compounds, **1** and **2**, show similar TA features, including ground-state bleaching (GSB) along with negative ΔOD signals to the

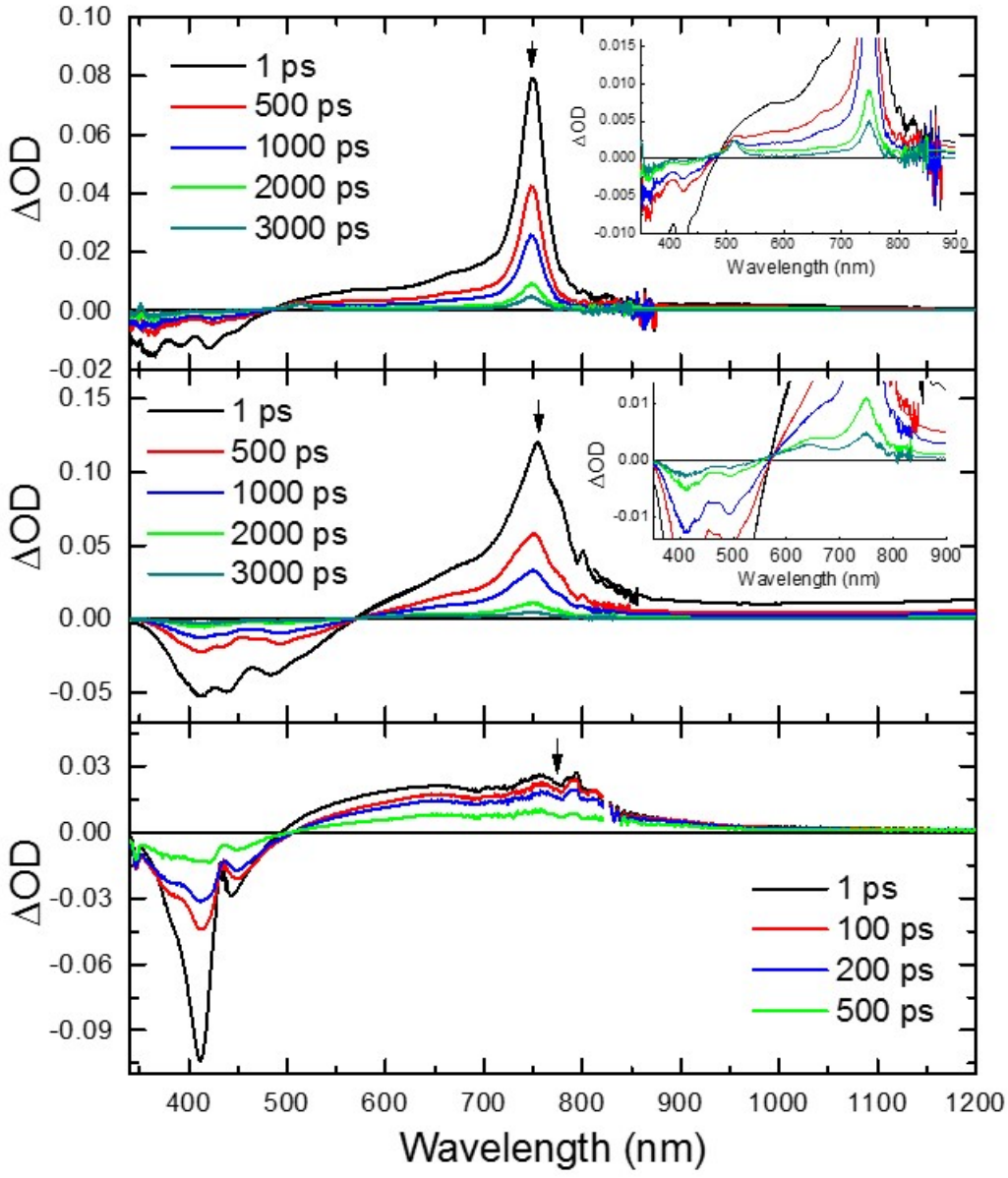

Figure 3.8. Femtosecond TA spectra of the linear model compounds and polymer in toluene: **1** (top plot), **2** (middle plot), and **3** (bottom plot) at various time delays. Inset: femtosecond TA of **1** (top) and **2** (middle). Excitation wavelengths were 350 nm, 380 nm, and 350 nm for **1**, **2**, and **3**, respectively.All samples were prepared at concentrations of 10^{-5} M and were excited with pulse energies of ~600 nJ/pulse.

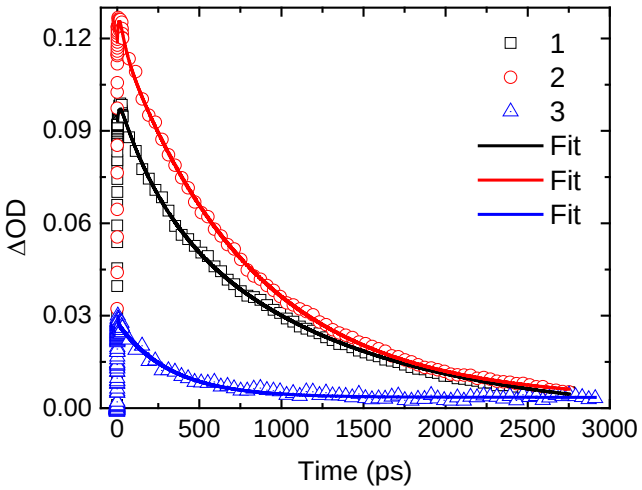

Figure 3.9. Representative femtosecond TA kinetic traces of **1**, **2**, and **3** at 750 nm overlaid with exponential fits. All samples were prepared at concentrations of 10^{-5} M and were excited with pulse energies of ~600 nJ/pulse. Excitation wavelengths were 350 nm, 380 nm, and 350 nm for **1**, **2**, and **3**, respectively.

red of the one-photon absorption band due to stimulated emission (SE). The TA spectra above 500 nm and 560 nm for **1** and **2**, respectively, can be assigned to excited-state absorption (ESA), and is structured with a well-defined peak at ~750 nm attributed to singlet-singlet ESA. The singlet ESA kinetic traces of the DSB chromophores are depicted in Figure 3.9 and well reproduced by a triexponential function with a risetime of ~9 ps for an intermediate species, followed by short and long-lived decay components of 260 ps and 1200 ps for **1**, and 22 ps and 800 ps for **2**. These time decays are consistent with those previously reported for unsubstituted trans,trans-distyrylbenzene where the multi- exponential decays were attributed to processes involving photoisomerization and emission [66, 67]. After the decay of the singlet species, a long-lived ESA band identified as a triplet-triplet ESA [56, 68] appears at 510 nm and 640 nm for **1** and **2**, respectively (see insets of Figure 3.8). This triplet-triplet ESA is very weak and shows a small yield of

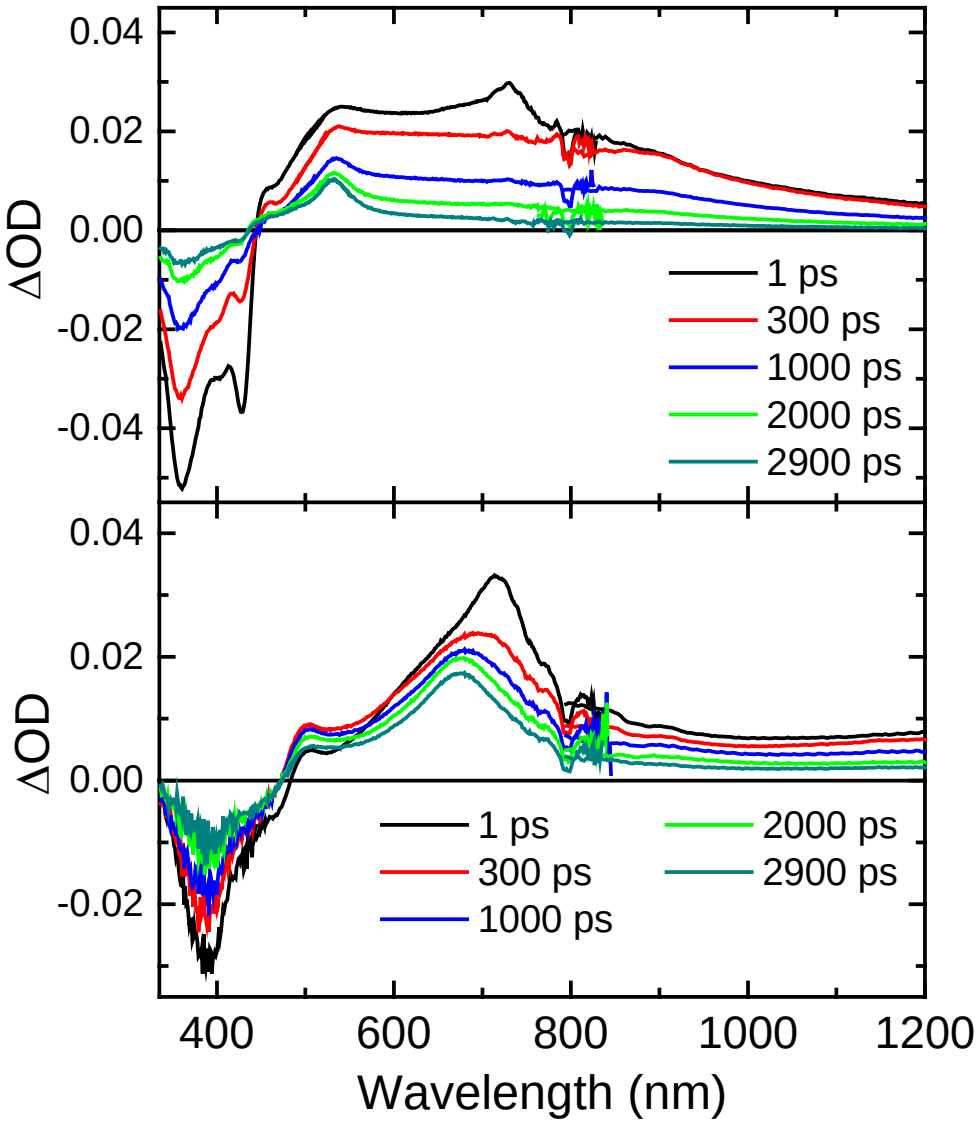

Figure 3.10. Femtosecond TA spectra of the PPE co-polymers at various probe delays: **4** (top plot) and **5** (bottom plot). All samples were prepared at concentrations of 10^{-5} M and were excited with pulse energies of ~600 nJ/pulse. Excitation wavelengths were 350 nm.

~4% and ~7% for **1** and **2**, respectively, which is expected given the high fluorescence yield of the DSB chromophores.[iii]

In contrast to the DSB molecules, the TA of **3** shows a broad and structureless ESA band, with absorption extending from the visible to the near IR region. Time profiles of **3** displayed in Figure 3.9 reveal a biexponential decay with a fast component of ~4 ps, and a slower component with a time decay of ~350 ps. These time constants agree with the biphasic decays reported for phenylene ethynylene oligomers [55], with the shorter component (t < 50 ps) attributed to initial structural relaxation of the S_1 state from a non-planar configuration to its preferred planar geometry, and the longer component corresponding to the decay of the relaxed S_1 state.

The TA of **4** and **5** depicts a combination of features from both the DSB molecules and PPE polymer. As shown in Figure 3.10, **4** shows broad ESA, similar to the PPE polymer, extending from the visible and near IR spectral region; however, like its DSB analogue, **1**, the co-polymer exhibits a structured absorption profile with a singlet-singlet ESA band that peaks at 730 nm and a long-lived ESA band that peaks at 530 nm. The ESA of **5** is also broad, but strongly resembles the DSB analogue, **2,** showing a slightly blue-shifted singlet-singlet ESA band peaking at 720 nm that overlaps with a long-lived ESA band peaking at 680 nm. The long-lived components of **4** and **5** which show absorption at time delays > 2.5 ns after the pump pulse that can be attributed to either long-lived singlet-singlet ESA or triplet-triplet ESA.

[iii] Triplet yields for **1**-**2** and **4**-**5** were estimated to be the quotient of the infinite component (y_0) and the sum of all amplitudes obtained from the exponential fit of the ground-state recovery: $yield^{Triplet} = y_0/(y_0 + \sum_{i=1}^{n} A_i)$, where y_0 and A_i were determined from $\Delta OD = y_0 + A_1 e^{-t-t_0/\tau_1} + A_2 e^{-t-t_0/\tau_2} + \cdots + A_n e^{-t-t_0/\tau_n}$.

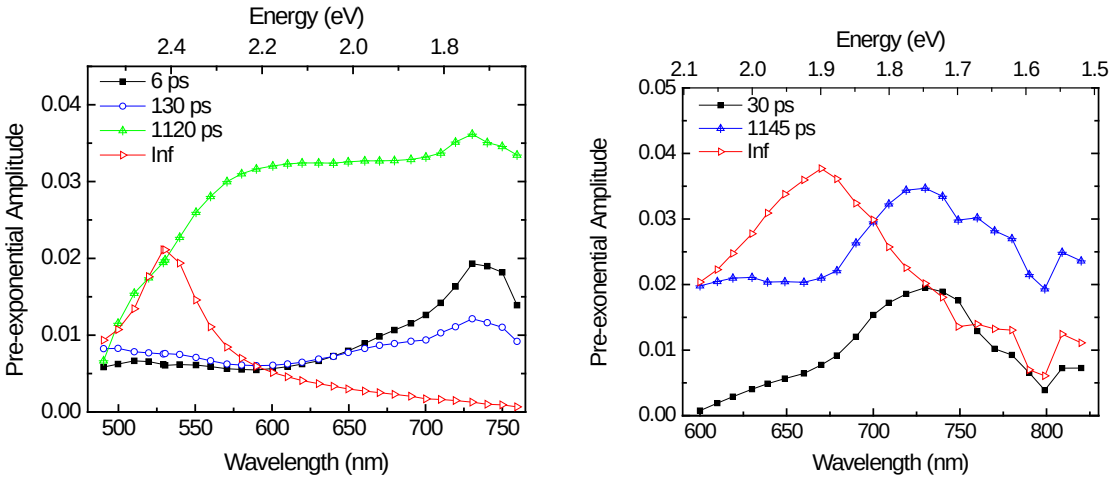

Figure 3.11. Global spectral analysis of **4** (left plot) and **5** (right plot) excited at 350 nm in toluene. Errors associated with values were determined to be ±10%.

Time profiles of the femtosecond TA measurements of **4** and **5** show multi-exponential decays with a very long ("infinite") time component (y_0). Because of broad and overlapping TA features, time decays at individual wavelengths gave conflicting results, thus a global spectral analysis method[iv] was applied to the femtosecond time traces of polymers **4** and **5** to extract the spectrum corresponding to the components of the excited-state decay kinetics. The pre-exponential amplitudes of the time constants for **4** and **5** have been graphed as a function of wavelength and are shown in Figure 3.11.

It should be noted that different data analysis methods, such as multivariate curve resolution [69], can be used to extract the TA spectra and the relative concentrations of individual excited state components. Multiexponential curve fitting techniques, such as

[iv] The transient data of **4** and **5** were analyzed using by global nonlinear regression (global fitting) of multiple wavelengths with the following multiexponential function: $\Delta OD = y_0 + A_1 e^{-t-t_0/\tau_1} + A_2 e^{-t-t_0/\tau_2} + \cdots + A_n e^{-t-t_0/\tau_n}$, where y_0 is the y-offset, t_0 is the x-offset or time-offset with respect to the pump/pulse temporal overlap, A is the pre-exponential amplitude of a transient species with lifetime of τ. For TA with femtosecond laser pulse excitation, y_0 is associated with an infinite component attributed to a long-lived singlet and/or triplet species that is considered infinite in the femtosecond timescale.

those employed for global fitting analysis, suffer from issues of uniqueness associated with covariance. However, as will be discussed below, the long-lived time decays (~1 ns) of **4** and **5** determined via global fitting methods correlate well with the τ_{Fl} values of the co-polymers (see Table 3.2). Additionally, the spectral position and band-shape of the infinite component of **4** and **5** agree with the ESA spectra of the co-polymers obtained via nanosecond TA (*vide infra*). For this reason, we consider the global analysis method utilized here reasonable representation of the numerous excited state components in these conjugated systems.

Both polymers show an ultra-fast component (t < 50 ps) that is ascribed to structural relaxation due to planarization. **4** shows an additional short-lived component of 130 ps, similar to the first relaxation time constant of **1**. Both **4** and **5** show a strong component with a relatively long decay time of ~1100 ps that is on the order of their fluorescence lifetime (see Table 3.2); however, the shape of the long-lived component differs between the two polymers. As shown in Figure 3.11a, the long-lived component of **4** is the dominant decay component in the dynamics of the polymer. The spectrum is also structureless similar to the ESA band seen in **3**. The long-lived component (~1100 ps) in **5** is also strong, but is of smaller amplitude than the infinite component (y_0). The infinite component of **5** also shows a structured band with a well defined peak that can be attributed to the ESA of DSB side chains. The fitting results from the global analysis suggests that both the DSB and PPE units of **4** and **5** strongly contribute to the S_1-S_n transition of the co-polymer, providing information on the degree of mixing between the excited states of the substituted polymers.

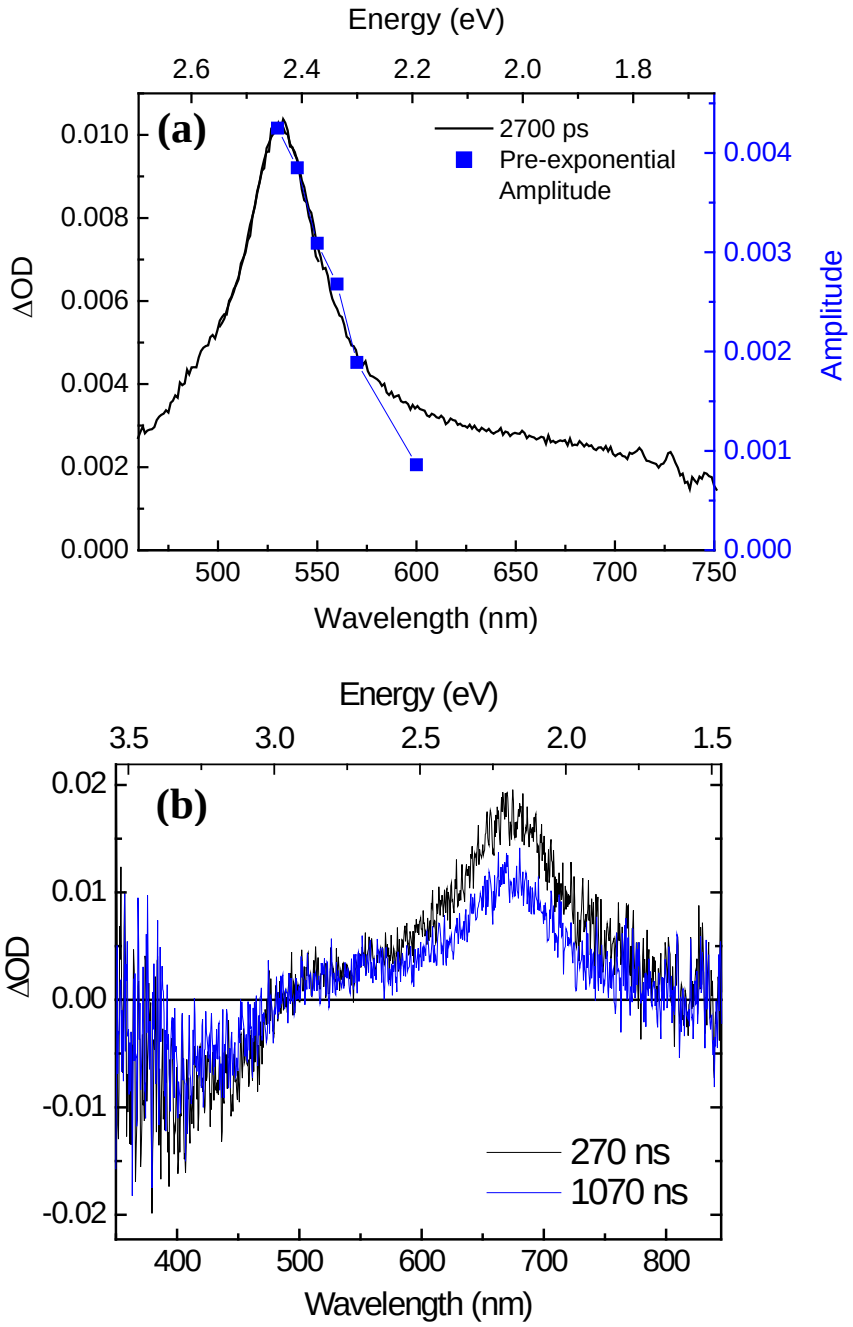

Figure 3.12. TA measurements **4** (a) and **5** (b) with nanosecond pulses in toluene at concentrations of 10^{-5} M: (a) global fitting of the decay kinetics of **4** at various wavelengths overlaid with the femotosecond TA spectra at a time delay of 2700 ps obtained from Figure 3.10; (b) ns-TA spectra of **5** at various probe delays. The excitation wavelengths were 355 nm and 465 nm for **4** and **5**, respectively. Samples were excited with a pump energy of ~200 nJ/pulse.

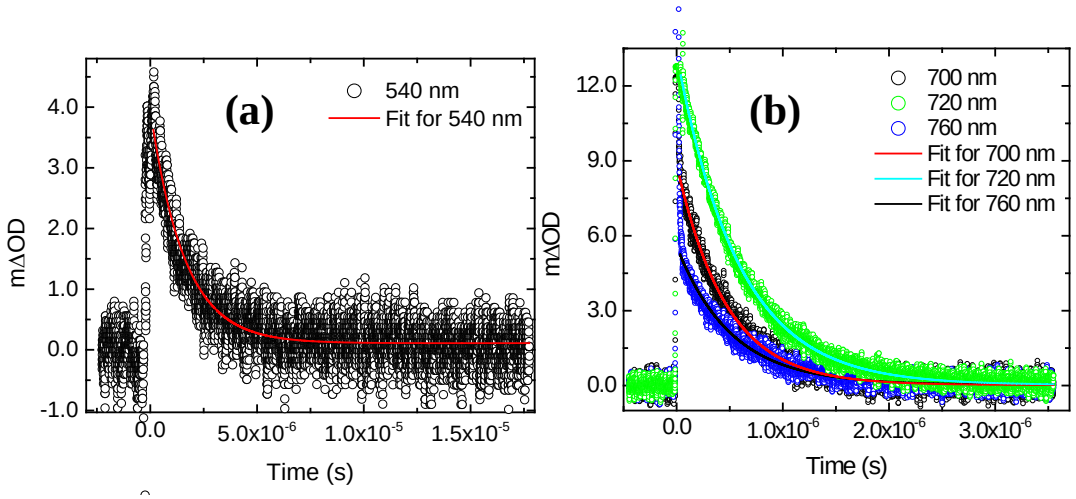

Figure 3.13. Nanosecond TA decay kinetics of the triplet state of **4** (a) and **5** (b) obtained in deoxygenated toluene solutions at concentrations of 10^{-5} M. The excitation wavelengths were 355 nm and 465 nm for **4** and **5**, respectively. Samples were excited with a pump energy of ~200 nJ/pulse.

Nanosecond transient absorption was utilized to determine the lifetime of the infinite component from the ultrafast species for **4** and **5**. Because of the relatively low yields of the long-lived excited-state species of **4** and the strong SE in the visible spectral region, the ESA of **4** were not obtained via nanosecond TA. Kinetic traces of **4** were, however, obtained and global fitting was utilized to correlate the excited-state species observed in nanosecond TA to the infinite component observed in femtosecond TA. The ESA spectra obtained for **5** also overlays well with the infinite components from the femtosecond TA. The relative ESA spectra and kinetics are displayed in Figure 3.12 and Figure 3. 13

The exited-state species observed via nanosecond TA for both **4** and **5** were assigned to the triplet state of these co-polymers, based on the oxygen quenching of this

component.[v] Nanosecond transient kinetic traces in the triplet-triplet absorption spectral region show monoexponential decays of 2 μs and 540 ns for **4** and **5**, respectively (see Figure 3. 13). Triplet yields of **4** and **5** were determined to be 8% and 28%, respectively,[iii] and are significantly higher than those of both the DSB analogues and alkyl-substituted PPEs (~0.10) [70]. Although triplet excitons in PPE-derivatives have been previously identified, they are not easily formed by direct photoexcitation and generally require extreme conditions such as pulse radiolysis [71], low temperatures in viscous hosts or solvents [72], or an addition of a metal to the molecule to increase the rate of intersystem crossing and triplet yield [73, 74]. In contrast, the triplet excitons of **4** and **5** were easily generated under ambient temperature conditions and in nonviscous solvents, demonstrating an increase of intersystem crossing (ISC) brought upon by the substitution of the distyryl units. This is consistent with work from Curtis [75] and Kasha [76] in their study of luminescence in molecular aggregates where they reported on the enhancement of the triplet state formation followed by fluorescence quenching due to high efficiency triplet excitation in dimers.

3.3.6. Concentration dependent excited-state measurements

Concentration-dependent femtosecond TA measurements were performed in order to investigate aggregation effects on the ESA and transient dynamics of **3**-**5**. TA measurements for each polymer were performed in toluene at a concentration of 1 mM. As shown in Figure 3.14, the principal TA features of **3**-**5** are preserved at relatively high concentrations, with the exception of ISP which shows slight broadening of the ESA

[v] Nanosecond TA measurements were conducted in both oxygenated and deoxygenated solvent environments. A significant quenching of the absorption and lifetime of the excited-state species by singlet oxygen was observed, verifying the presence of a triplet species.

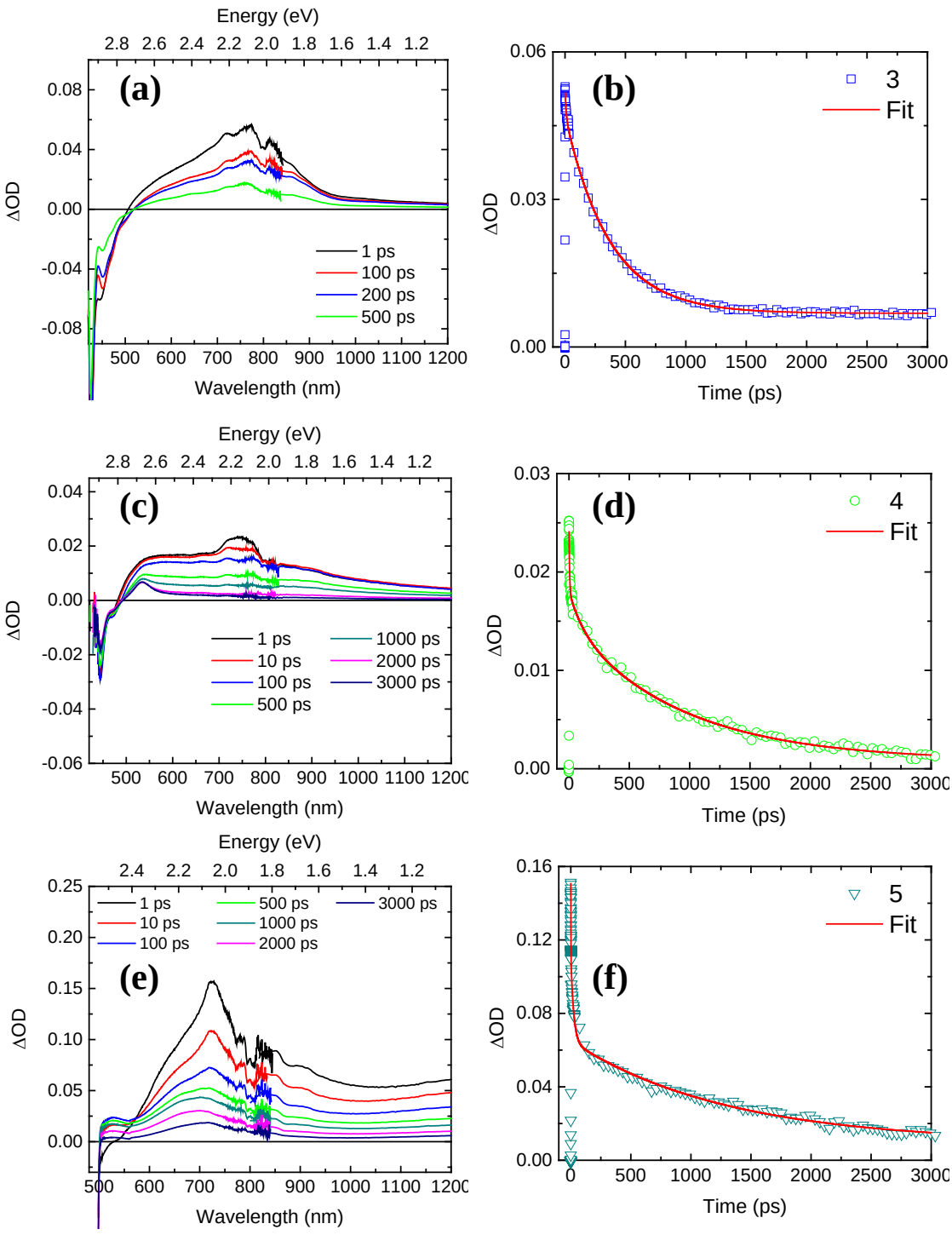

Figure 3.14. Femtosecond TA spectra and decay kinetics of concentrated solutions of **3** (a and b), **4** (c and d), and **5** (e and f). Excitation wavelengths were 350 nm for **3** and **4** and 480 for **5**. Samples were prepared in $CHCl_3$ at 1 mM and were excited with a pump energy of ~600 nJ/pulse.

band maxima at ~750 nm. The time profiles of all of the polymers show decay kinetics that are similar to those observed at lower concentrations. The behavior of **3-5** at 1 mM suggests that the substitution of the polymers strongly hinders π- π interactions in the ground state and, subsequently, excimer formation in the excited state. This is extremely important for the use of these crucifrom-like polymers in nonlinear applications that require a high concentrations of chromophores. Excimer formation can provide additional nonradiative decay channels that may, in turn, lead to significant quenching of excited state species.

3.3.7. Wavelength-dependent optical limiting studies of PPE co-polymers

Co-polymers **4** and **5** exhibit 2PA bands with relatively large δ values that overlap with their singlet-singlet and triplet-triplet ESA bands, indicating their potential as optical power limiters via two-photon processes. To determine the optical limiting capabilities of these distyryl-substituted polymers, experiments were performed using femtosecond- and nanosecond- pulsed excitation on solutions at various wavelengths covering the visible and near-IR spectral region. The results are shown in Figure 3.15.

Both **4** and **5** show high transparencies (>65%) for all wavelengths considered, which is a desirable characteristic for an optical limiting material. The energy-dependent transmittance curves of **4** observed in the ns-pulse regime (Figure 3.15b) are characterized by a high turn-on energy and a subsequent steep reduction of the transmittance. Such energy-dependent curves are indicative of a limiting mechanism involving 2PA-ESA, which is expected given the high linear transmittance (T_{Lin}) of **4** in across the visible and near-IR spectral region (>94%). **5** shows lower T_{Lin} values in the ns-pulse OPL measurements compared to **4**, resulting in energy-dependent transmittance

curves with a more gradual reduction of transmittance prior to the steep reduction, suggesting a 1PA-ESA contribution to the limiting mechanism. A gradual reduction of the transmittance of **5** is also observed in fs-pulse regime (see Figure 3.15c); however, especially in the case of **5** at 680 nm, the response is closely correlated to that of the solvent ($CHCl_3$).

We can compare the OPL performance of the co-polymers by quantifying the nonlinear response in terms of the energy threshold (E_{Th}) value and optical pulse suppression figure-of-merit (FOM) given by the following equations:

$$E_{Th} = \frac{T_{Lin}}{2} \quad \text{(Eq 3.3)}$$

$$FOM = \frac{T_{Lin}}{T_F} \quad \text{(Eq 3.4)}$$

where FOM of the OPL performance is defined by the ratio of the linear transmittance and the final transmittance (T_F). The E_{Th} and FOM values for **4** and **5** are displayed in Table 3.4 and Table 3.5. The onset of attenuation due to NLA begins at lower energies for co-polymer **4** in comparison to **5** in both the fs- and ns-time regime. For example, **4** shows an E_{Th} as low as ~140 nJ for fs pulses and ~57 μJ and ns pulses at 532 nm. Wavelength-dependent OPL studies of **4** show that the E_{Th} and FOM values with the δ of the co-polymer in both the fs- and ns-pulse regimes, further suggesting that the limiting mechanism is 2PA-ESA regardless of the length of the laser pulse. The E_{Th} of **5** also scales with δ; however, similar FOM values were determined over the wavelengths considered. Although the suppression values determined for **4** and **5** are lower than that those reported from other conjugated polymers in similar spectral regimes [18, 77] , it should be noted that the co-polymer concentration was relatively low (1 mM) due to the

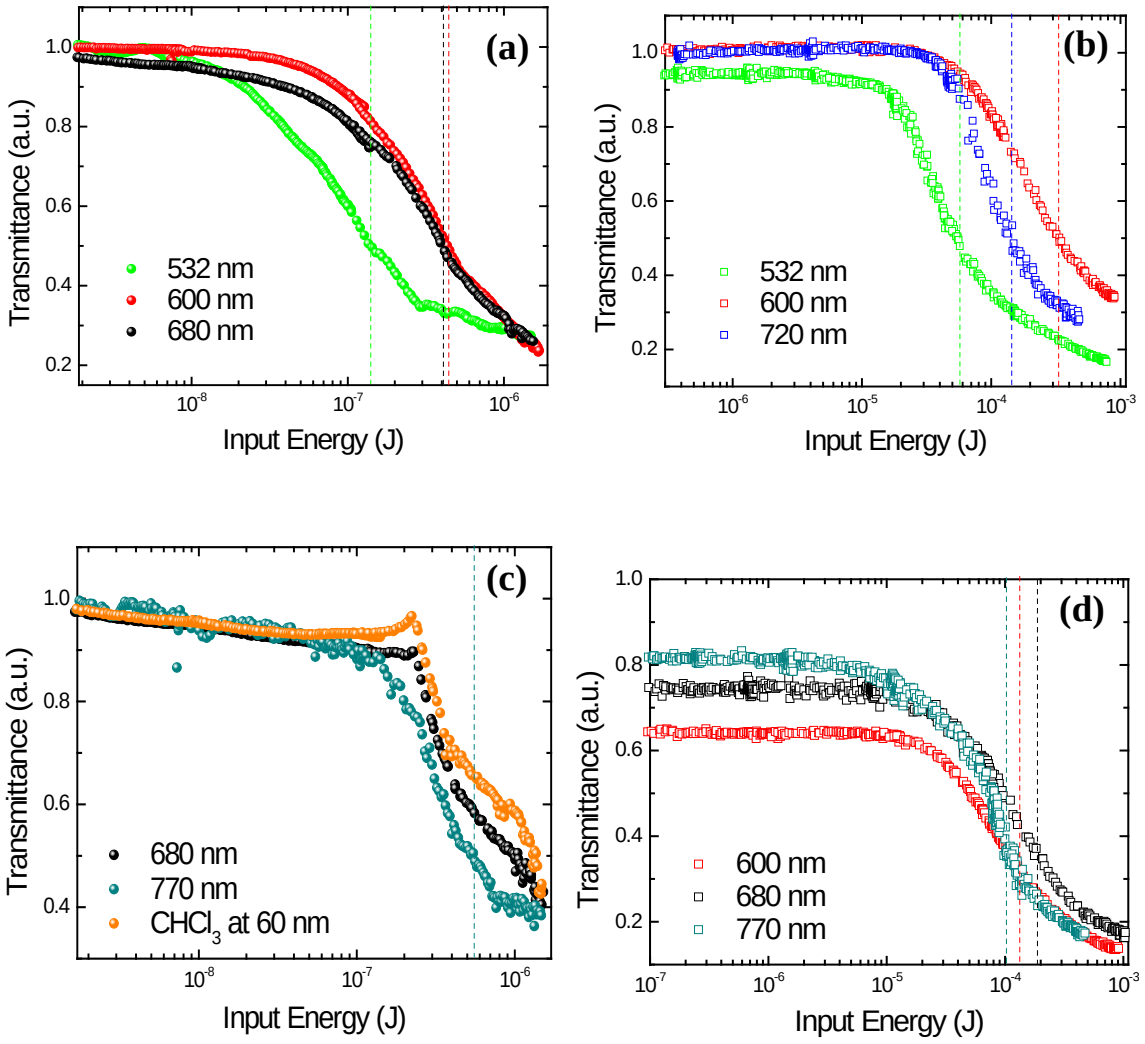

Figure 3.15. Broadband optical limiting of PPE co-polymers in solution: (a) fs- and (b) ns-pulsed optical liming on solutions of **4**; (c) fs- and (d) ns-pulsed optical limiting on solutions of **5**. The OPL response of $CHCl_3$ is also shown. Dotted lines depicting the E_{Th} for each wavelength are overlaid with the energy dependent transmission curves for comparison purposes. All sample solutions were degassed and were prepared in $CHCl_3$ at concentrations of 1 mM. Fs-pulsed measurements were conducted in 1 mm cells and ns-pulsed measurements were conducted in 1 cm cells while stirring continuously. Experimental parameters are given in the Experimental Methods section.

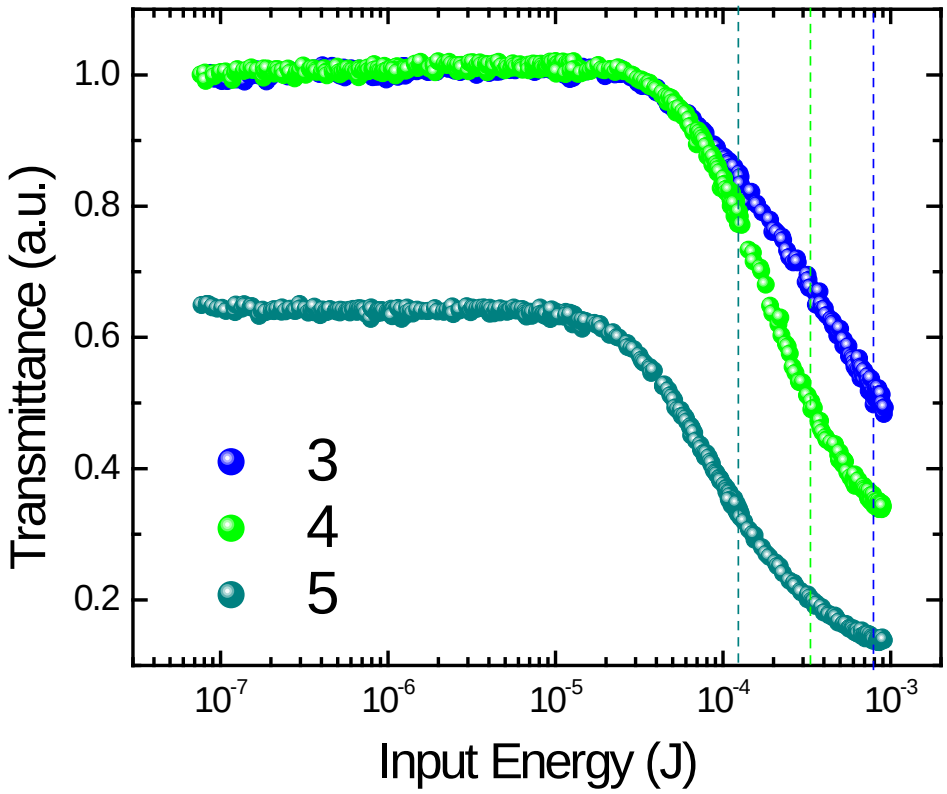

Figure 3.16. Energy-dependent transmittance curves for ns-pulse OPL measurements of PPE polymer solutions (**3**-**5**) at 600 nm**.** Degassed polymer solutions were prepared in $CHCl_3$ at a concentration of 1 mM. Measurements were conducted in a 1 cm pathlength cell while stirring continuously.

Table 3.4. Energy threshold (E_{Th}) values for wavelength-dependent optical limiting studies on solutions of **4** and **5**

	532 nm		**600 nm**		**680 nm**		**720 nm**		**770 nm**	
	fs	ns	fs	ns	fs	ns	fs	ns	fs	ns
4[a]	1.43×10^{-7}	5.71×10^{-5}	4.33×10^{-7}	3.36×10^{-4}	4.49×10^{-7}	---	---	1.45×10^{-4}	---	---
5[a]	---	---	---	1.34×10^{-4}	solvent response[b]	1.83×10^{-4}	---	---	5.60×10^{-7}	1.02×10^{-4}

[a]All E_{Th} values are measured in Joules (J). [b] The energy-dependent curves obtained from **5** at 680 nm with fs-pulsed excitation were very similar to the solvent ($CHCl_3$) response.

Table 3.5. Figure-of-merit (*FOM*) values for wavelength-dependent optical limiting studies on solutions of **4** and **5**

	532 nm		**600 nm**		**680 nm**		**720 nm**		**770 nm**	
	fs	ns	fs	ns	fs	ns	fs	ns	fs	ns
4[a]	3.7	5.7	4.3	2.9	3.8	---	---	3.5	---	---
5[a]	---	---	---	4.7	solvent response[a]	4.3	---	---	2.6	4.7

[a] The energy-dependent curves obtained from **5** at 680 nm with fs-pulsed excitation were very similar to the solvent ($CHCl_3$) response.

limited solubility of **5**. Co-polymer **4**, however, shows relatively high solubility (>50 mM) in organic solvents and, as δ is proportional to dye concentration, is expected to exhibit larger suppression values.

The OPL performances of the distyryl-substituted co-polymers were also compared to that of the dioctyl *p*-PPE polymer (**3**) and are displayed in Figure 3.16. **3** exhibits a high E_{Th} value of ~800 μJ, which is ~2 and ~6 times higher than that of **4** and **5**, respectively. Stark contrasts are also observed in *FOM* values. Polymer **3** shows a *FOM* of 2.0, which is considerably less than that of the distyryl-substituted co-polymers (see Table 3.5). The determined for **3** compares well to that of the alkoxy-substituted PPE derivative reported by Prasad and coworkers (*FOM* = 3.3 at concentration per repeat unit of 30 mM) [25]. As the T_{Lin} of **3** is ~1, the limiting in the PPE polymer is attributed to 2PA-ESA. Therefore, it follows that the OPL performance of **3** does not compare favorably with that of **4** and **5,** given the differences in δ among the polymers.

3.4. Comparison of spectral features and electronic coupling observed in cruciform-like PPE co-polymer to that of cruciform small molecules

As discussed above, the photophysical behavior of the cruciform-like PPE polymers give rise to interesting changes in 1PA, 2PA, and ESA characteristics with respect to the linear model compounds. We will also discuss the differences of the PPE co-polymers compared to the cruciform analogues. Specifically, we will compare the 1PA and 2PA behavior of the polymers to the spectral properties that have been reported for small molecule analogs. We will also discuss the degree of electronic coupling within the polymer, and how the coupling of the conjugated side-arms to the polymer main chain compares to the coupling experienced in cruciform molecules.

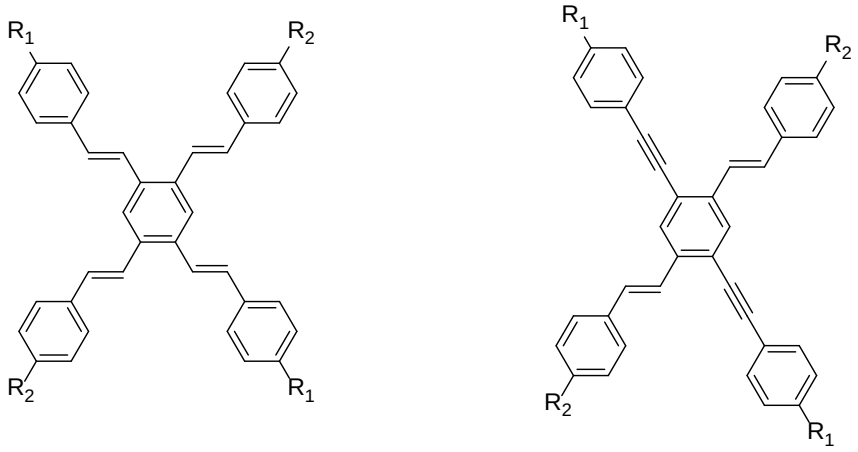

6a: R_1=NEt_2; R_2=NEt_2
6b: R_1=NEt_2; R_2=NO_2

7a: R_1=H; R2=$CH(CH3)_2$
7b: R_1=H; R_2=NBu_2

Figure 3.17. Molecular structures of linear and cross-shaped chromophores reported in the literature and used as examples for comparisons in the present work. Molecule **6** was reported in Pond et. al. [26]. Compound **7** was reported in Siegel [77].

The molecular structures of the cruciforms reported in the literature that are being considered in this discussion are shown in Figure 3.17. All molecules show a two-dimensional architecture and can be described as possessing two linear units that are joined together through a central phenylene ring. While many other cruciform structures exist, we consider the compounds displayed in Figure 3.17 to be the most relevant for an accurate comparison to the PPE co-polymers considered in this study.

3.4.1. Comparison of 1PA and 2PA properties

Similar to co-polymers **4** and **5**, the 1PA spectra of each four-branch chromophore is significantly different from that of the corresponding linear molecules. In general, the high-energy absorption band is blue-shifted with respect to the linear models, or in the case of the

non-centrosymmetric cruciforms, the linear model possessing the higher energy absorption band. An additional band or weak shoulder appears on the low energy side of the 1PA spectra of the cruciforms with tails that extend beyond that of the linear model or lower-energy linear model. This is most clear in the 1PA of **6b** and **7a** depicted in Figure 3.18 and Figure 3.19, respectively. The significant splitting of the 1PA band of **6b** and **7a** contrasts to the modest spectral changes observed in the 1PA of the co-polymers. Whereas both co- polymers show a red-shift in the 1PA tail, the blue-shift of the higher-energy band was small (<100 cm^{-1}) and only observed in **4**.

The cruciform-like PPE co-polymers also show differences in 2PA relative to their small molecules cruciform analogues. While the 2PA of the centrosymmetric cruciform, **6a**, and the noncentrosymmetric, **7a**, are quite similar to their linear models, significant changes are observed when comparing the donor/acceptor-substituted noncentrosymmetric cruciforms to their linear analogues. For example, **6b** shows increased 2PA in the near-IR with a band maximum ($\lambda_{abs}^{(2)}$ = 830 nm) that does not appear to be closely related to the $\lambda_{abs}^{(2)}$ of ether **2** or **Ph-2A** ($\lambda_{abs}^{(2)}$ of **2** = 718 nm and $\lambda_{abs}^{(2)}$ of **Ph-2A**= 740 nm). Furthermore, **7b** exhibits two 2PA bands: a prominent peak at 770 nm and a secondary band with a local maximum in the near-IR spectral region at ~950 nm which is beyond the 2PA region of both model compounds. The similarities in the 2PA band structure of **6b** and **7b** suggests that interactions between the donor and acceptor units governs the 2PA character of these noncentrosymmetric cruciforms. Indeed, Siegel demonstrated that in the case of phenylene vinylene / phenylene ethynylene based cruciforms with D/A groups, the $\lambda_{abs}^{(2)}$ overlaps with the CT band determined by a Franck Condon fitting of the absorption spectra [78].

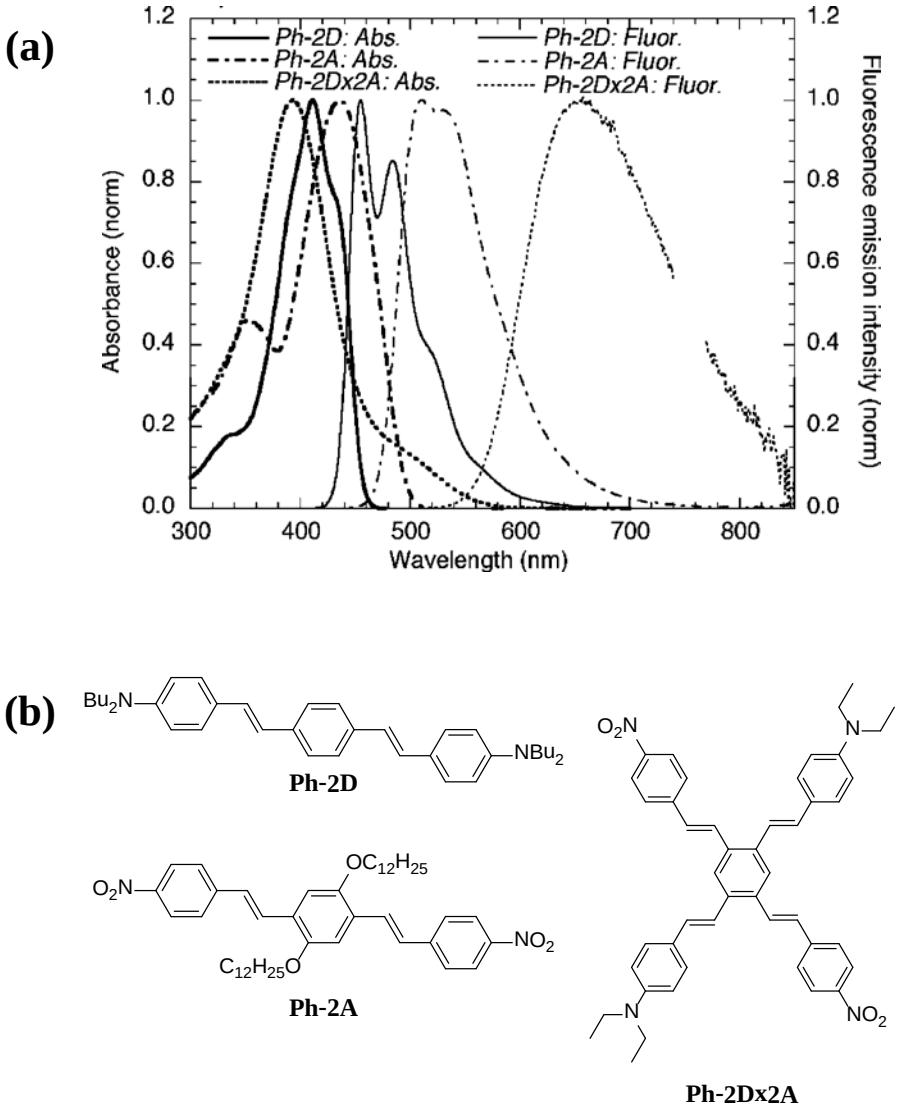

Figure 3.18. Normalized 1PA and emission spectra (a) and molecular structures of chromophores (b) from Rumi et. al. The molecules **Ph-2D** and **Ph-2Dx2A** in Rumi et. al. are referred to as **2** and **6b**, respectively, in this work. Reprinted with permission from Mariacristina Rumi; Stephanie J. K. Pond; Timo Meyer-Friedrichsen; Qing Zhang; Maximilienne Bishop; Yadong Zhang; Stephen Barlow; Seth R. Marder; Joseph W. Perry; J. Phys. Chem. C 2008, 112, 8061-8071. DOI: 10.1021/jp710682z. Copyright © 2008 American Chemical Society.

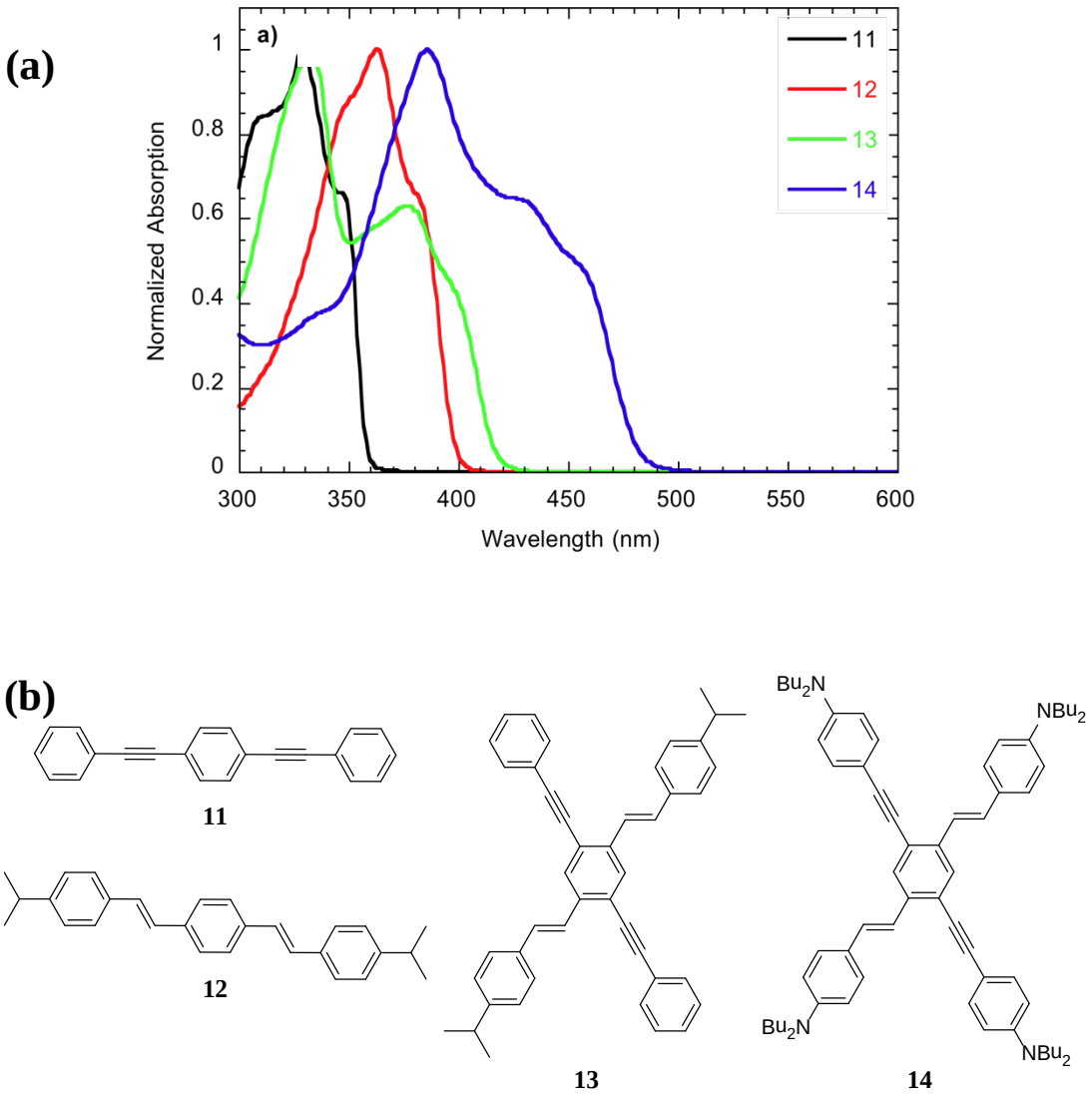

Figure 3.19. Normalized 1PA (a) ad molecular structures of chromophores (b) from Siegel. The molecules **12** and **13** in Siegel is referred to as **1** and **7a**, respectively, in this work. Reprinted with permission from Siegel, N.N., *Two-photon absorption in cruciform and dipolar chromophores: excitonic interactions and response to metal ions.* Ph.D. Thesis, The Georgia Institute of Technology, August 2010. Copyright © 2010 Georgia Institute of Technology.

In comparison to the two distinct 2PA bands observed from **6b** and **7b**, **4** and **5** show 2PA with maxima that overlap with the $\lambda_{abs}^{(2)}$ of the PPE polymer and the respective DSB molecules. Additionally, as opposed to the weak secondary 2PA transition in the near-IR observed from **6b** and **7b**, the prominent 2PA band of **4** and **5** is broadened and extends to regions of the spectra where nether **1**-**3** show 2PA. Based on earlier findings from Rumi et. al and Siegel, we can assume that the CT character in **4** and **5** plays a slight role in the 2PA properties they exhibit. This is particularly true for **5** which shows reasonable CT as evidenced by the positive solvatochromism observed in its emission. However, the overlap of the 2PA bands of **4** and **5** with that of their linear models would suggest the two-photon allowed states of the conjugated side-arms and the PPE main chain are not significantly coupled, and thus, are behaving independently.

The increase in δ and the bandwidth of the 2PA band may also be ascribed to the increase in molecular size of the co-polymers. Yang et. al attribute the increased 2PA observed in donor-acceptor substituted anthracene-centered cruciforms to the increased molecular size of the cruciform relative to the one-dimensional analogues [79]. As the effective conjugation length of

PPE polymers is ~9 repeat units, it is possible that the substitution may extend the size of π-conjugation substantially and provide more effective optical coupling between the ground and two-photon allowed states. This extended conjugation would increase the density of states and, in turn, increase the δ over a wider range of wavelengths [80, 81].

3.4.2. Exciton analysis of PPE co-polymers

To explain the spectral changes observed and to determine the degree of coupling between the conjugated polymer backbone and conjugated arms, we will utilize a

molecular exciton coupling model. According to molecular exciton theory, two molecules in close proximity (through intermolecular interaction or by virtue of covalent attachment) may interact through a coupling mechanism leading to a mixing of their excited-state wave functions [52]. This coupling results in both shifts and splittings of the electronic absorption bands of the resultant molecular aggregate or supramolecule. Perry and co-workers have previously shown that the molecular exciton model can be used to describe the degree of coupling between equivalent and nonequivalent oligo(phenylene vinylene) and phenylene vinylene / phenylene ethynylene chromophoric arms in cruciform oligomers [26, 78]. Because of the configuration of the repeat monomer units, this same approach will be used to rationalize the spectral properties observed for the substituted PPE co-polymers.

A derivation of the excited-state energies for a non-identical dimer as a function of the properties of its subunits is given in detail by Siegel [78]. The distyryl-substituted PPE co-polymers can be divided into two linear nondegenerate units connected through a central aromatic ring at angle α. For this reason we will consider the electronic states of the DSB analogues (**1** or **2**) and the dioctyl *p*-PPE polymer (**3**) to describe the resultant electronic properties of the substituted polymer. It is noted that dioctyl phenylene is not a monomer unit of co-polymers **4** and **5**. While the degree of electron donation may differ between ethylhexyl and octyl alkyl units, we assume that **3** provides an acceptable model for the coupling contribution expected from a dialkyl *p*-PPE to this particular cross geometry.

The ground state interaction between nondegenerate units *a* and *b* results in an energy shift of the aggregate ground state due to the van der Waals interaction term

(V_{gg}^{diag}). As described by Siegel [78], the lowest excited state energy of an aggregate composed of non-identical components can be written as

$$E_{\pm} = \frac{E_e^{(a)} + E_e^{(b)}}{2} + \frac{\sqrt{(E_{eg}^{(a)} - E_{eg}^{(b)} + \Delta V^{diag})^2 + 4V^2}}{2} \qquad \text{(Eq 3.5)}$$

where $E_{\pm}$ are the energies of the symmetric and antisymmetric combinations of the excited state wavefunctions, respectively, $E_e^{(a)}$ and $E_e^{(b)}$ are the excited state energies of units *a* and *b*, $E_{eg}^{(a)}$ and $E_{eg}^{(b)}$ are the one-photon ground to excited state ($g \rightarrow e$) transition energies of units *a* and *b*, $\Delta V^{diag} = V_{eg}^{diag} - V_{ge}^{diag}$ is the difference between the van der Waals interaction energy between unit *a* in the ground state and unit *b* in the excited state (V_{eg}^{diag}) and vice versa (V_{ge}^{diag}), and *V* is the coupling energy between the two units. A pictorial representation of Eq.3.5 and the relevant terms is depicted in Figure 3.20.

The excited-state, transition, and van der Waals energy terms for the PPE co-polymers can be deduced from the 1PA measurements, allowing for the experimental determination of *V* using the following equation:

$$V = \frac{\sqrt{(\Delta E_+^{(c)} - \Delta E_-^{(c)})^2 - (E_{eg}^{(DSB)} - E_{eg}^{(PPE)})^2}}{4} \qquad \text{(Eq 3.6)}$$

where $\Delta E_{\pm}^{(c)}$ are the 0-0 transition energies of the exciton-like transitions of the PPE co-polymers. The DSB molecules, **1** and **2**, and the dioctyl *p*-PPE polymer, **3,** has taken the place of units *a* and *b* from Eq. 3.5. The ΔV^{diag} has been neglected, which is a common assumption in such cases [82].

Because of the spectral overlap of DSB molecules and the PPE polymer main chain, it is difficult to obtain *V* directly from the 1PA of **4** and **5**. Therefore, an

approximate separation of the two linear components from the co-polymer 1PA spectrum was performed (see Figure 3.20). In the case of **4**, the c_+ band, which corresponds to the higher-energy component of the co-polymer, can be obtained by slightly shifting the 1PA of **1** (Spectrum I) to higher energy (Spectrum II), such that the peak position moves from 27,590 cm^{-1} to 27,860 cm^{-1}. As shown in Figure 3.20a, the high-energy side of this shifted spectrum is close to the actual 1PA spectrum of **4** (Spectrum III). A slight misalignment of Spectrum II and Spectrum III is observed between 30,000-33,000 cm^{-1}, which can be attributed to the high-energy absorption of the PPE polymer backbone. The c_- band (the lower-energy component of the co-polymer) is displayed as Spectrum IV and was obtained by subtracting Spectrum II from Spectrum III. Spectrum IV appears as a well-defined band peaking at $E_{-}^{(c)}$= 25,090 cm^{-1}. Using Eq. 3.6, the value of the coupling is then 1010 cm^{-1} or 0.12 eV.

The coupling of co-polymer **5** was determined in a similar fashion; however, because the PPE polymer is the higher energy unit, the 1PA of **3** was used. The coupling value of **5** was experimentally determined as 900 cm^{-1} or 0.11 eV. The coupling values for **4** and **5** are on the order of coupling energies calculated for noncentrosymmetric cruciform oligomers [78], suggesting similar electronic interactions occur within the repeating unit of the polymer despite the additional number of repeating units and extended conjugation length of the PPE polymer.

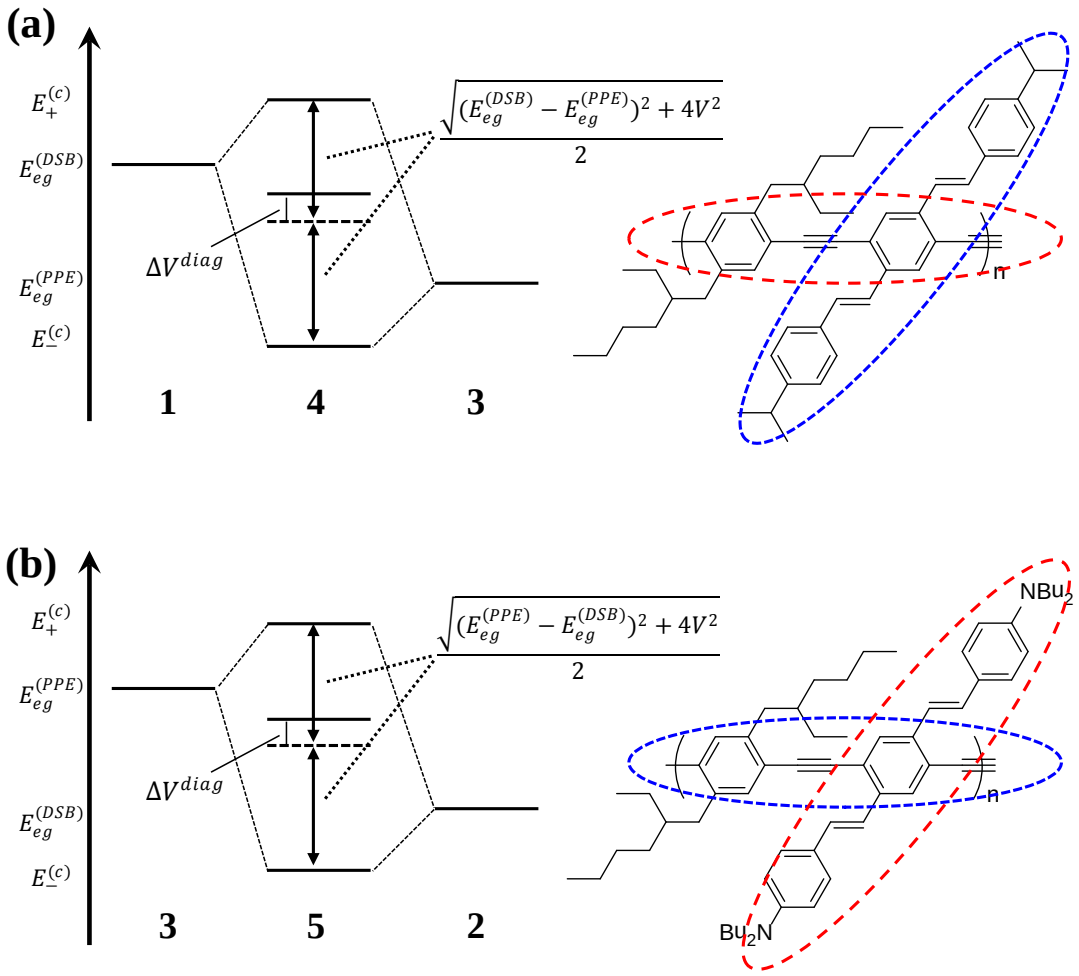

Figure 3.20. Energy level diagram and schematic representation of the linear subunits that join together to make the molecular orbitals of the cruciform-like PPE polymers, **4** (a) and **5** (b). Adapted with permission from Siegel, N.N., *Two-photon absorption in cruciform and dipolar chromophores: excitonic interactions and response to metal ions.* Ph.D. Thesis, The Georgia Institute of Technology, August 2010. Copyright © 2010 Georgia Institute of Technology.

(b)

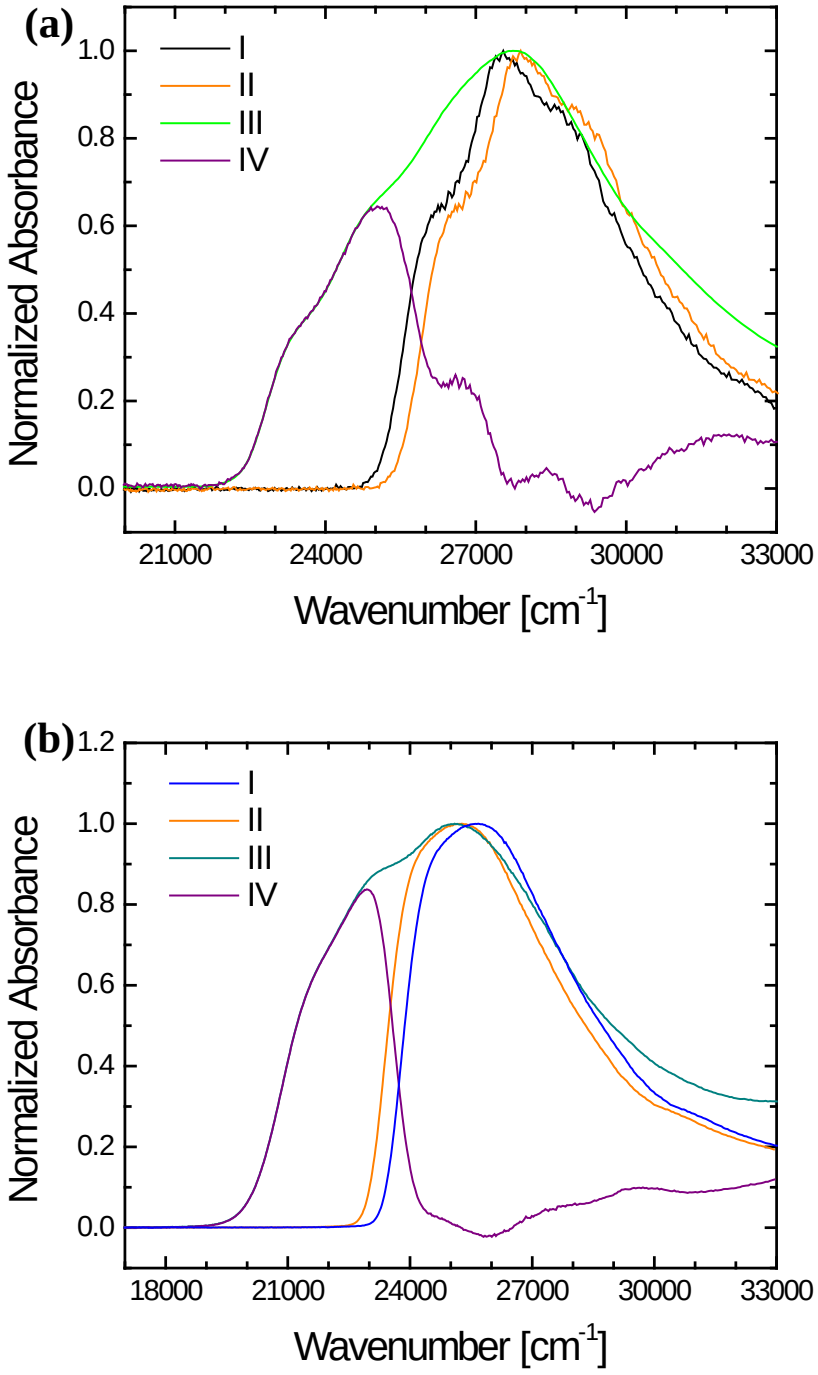

Figure 3.21. Linear absorption spectra of (a) **4** and (b) **5** depicting the approximate contributions of their respective linear units and excitonic band. I: spectrum of **1** (a) or **3**(b); II: spectrum of **1**(a) or **3** (b) shifted to match the high-energy side of the co-polymer; III: spectrum of **4** (a) or **5**(b); IV: difference between III and II.

3.5. Summary

In summary, two phenylene ethynylene-based co-polymers with conjugated side chains were characterized via linear and nonlinear spectroscopic methods. The cruciformic-like configuration of the PPE co-polymer with its substituted styryl arms greatly enhances the nonlinear response compared to that of the alkyl-substituted PPE polymer, increasing the 2PA band area and 2PA cross section values considerably. Furthermore, the slight exciton splitting of the lowest singlet state results in strong, broadband singlet-singlet and triplet-triplet ESA with contributions from both the DSB model and PPE polymer. Because of the coupling between the polymer chain with the conjugated side-arms, an enhancement of triplet formation is observed, relative to the linear models. The overlapping ESA and 2PA bands of the cruciform-like co-polymer give rise to effective OPL of both femtosecond and nanosecond pulses via 2PA-ESA. OPL measurements suggest NLA bandwidths as large as 250 nm, extending from the visible to the NIR region. A comparison study of the OPL performance of the cruciform-like PPE co-polymers to that of the linear PPE model reveals improved optical pulse suppression from the substituted polymers. Particularly for the donor-substituted cruciform-like PPE, the E_{Th} was reduced by 650 μJ and a 2.3-fold increase in FOM (relative to the octyl-substituted PPE) is reported.

The 1PA and 2PA behavior and the excitonic coupling of the electronic states of the cruciform co-polymers were also investigated and compared to that of small molecule cruciform analogues. The coupling energy between the conjugated side-arms and polymer backbone were found to be of similar value to small molecule cruciforms,

presenting an interesting synthetic route towards selectively altering the 1PA and 2PA properties of conjugated polymers for NLO applications.

3.6. Experimental Details

Materials. The synthesis of **1**-**5** were performed by the Uwe Bunz Research Group, formerly of the Georgia Institute of Technology. The syntheses of compounds **1** and **2** and polymers **3** and **5** have been reported previously [33, 35, 45, 83]. The synthesis of polymer **4**, 2,5-bis(4-isopropylstyryl)-1,4-phenylene-*co*-alkyne-*co*-1,4-bis(2-ethylhexyl)benzene-*co*-alkyne tetra-polymer, is described in elsewhere.[vi] Spectroscopic measurements were performed using toluene, chloroform, cyclohexane, methanol, and acetonitrile (spectrophotometric grade, Aldrich). Coumarin 307, Coumarin 485, 1,4-bis(2-methylstyryl)benzene, Fluorescein, and Rhodamine 590 (6G) dyes (Laser dye grade, Exciton) were used as reference compounds for quantum yield and 2PA cross section measurements.

Spectroscopic Measurements. UV-Vis. absorption spectra were measured with a UV-Vis-NIR scanning spectrophotometer (UV-3101PC, Shimadzu). Polymer concentrations in this paper are specified as the concentration per terpolymer repeating unit. Peak molar extinction coefficients (ε_{max}) per repeat unit were obtained from a linear regression analysis of absorbance versus the polymer concentration using the Beer-Lambert equation. A spectrofluorometer (Fluorolog-2, Spex) was used for the measurement of fluorescence spectra. To obtain fluorescence spectra, all polymers were

[vi] The synthesis and characterization details of **1**-**5** are included in *Distyryl substituted phenylene ethynylene polymers with broadband nonlinear absorption for optical power limiting in the visible and near infrared*, **Marshall, A. S.**, Sartin, M., Hales, J. M., Zappas, A. J., Zucchero, A. J., Bunz, U. W., and Perry, J. W. *In preparation.*

excited at their one-photon absorption maximum wavelength ($\lambda_{abs}^{(1)}$). All spectra have been corrected via subtraction of the scattering response from the solvent and the instrument's spectral response. Low concentration polymer solutions (10^{-6} M) were used for all steady-state fluorescence measurements to minimize inner filter effects. Fluorescence quantum yields (η) were determined using Coumarin 307 in acetonitrile (η_{std}=0.58) as a reference compound [84].

2PA cross sections (δ) were determined using two-photon excited fluorescence (2PEF) experimental methods with femtosecond excitation sources. A one-arm, dual-channel referential 2PEF technique was utilized [85]. The excitation source was an optical parametric amplifier (OPA; TOPAS, Spectra-Physics) that produces tunable laser pulses over the range of 190 nm-2600 nm. The OPA was pumped by a Ti:Sapphire regenerative amplifier (Spitfire, Spectra-Physics) operating at a 1 kHz repetition rate. The output of the OPA was used to excite the two-photon absorbing compounds under study and was weakly focused between two cuvettes in series containing the reference dye (*r*) whose 2PA properties have been well characterized (Coumarin 485 in methanol and Rhodamine 590 (6G) in methanol [86]) and the sample of interest (*s*). Measurements were repeated with the sample and reference positions exchanged. At each wavelength (λ_0), δ for the sample of interest was determined using the following equation:

$$\delta_2^s(\lambda_0) = \delta_2^r(\lambda_0)\frac{C^r}{C^s}\sqrt{\frac{F_1^s(\lambda_0)F_2^s(\lambda_0)}{F_1^r(\lambda_0)F_2^r(\lambda_0)}}\frac{\varphi^r(\lambda')}{\varphi^s(\lambda')}$$

where *C* is the concentration, *F* is the detected 2PEF signal, (φ) is the differential fluorescence quantum yield at a common emission wavelength (λ') for the sample and reference, superscripts *r* and *s* signify reference and sample of interest, respectively, and

subscripts 1 and 2 indicate channel positions one and two. All samples were prepared in toluene at a concentration of ~10^{-5} M and contained in 1 cm path-length fused silica cuvettes.

Fluorescence lifetimes were measured using time-correlated single-photon counting (TCSPC). A femtosecond mode-locked Ti:Sapphire laser (Mai Tai HP, Spectra-Physics) operating at 80 MHz with tunable wavelength range of 690-1040 nm was used as an excitation source. The output of laser was frequency doubled by a BBO crystal and was used to excite fluorescence from the molecules under study via one-photon excitation. The details of the experimental setup and the method of analysis have been previously described [87]. All samples were prepared in toluene at low concentration (~10^{-6} M) and were stirred continuously during measurements in 1 cm path-length fused silica cuvettes.

Femtosecond transient absorption spectra and kinetic traces were measured with a commercially available broadband pump-probe spectrometer (HELIOS, Ultrafast Systems LLC) using a femtosecond Ti:Sapphire regenerative amplifier laser source (Spitfire, Spectra-Physics). The probe beam was produced by splitting a portion (~5%) of the laser source (800 nm, 1 kHz repetition rate) and focusing into a sapphire crystal in order to generate a white-light continuum (WLC; 400-950 nm). The tunable pump beam was generated by directing the remainder from the laser source to the OPA discussed above. The pump beam was chopped at 500 Hz to allow for the collection of a pumped (WLC plus pump) and a non-pumped (WLC only) sample spectrum, which were used to generate a transient optical density difference (ΔOD) spectrum of the sample. The transmitted probe signal was collected using a fiber optic cable that was coupled to a

multichannel spectrometer with a silicon CCD detector. Spectra at each time delay were averaged for 2 seconds. The linear and excited state spectra of the samples were monitored after every measurement to ensure that no photodegradation had occurred during the experiment. To correct for temporal dispersion of the probe light, a chirp correction function was obtained using spectrophotometric grade carbon tetrachloride (Fisher Scientific) and was applied to all spectra. All samples were prepared in toluene (concentrations at ~10^{-4} M) and were stirred continuously during measurements in 2 mm path-length fused silica cuvettes.

For nanosecond transient absorption measurements, the ns-OPO described above was used as the excitation source. The white-light probe beam was produced by a 250 W tungsten-halogen lamp (300 W radiometric power supply, model Oriel 69931, Newport). The pump and probe were overlapped at a slight angle as they passed through the sample. For nanosecond transient kinetic measurements, the white light was focused onto the slit of a monochromator (Acton SpectraPro 2150i monochromator, Princeton Instruments) set to the selected probe wavelength and was detected using a high-speed InGaAs PIN photodiode (HCA-S-200M-Si, Femto). The temporal responses of oxygenated and deoxygenated samples (accomplished via purging with nitrogen gas) were compared in order to test for the presence of triplet species. To acquire nanosecond transient absorption spectra, the transmitted white light probe beam was directed into a spectrometer (320PI, Acton) equipped with a gated-intensified CCD camera (ST-133, Princeton Instruments). A pulse delay generator (model 575, Berkeley Nucleonics) was used to control the time delay of the CCD gate relative to the pump pulse. The solutions

used in these experiments were prepared in toluene (concentrations at ~10^{-5} M) and contained in 1 cm cuvettes and were stirred continuously.

Energy-dependent OPL measurements were carried out using both femtosecond and nanosecond laser pulses. For femtosecond OPL, polymer solutions were prepared in chloroform at relatively high concentrations (~10^{-3} M) and contained in 1 mm path-length fused-silica cuvettes. The fs-OPA was used as an excitation source and the repetition rate was reduced to 50 Hz to minimize potential contributions from thermal nonlinearities. The excitation beam was focused using a 50 mm focal length lens (f/20 geometry) with the focus placed in the middle of the 1 mm cuvette. The transmitted excitation beam as well as a reference beam (used to minimize pulse-to-pulse energy fluctuations) were detected using large area visible photoreceivers (model 2031, New Focus, Inc.) and integrated using Boxcar integrators (SR250, Stanford Research Systems). A scanning knife-edge method was used to determine the beam waist, which was 17 ± 2 μm with a nearly Gaussian shape (M^2 range of 1.1-1.2). The energies at the sample were measured using a power meter (PD300-UV-SH, Ophir) and were varied using a computer-controlled half-waveplate rotator (ESP300, Newport) in conjunction with a Glan-laser polarizer. Energy-dependent reference and excitation signals were acquired using a Labview-based data acquisition program.

Nanosecond OPL measurements were performed similarly to the femtosecond measurements, using the ns-OPO as the excitation source. The optical geometry was more tightly focused (f/5) than for the fs measurements. Sample solutions (~10^{-3} M) used in nanosecond OPL measurements were prepared in chloroform, deoxygenated and contained in 1 cm quartz cuvettes which were stirred continuously.

3.7. References

[1] He, G.S., Yuan, L., Bhawalkar, J.D. and Prasad, P.N., *Optical limiting, pulse reshaping, and stabilization with a nonlinear absorptive fiber system.* Appl. Opt., 1997. **36**(15): p. 3387-3392.

[2] Kieu, K., Schneebeli, L., Merzlyak, E., Hales, J.M., DeSimone, A., Perry, J.W., Norwood, R.A. and Peyghambarian, N., *All-optical switching based on inverse Raman scattering in liquid-core optical fibers.* Opt. Lett., 2012. **37**(5): p. 942-944.

[3] Tutt, L.W. and Boggess, T.F., *A review of optical limiting mechanisms and devices using organics, fullerenes, semiconductors and other materials.* Progress in Quantum Electronics, 1993. **17**(4): p. 299-338.

[4] Bhawalkar, J.D., He, G.S. and Prasad, P.N., *Nonlinear multiphoton processes in organic and polymeric materials.* Reports on Progress in Physics, 1996. **59**(9): p. 1041.

[5] Perry, J.W., Mansour, K., Lee, I.Y.S., Wu, X.L., Bedworth, P.V., Chen, C.T., Ng, D., Marder, S.R., Miles, P., Wada, T., Tian, M. and Sasabe, H., *Organic Optical Limiter with a Strong Nonlinear Absorptive Response.* Science, 1996. **273**(5281): p. 1533-1536.

[6] Perry, J.W., *Organic and Metal-Containing Reverse Saturable Absorbers for Optical Limiting*, in *Nonlinear optics of organic molecules and polymers*, H.S. Nalwa and S. Miyata, Editors. 1997, CRC press: Boca Raton, FL. p. 813-840.

[7] Tutt, L.W. and Kost, A., *Optical limiting performance of C_{60} and C_{70} solutions.* Nature, 1992. **356**(6366): p. 225-226.

[8] Perry, J.W., Mansour, K., Marder, S.R., Perry, K.J., Alvarez, J.D. and Choong, I., *Enhanced reverse saturable absorption and optical limiting in heavy-atom-substituted phthalocyanines.* Opt. Lett., 1994. **19**(9): p. 625-627.

[9] Ehrlich, J.E., Wu, X.L., Lee, I.Y.S., Hu, Z.Y., Röckel, H., Marder, S.R. and Perry, J.W., *Two-photon absorption and broadband optical limiting with bis-donor stilbenes.* Opt. Lett., 1997. **22**(24): p. 1843-1845.

[10] He, G.S., Xu, G.C., Prasad, P.N., Reinhardt, B.A., Bhatt, J.C. and Dillard, A.G., *Two-photon absorption and optical-limiting properties of novel organic compounds.* Opt. Lett., 1995. **20**(5): p. 435-437.

[11] He, G.S., Gvishi, R., Prasad, P.N. and Reinhardt, B.A., *Two-photon absorption based optical limiting and stabilization in organic molecule-doped solid materials.* Optics Communications, 1995. **117**(1-2): p. 133-136.

[12] He, G.S., Lin, T.-C., Prasad, P.N., Cho, C.-C. and Yu, L.-J., *Optical power limiting and stabilization using a two-photon absorbing neat liquid crystal in isotropic phase.* Applied Physics Letters, 2003. **82**(26): p. 4717-4719.

[13] Charlot, M., Izard, N., Mongin, O., Riehl, D. and Blanchard-Desce, M., *Optical limiting with soluble two-photon absorbing quadrupoles: Structure–property relationships.* Chemical Physics Letters, 2006. **417**(4–6): p. 297-302.

[14] Morel, Y., Irimia, A., Najechalski, P., Kervella, Y., Stephan, O., Baldeck, P.L. and Andraud, C., *Two-photon absorption and optical power limiting of bifluorene molecule.* The Journal of Chemical Physics, 2001. **114**(12): p. 5391-5396.

[15] Riehl, D., Izard, N., Vivien, L., Anglaret, E., Doris, E., Menard, C., Mioskowski, C., Porres, L., Mongin, O., Charlot, M., Blanchard-Desce, M., Anemian, R., Mulatier, J.-C., Barsu, C. and Andraud, C. *Broadband optical limiting optimization by combination of carbon nanotubes and two-photon absorbing chromophores in liquids*. 2003.

[16] Perry, J.W., Barlow, S., Ehrlich, J.E., Heikal, A.A., Hu, Z.-Y., Lee, L.-Y.S., Mansour, K., Marder, S.R., Rockel, H., Rum, M., Thayumanavan, S. and Wu, X.L., *Two-photon and higher-order absorptions and optical limiting properties of bis-donor substituted conjugated organic chromophores.* Principles, Materials, Phenomena, and Devices, 1999. **21**: p. 225-243.

[17] Zidan, M.D., Alsous, M.B., Allaf, A.W., Allahham, A. and Al-Zier, A., *Optical limiting action of C60 doped poly(ethylacetylenecarboxylate).* Optics & Laser Technology, 2012. **44**(7): p. 2282-2285.

[18] Chi, S.-H., Hales, J.M., Cozzuol, M., Ochoa, C., Fitzpatrick, M. and Perry, J.W., *Conjugated polymer-fullerene blend with strong optical limiting in the near-infrared.* Opt. Express, 2009. **17**(24): p. 22062-22072.

[19] Hales, J.M., Cozzuol, M., Screen, T.E.O., Anderson, H.L. and Perry, J.W., *Metalloporphyrin polymer with temporallyagile, broadband nonlinear absorption foroptical limiting in the near infrared.* Opt. Express, 2009. **17**(21): p. 18478-18488.

[20] Li, C., Liu, C., Li, Q. and Gong, Q., *Broadband optical limiting and nonlinear optical absorption properties of a novel hyperbranched conjugated polymer.* Chemical Physics Letters, 2004. **400**(4–6): p. 569-572.

[21] Vishnumurthy, K.A., Sunitha, M.S. and Adhikari, A.V., *New optical limiting polymeric materials with different π-electron conjugation bridge structures: Synthesis and characterization.* European Polymer Journal, 2012. **48**(9): p. 1575-1585.

[22] Poornesh, P., Hegde, P.K., Umesh, G., Manjunatha, M.G., Manjunatha, K.B. and Adhikari, A.V., *Nonlinear optical and optical power limiting studies on a new*

thiophene-based conjugated polymer in solution and solid PMMA matrix. Optics & Laser Technology, 2010. **42**(1): p. 230-236.

[23] Duncan, T.V., Susumu, K., Sinks, L.E. and Therien, M.J., *Exceptional Near-Infrared Fluorescence Quantum Yields and Excited-State Absorptivity of Highly Conjugated Porphyrin Arrays.* Journal of the American Chemical Society, 2006. **128**(28): p. 9000-9001.

[24] Guijiang, Z., Yunqi, L. and Cheng, Y., *Optical-limiting properties of poly(arylene ethynylenes) containing thiophene ring.* Journal of Applied Polymer Science, 2004. **93**(1): p. 131-135.

[25] He, G.S., Weder, C., Smith, P. and Prasad, P.N., *Optical power limiting and stabilization based on a novel polymer compound.* IEEE Journal of Quantum Electronics, 1998. **34**(12): p. 2279-2285.

[26] Rumi, M., Pond, S.J.K., Meyer-Friedrichsen, T., Zhang, Q., Bishop, M., Zhang, Y., Barlow, S., Marder, S.R. and Perry, J.W., *Tetrastyrylarene Derivatives: Comparison of One- and Two-Photon Spectroscopic Properties with Distyrylarene Analogs.* The Journal of Physical Chemistry C, 2008. **112**(21): p. 8061-8071.

[27] Kang, H., Evmenenko, G., Dutta, P., Clays, K., Song, K. and Marks, T.J., *X-Shaped Electro-optic Chromophore with Remarkably Blue-Shifted Optical Absorption. Synthesis, Characterization, Linear/Nonlinear Optical Properties, Self-Assembly, and Thin Film Microstructural Characteristics.* Journal of the American Chemical Society, 2006. **128**(18): p. 6194-6205.

[28] Samori, S., Tojo, S., Fujitsuka, M., Spitler, E.L., Haley, M.M. and Majima, T., *Donorâˆ’Acceptor-Substituted Tetrakis(phenylethynyl)benzenes as Emissive Molecules during Pulse Radiolysis in Benzene.* The Journal of Organic Chemistry, 2007. **72**(8): p. 2785-2793.

[29] Ohta, K., Yamada, S., Kamada, K., Slepkov, A.D., Hegmann, F.A., Tykwinski, R.R., Shirtcliff, L.D., Haley, M.M., Salek, P., Gel'mukhanov, F. and Agren, H., *Two-Photon Absorption Properties of Two-Dimensional π-Conjugated Chromophores: Combined Experimental and Theoretical Study.* Journal of Physical Chemistry A. **115**(2): p. 105-117.

[30] Wilson, J.N. and Bunz, U.H.F., *Switching of Intramolecular Charge Transfer in Cruciforms: Metal Ion Sensing.* Journal of the American Chemical Society, 2005. **127**(12): p. 4124-4125.

[31] Zucchero, A.J., McGrier, P.L. and Bunz, U.H.F., *Cross-Conjugated Cruciform Fluorophores.* Accounts of Chemical Research, 2009. **43**(3): p. 397-408.

[32] Zucchero, A.J., Wilson, J.N. and Bunz, U.H.F., *Cruciforms as Functional Fluorophores: Response to Protons and Selected Metal Ions.* Journal of the American Chemical Society, 2006. **128**(36): p. 11872-11881.

[33] Siegel N. N.; Zucchero, A.J.W., J. N.; Rumi, M.; Bunz, U. H. F.; Perry, J. W., *One- and Two-Photon Spectroscopy of Cruciform Chromophores with Phenylethynyl and Styryl Arms: Effects of Electron Donor/Acceptor Substitution.* In production.

[34] Albota, M., Beljonne, D., Brédas, J.-L., Ehrlich, J.E., Fu, J.-Y., Heikal, A.A., Hess, S.E., Kogej, T., Levin, M.D., Marder, S.R., McCord-Maughon, D., Perry, J.W., Röckel, H., Rumi, M., Subramaniam, G., Webb, W.W., Wu, X.-L. and Xu, C., *Design of Organic Molecules with Large Two-Photon Absorption Cross Sections.* Science, 1998. **281**(5383): p. 1653-1656.

[35] Rumi, M., Ehrlich, J.E., Heikal, A.A., Perry, J.W., Barlow, S., Hu, Z., McCord-Maughon, D., Parker, T.C., Röckel, H., Thayumanavan, S., Marder, S.R., Beljonne, D. and Bredas, J.-L., *Structure-Property Relationships for Two-Photon Absorbing Chromophores: Bis-Donor Diphenylpolyene and Bis(styryl)benzene Derivatives.* J. Am. Chem. Soc., 2000. **122**(39): p. 9500-9510.

[36] Zojer, E., Beljonne, D., Kogej, T., Vogel, H., Marder, S.R., Perry, J.W. and Brédas, J.L., *Tuning the two-photon absorption response of quadrupolar organic molecules.* The Journal of Chemical Physics, 2002. **116**(9): p. 3646-3658.

[37] Chiang, C.K., Fincher, C.R., Park, Y.W., Heeger, A.J., Shirakawa, H., Louis, E.J., Gau, S.C. and MacDiarmid, A.G., *Electrical Conductivity in Doped Polyacetylene.* Physical Review Letters, 1977. **39**(17): p. 1098-1101.

[38] Skotheim, T.A., *Handbook of conducting polymers*. 1997: CRC press.

[39] Sun, S.-S. and Sariciftci, N.S., *Organic photovoltaics: mechanisms, materials, and devices*. 2005: CRC press.

[40] Yang, J.-S. and Swager, T.M., *Fluorescent Porous Polymer Films as TNT Chemosensors: Electronic and Structural Effects.* Journal of the American Chemical Society, 1998. **120**(46): p. 11864-11873.

[41] Swanson, L.S., Shinar, J., Ding, Y.W. and Barton, T.J., *Photoluminescence, electroluminescence, and optically detected magnetic resonance study of 2,5-dialkoxy derivatives of poly(p-phenyleneacetylene) (PPA) and PPA-based light-emitting diodes.* Synthetic Metals, 1993. **55**(1): p. 1-6.

[42] Montali, A., Smith, P. and Weder, C., *Poly(p-phenylene ethynylene)-based light-emitting devices.* Synthetic Metals, 1998. **97**(2): p. 123-126.

[43] Zhou, Q. and Swager, T.M., *Fluorescent Chemosensors Based on Energy Migration in Conjugated Polymers: The Molecular Wire Approach to Increased*

Sensitivity. Journal of the American Chemical Society, 1995. **117**(50): p. 12593-12602.

[44] Weder, C., Sarwa, C., Bastiaansen, C. and Smith, P., *Highly polarized luminescence from oriented conjugated polymer/polyethylene blend films.* Advanced Materials, 1997. **9**(13): p. 1035-1039.

[45] Yifan, X., Paul, R.B., James, N.W. and Uwe, H.F.B., *Photoresponsivity of polymer thin-film transistors based on polyphenyleneethynylene derivative with improved hole injection.* Applied Physics Letters, 2004. **85**(18): p. 4219-4221.

[46] Hoppe, H., Sariciftci, N.S., Egbe, D.A.M., Mühlbacher, D. and Koppe, M., *Plastic Solar Cells Based on Novel PPE-PPV-Copolymers.* Molecular Crystals and Liquid Crystals, 2005. **426**(1): p. 255-263.

[47] Holzer, W., Penzkofer, A., Pichlmaier, M., Bradley, D.D.C. and Blau, W.J., *Photodegradation of some luminescent polymers.* Chemical Physics, 1999. **248**(2–3): p. 273-284.

[48] Holzer, W., Penzkofer, A., Gong, S.H., Davey, A.P. and Blau, W.J., *Laser performance studies of para-(phenylene-ethynylene) polymers in organic solvents.* Optical and Quantum Electronics, 1997. **29**(7): p. 713-724.

[49] Sluch, M.I., Godt, A., Bunz, U.H.F. and Berg, M.A., *Excited-State Dynamics of Oligo(p-phenyleneethynylene): Quadratic Coupling and Torsional Motions.* Journal of the American Chemical Society, 2001. **123**(26): p. 6447-6448.

[50] Bunz, U.H.F., *Poly(aryleneethynylene)s.* Macromolecular Rapid Communications, 2009. **30**(9-10): p. 772-805.

[51] Slepkov, A.D., Hegmann, F.A., Tykwinski, R.R., Kamada, K., Ohta, K., Marsden, J.A., Spitler, E.L., Miller, J.J. and Haley, M.M., *Two-photon absorption in two-dimensional conjugated quadrupolar chromophores.* Opt. Lett., 2006. **31**(22): p. 3315-3317.

[52] Kasha, M., *Energy Transfer Mechanisms and the Molecular Exciton Model for Molecular Aggregates.* Radiation Research, 1963. **20**(1): p. 55-70.

[53] Letard, J.F., Lapouyade, R. and Rettig, W., *Structure-photophysics correlations in a series of 4-(dialkylamino)stilbenes: intramolecular charge transfer in the excited state as related to the twist around the single bonds.* Journal of the American Chemical Society, 1993. **115**(6): p. 2441-2447.

[54] Pu, K.-Y., Qi, X.-Y., Yang, Y.-L., Lu, X.-M., Li, T.-C., Fan, Q.-L., Wang, C., Liu, B., Chan, H.S.O. and Huang, W., *Supramolecule-Regulated Photophysics of Oligo(p-phenyleneethynylene)-Based Rod–Coil Block Copolymers: Effect of Molecular Architecture.* Chemistry – A European Journal, 2008. **14**(4): p. 1205-1215.

[55] Duvanel, G.G., J.; Schuwey, A.; Gossauer, A.; Vauthey, E., *Ultrafast excited-state dynamics of phenyleneethynylene oligomers in solution.* Photochem. Photobiol. Sci., 2007. **6**: p. 956-963.

[56] Ginocchietti, G., Cecchetto, E., De Cola, L., Mazzucato, U. and Spalletti, A., *Photobehaviour of thio-analogues of stilbene and 1,4-distyrylbenzene studied by time-resolved absorption techniques.* Chemical Physics, 2008. **352**(1–3): p. 28-34.

[57] Demas, J., *Excited state lifetime measurements*. 1983, New York: Academic Press, Inc.

[58] Kennedy, S.M. and Lytle, F.E., *p-Bis(o-methylstyryl)benzene as a power-squared sensor for two-photon absorption measurements between 537 and 694 nm.* Analytical Chemistry, 1986. **58**(13): p. 2643-2647.

[59] Fisher, W.G., Wachter, E.A., Lytle, F.E., Armas, M. and Seaton, C., *Source-Corrected Two-Photon Excited Fluorescence Measurements between 700 and 880 nm.* Applied Spectroscopy, 1998. **52**(4): p. 536-545.

[60] Hales, J.M., Hagan, D.J., Stryland, E.W.V., Schafer, K.J., Morales, A.R., Belfield, K.D., Pacher, P., Kwon, O., Zojer, E. and Brédas, J.L., *Resonant enhancement of two-photon absorption in substituted fluorene molecules.* Journal of Chemical Physics, 2004. **121**(7): p. 3152-3160.

[61] Drobizhev, M., Karotki, A., Kruk, M. and Rebane, A., *Resonance enhancement of two-photon absorption in porphyrins.* Chemical Physics Letters, 2002. **355**(1–2): p. 175-182.

[62] Boggess, T., Bohnert, K., Mansour, K., Moss, S.C., Boyd, I. and Smirl, A., *Simultaneous measurement of the two-photon coefficient and free-carrier cross section above the bandgap of crystalline silicon.* Quantum Electronics, IEEE Journal of, 1986. **22**(2): p. 360-368.

[63] Oulianov, D.A., Tomov, I.V., Dvornikov, A.S. and Rentzepis, P.M., *Observations on the measurement of two-photon absorption cross-section.* Optics Communications, 2001. **191**(3–6): p. 235-243.

[64] Rumi, M. and Perry, J.W., *Two-photon absorption: an overview of measurements and principles.* Adv. Opt. Photon., 2010. **2**(4): p. 451-518.

[65] Ehrlich, J.E., Wu, X.L., Lee, I.-Y.S., Heikal, A.A., Hu, Z.-Y., Röckel, H., Marder, S.R. and Perry, J.W., *Two-Photon Absorbing Organic Chromophores for Optical Limiting.* MRS Online Proceedings Library, 1997. **479**: p. 9-15.

[66] Hsu, F.-C., Lin, S.H. and Wang, J.-K., *Excited-state dynamics of trans,trans-distyrylbenzene: A femtosecond transient absorption study.* Chemical Physics Letters, 2005. **411**(1–3): p. 103-107.

[67] Hsu, F.-C., Hayashi, M., Wang, H.-W., Lin, S.H. and Wang, J.-K., *Excited-State Dynamics of trans,trans-Distyrylbenzene: Transient Anisotropy and Excitation Energy Dependence.* The Journal of Physical Chemistry A, 2007. **111**(5): p. 759-763.

[68] Marri, E., Elisei, F., Mazzucato, U., Pannacci, D. and Spalletti, A., *Triplet-sensitized photobehaviour of the three stereoisomers of 1,4-distyrylbenzene and some aza-analogues.* Journal of Photochemistry and Photobiology A: Chemistry, 2006. **177**(2–3): p. 307-313.

[69] Ruckebusch, C., Aloïse, S., Blanchet, L., Huvenne, J.P. and Buntinx, G., *Reliable multivariate curve resolution of femtosecond transient absorption spectra.* Chemometrics and Intelligent Laboratory Systems, 2008. **91**(1): p. 17-27.

[70] Walters, K.A., *Triplet state photophysics in an aryleneethynylene π-conjugated polymer.* Chem. Commun., 1998: p. 1115-1116.

[71] Funston, A.M., Silverman, E.E., Schanze, K.S. and Miller, J.R., *Spectroscopy and Transport of the Triplet Exciton in a Terthiophene End-Capped Poly(phenylene ethynylene).* The Journal of Physical Chemistry B, 2006. **110**(36): p. 17736-17742.

[72] Levitus, M., Schmieder, K., Ricks, H., Shimizu, K.D., Bunz, U.H.F. and Garcia-Garibay, M.A., *Steps To Demarcate the Effects of Chromophore Aggregation and Planarization in Poly(phenyleneethynylene)s. 1. Rotationally Interrupted Conjugation in the Excited States of 1,4-Bis(phenylethynyl)benzene.* Journal of the American Chemical Society, 2001. **123**(18): p. 4259-4265.

[73] Köhler, A., Wilson, J.S., Friend, R.H., Al-Suti, M.K., Khan, M.S., Gerhard, A. and Bassler, H., *The singlet--triplet energy gap in organic and Pt-containing phenylene ethynylene polymers and monomers.* The Journal of Chemical Physics, 2002. **116**(21): p. 9457-9463.

[74] Wilson, J.S., Chawdhury, N., Al-Mandhary, M.R.A., Younus, M., Khan, M.S., Raithby, P.R., Köhler, A. and Friend, R.H., *The Energy Gap Law for Triplet States in Pt-Containing Conjugated Polymers and Monomers.* Journal of the American Chemical Society, 2001. **123**(38): p. 9412-9417.

[75] Levinson, G.S., Simpson, W.T. and Curtis, W., *Electronic Spectra of Pyridocyanine Dyes with Assignments of Transitions.* Journal of the American Chemical Society, 1957. **79**(16): p. 4314-4320.

[76] Kasha, M., Rawls, H. and El-Bayoumi, M.A., *The exciton model in molecular spectroscopy.* Pure Appl. Chem, 1965. **11**(3-4): p. 371-392.

[77] Cha, M., Sariciftci, N.S., Heeger, A.J., Hummelen, J.C. and Wudl, F., *Enhanced nonlinear absorption and optical limiting in semiconducting*

polymer/methanofullerene charge transfer films. Applied Physics Letters, 1995. **67**(26): p. 3850-3852.

[78] Siegel, N.N., *Two-photon absorption in cruciform and dipolar chromophores: excitonic interactions and response to metal ions,* in *Chemistry and Biochemistry*2010, Georgia Institute of Technology: Atlanta, GA.

[79] Zhang, H.C., Guo, E.Q., Zhang, Y.L., Ren, P.H. and Yang, W.J., *Donorâ^'Acceptor-Substituted Anthracene-Centered Cruciforms: Synthesis, Enhanced Two-Photon Absorptions, and Spatially Separated Frontier Molecular Orbitals.* Chemistry of Materials, 2009. **21**(21): p. 5125-5135.

[80] Chung, S.-J., Kim, K.-S., Lin, T.-C., He, G.S., Swiatkiewicz, J. and Prasad, P.N., *Cooperative Enhancement of Two-Photon Absorption in Multi-branched Structures.* The Journal of Physical Chemistry B, 1999. **103**(49): p. 10741-10745.

[81] Yoo, J., Yang, S.K., Jeong, M.-Y., Ahn, H.C., Jeon, S.-J. and Cho, B.R., *Bis-1,4-(p-diarylaminostryl)-2,5-dicyanobenzene Derivatives with Large Two-Photon Absorption Cross-Sections.* Organic Letters, 2003. **5**(5): p. 645-648.

[82] Ferguson, J., *Absorption spectroscopy of sandwich dimers and cyclophanes.* Chemical Reviews, 1986. **86**(6): p. 957-982.

[83] Kloppenburg, L., Jones, D. and Bunz, U.H.F., *High Molecular Weight Poly(p-phenyleneethynylene)s by Alkyne Metathesis Utilizing "Instant" Catalysts: A Synthetic Study.* Macromolecules, 1999. **32**(13): p. 4194-4203.

[84] Jones, G., II, Jackson, W.R., Choi, C.Y. and Bergmark, W.R., *Solvent effects on emission yield and lifetime for coumarin laser dyes. Requirements for a rotatory decay mechanism.* Journal of Physical Chemistry, 1985. **89**(2): p. 294-300.

[85] Makarov, N.S., Campo, J., Haley, M.M. and Perry, J.W., *Rapid, broadband two-photon-excited fluorescence spectroscopy and its application to red-emitting reference compounds.* Opt. Express, 2011. **1**(4): p. 551-563.

[86] Makarov, N.S., Drobizhev, M. and Rebane, A., *Two-photon absorption standards in the 550-1600 nmexcitation wavelength range.* Opt. Express, 2008. **16**(6): p. 4029-4047.

[87] Malicki, M., Hales, J.M., Rumi, M., Barlow, S., McClary, L., Marder, S.R. and Perry, J.W., *Excited-state dynamics and dye-dye interactions in dye-coated gold nanoparticles with varying alkyl spacer lengths.* Physical Chemistry Chemical Physics, 2010. **12**(23): p. 6267-6277.

CHAPTER 4

THE TWO-PHOTON AND EXCITED-STATE SPECTROSCOPY OF DONOR-ACCEPTOR-DONOR TYPE BORAZINE OLIGOMERS

4.1. Introduction

Substantial efforts have been directed towards identification of structure-property relationships of organic chromophores in an effort to design molecules with large 2PA cross sections (δ), along with optical and material features specific to particular 2PA applications [1-4]. For example, two-photon imaging applications require chromophores that are photostable and nontoxic, with high fluorescence quantum yields (Φ_{fl}), as well as sizable δ values [5, 6]. Such specificity of desired optical and material traits has resulted the exploration of a broad range of chromophores and structural motifs.

In particular, quadrupolar molecular configurations with electron donor (D) or electron acceptor (A) units, arranged in a general structure motif of D-π-D or A- π -A, results in more than a one order-of-magnitude increase in δ relative to the corresponding unsubstituted analogues due to symmetric intramolecular charge transfer (ICT) upon excitation [1]. Moreover, incorporating donor or acceptor units as side groups on the π-bridge (i.e. D- π-A- π -D or A- π -D- π -A) resulted in increased δ values, further demonstrating the importance of ICT character of 2PA chromophores [1, 2]. Increases in δ have also been observed in quadrupolar molecules when the conjugation length of the π-system is increased, as the charge is transferred over a longer distance [4].

Surprisingly, only a few electron donor (e.g. diphenyl- or dialkyl-amino [1, 2, 4, 7, 8]) and electron acceptor substitutents (e.g. nitro [9, 10], sulfonyl [1, 8], and cyano [1, 2]) have been used in the design of carbon-based, 2PA chromophores. More recent work has incorporated boryl groups into the π-conjugated structure [11-13]. Because of its empty *p* orbital, three-coordinate boron is electron deficient and a strong electron acceptor. Furthermore, the vacant p_z orbital of boron allows for conjugation in organic systems, giving rise to unique photophysical and electronic properties [14-16]. For example, organoborane chromophores possess interesting emissive properties and have shown their efficacy as two-photon chemosensors [17].

Discrete molecules that combine organoboranes with triarylamines have been investigated and show interesting nonlinear optical (NLO) properties [18, 19]. Notable work by Lambert [20-22], Müllen and Perry [23, 24], Wenger [25] and Marder [12, 16, 26] have shown dipolar, quadrupolar, octupolar, and dendrimer structures that possess δ values as large as 1300 GM [13]. Polymeric systems of this type are comparatively less explored [27-29]. A high molecular weight linear polymeric system, in which arylamine donors and arylborane acceptors alternate in the polymer main chain, has been introduced by Jäkle and coworkers [30]. The investigation of such a D/A polymers pose important questions in regards to structural conformation, electron delocalization, ICT characteristics, and nonlinear optical properties in organoborane polymeric systems. Further study of the NLO properties of organoborane polymers may allow for new design strategies towards enhancement of 2PA and Φ_{Fl} in organic fluorophores for 2PA-based fluorescence applications. Additionally, continued investigation of the photophysics and dynamics of organoborane 2PA dyes may present new candidates for other NLO applications, such as OPL [31].

Comparative investigations of well-defined oligofluorenes (***OFn***) [32, 33], oligothiophenes (***OTn***) [34, 35], and oligoanilines (***OAn***)[36] (structures are depicted in Figure 4.1) in what since has been termed “the oligomer approach” [37] have provided important information on the photophysical attributes and electronic structures of the corresponding polymers [38]. In the same regard, we report on a comprehensive study of the one-photon absorption (1PA), 2PA, and excited-state absorption (ESA) properties of well-defined organoborane oligomers with alternating triarylamine donor and triarylborane acceptor groups arranged in a quadrupolar and bent dipolar geometry. The alternating electron donor and acceptor pairing in these oligomers can be visualized as the linear counterpart to a π-expanded borazine reported by Jäkle *et. al.* [39], as such, the chromophores in this work have been coined as "linear borazine oligomers". Because the molecules feature strong donor and acceptor groups, interesting changes in the spectra and photophysics are expected with increased conjugation. We also examine the solvent effects on the photophysics of the chromophores in order to understand the structural conformation configuration and charge transfer characteristics of the oligomers.

4.2. Background

4.2.1. Organoboranes as Ambipolar Materials

Considerable efforts have been devoted to developing ambipolar molecules, in which donor and acceptor groups are linked by a π-conjugated bridging moiety [39-41]. They are attractive for applications in the area of materials science, such as electronic devices including organic light-emitting diodes (OLEDs) [40], organic field-effect transistors (OFETs) [42, 43], and organic photovoltaics (OPVs) [44], as well as for use in bioimaging and photodynamic therapy (PDT) [41].

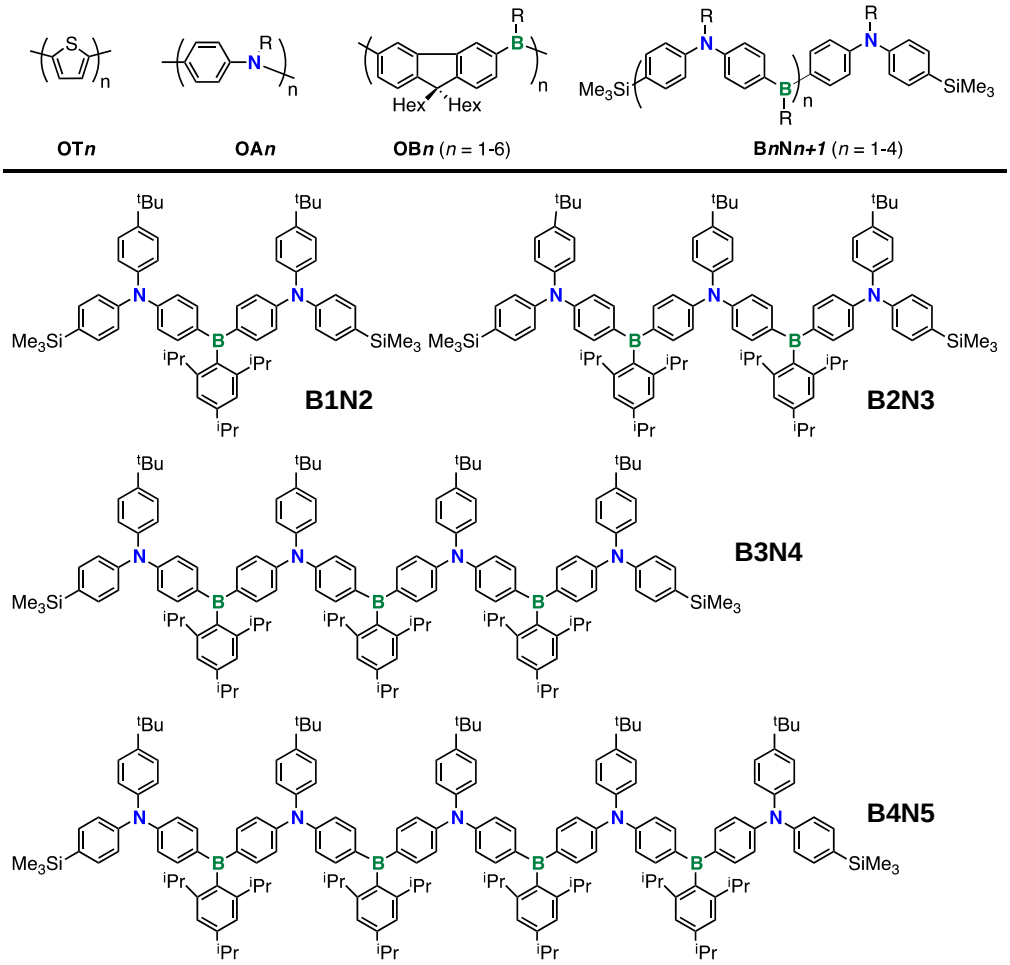

Figure 4.1 Examples of well-defined conjugated oligomers with electron donor and electron acceptor moieties and structures of the linear borazine oligomers (**B*n*N*n+1***) considered in this study.

Ambipolar molecules that combine organoboranes with triarylamines are attractive as multifunctional compounds. Triarylamines have been extensively exploited as p-type semiconductor materials that enable hole transport due to their inherent electron-donating capability [45, 46]. Among the wide range of n-type acceptor materials studied, triarylboranes bearing an empty p orbital are of particular significance since p-π orbital interactions with attached π-conjugated organic groups favor extended π-conjugation [14, 15]. In addition, the binding of anions (such as fluoride or cyanide) perturbs this orbital overlap, allowing for use of

organoborane fluorophores as materials for sensing [47-52]. Therefore, such B/N compounds with the simultaneous n- and p-type behavior and the possibility for interesting ICT processes favor the exploitations in NLO materials [18, 19, 53], OLEDs [54-58], and luminescent anion sensors [39, 57].

4.2.2. Synthetic and Electrochemical Characterization and DFT Calculations on B*n*N*n+1* Oligomers

The work presented in this chapter is part of a collaborative effort between Ariel Marshall and Dr. San-hui Chi of the Joseph Perry group[i] and Xiaodong Yin and Dr. Pangkuan Chen of the Frieder Jäkle group[ii]. The electrochemical measurements were conducted by the Jäkle group and are included here for additional background on this set of oligomers. The synthetic details can be found in Appendix A.

Electrochemical measurements were carried out with cyclic voltammetry and square wave voltammetry experiments, using THF as the solvent for reduction and CH_2Cl_2 for oxidation processes. The results are summarized in Table 4.1. All the oligomers are reversibly reduced and the redox potentials are reported relative to the Fc/Fc^+ couple at 298 K. The first reduction wave for **B1N2** was observed at $E_{1/2}$ = –2.60 V, and those for the higher oligomers occur at increasingly less negative potentials. For the higher oligomers, successive reduction of the individual boron sites gave rise to multiple waves as a consequence of electronic interactions between the resulting radical anions in the conjugated chain. The square wave voltammetry plots

[i] The Joseph Perry group is associated with the Center of Organic Photonics and Electronics at the Georgia Institute of Technology.
[ii] The Frieder Jäkle group is associated with the Department of Chemistry at Rutgers University.

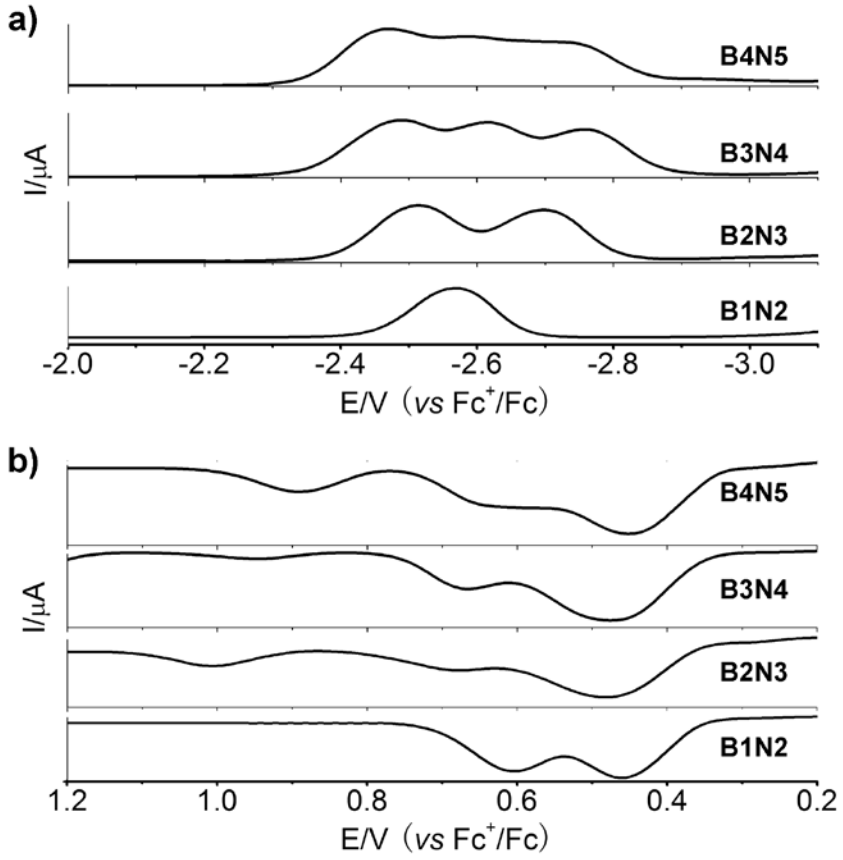

Figure 4.2 Square wave voltammograms for borazine oligomers provided by the Frieder Jäkle group in the Department of Chemistry at Rutgers University. a) Reduction in THF/0.1 M Bu_4NPF_6; b) oxidation in CH_2Cl_2/0.1 M Bu_4NPF_6; recorded vs. Fc^+/Fc redox couple.

are consistent with separate one-electron transfer reduction processes, with the exception that the redox waves partially overlap in the voltammogram for **B4N5** (Figure 4.2a).

Table 4.1 Electrochemical Data for Oligomers **B*n*N*n+1***

	B1N2 [a]	**B2N3** [a]	**B3N4** [a]	**B4N5** [a]
E^{p1}_{red}	-2.57 (1e)	-2.51 (1e)	-2.49 (1e)	-2.47 (2 e)
E^{p2}_{red}		-2.70 (1e)	-2.62 (1e)	-2.58 (1e)
E^{p3}_{red}			-2.76 (1e)	-2.72 (1e)
E^{p1}_{ox}	0.46 (1e)	0.48 (2e)	0.47 (3e)	0.45 (3e)
E^{p2}_{ox}	0.60 (1e)	0.68 (1e)	0.66 (1e)	0.60 (2e)
E^{p3}_{ox}		1.01 [b]	0.95 [b]	0.89 [b]
E_{HOMO} [c]	-5.26	-5.28	-5.27	-5.25
E_{LUMO} [c]	-2.23	-2.29	-2.31	-2.33
ΔE_{gap}	3.03	2.99	2.96	2.92

[a] Derived from square wave voltammetry data. [b] Assigned to further oxidation to dication states. [c] $E_{HOMO} = -(E^{p1}_{ox} + 4.8)$ (eV); $E_{LUMO} = -(E^{p1}_{red} + 4.8)$ (eV). Values provided by the Frieder Jäkle group in the Department of Chemistry at Rutgers University.

In contrast to the reduction waves, which are generally well separated, the oxidation profiles in CH_2Cl_2 are more complex. Two reversible oxidation waves are detected for the D-A-D species **B1N2** at $E_{1/2}$ = 0.46 and 0.60 V and they are easily assigned to successive oxidation of amines. All the higher oligomers give rise to three redox waves with different relative intensities. Based on the square wave voltammograms in Figure 4.2b, we assign the first two redox waves to 2e/1e, 3e/1e and 3e/2e oxidation processes for **B2N3**, **B3N4** and **B4N5**, respectively, resulting in the corresponding cation radical states. A third wave at higher potentials (>0.8 V) is attributed to further oxidation of the terminal arylamines to dication states. The imperfect reversibility of the oxidation processes for the higher oligomers in the CV plots could be due to partial

decomposition of the resulting highly charged species or possibly subsequent reactions of the radical cations generated at the electrode.

4.3. Photophysical Characterization of Linear Borazine Oligomers

4.3.1. Steady-State Absorption and Fluorescence Measurements

In order to understand the ICT and photophysical characteristics of D-A-D organoborane oligomers, we have investigated the relevant 1PA and emission properties of all molecules considered in this study. The 1PA and emission spectra of the linear borazine oligomers are displayed in Figure 4.3 with corresponding properties listed in Table 4.2. As shown in Figure 4.3a, the 1PA spectra for all **B*n*N*n+1*** oligomers are characterized by a dominant absorption band at ~400-430 nm, along with two high-energy bands at ~310 nm and above 250 nm. The lowest energy 1PA band can be assigned to an ICT transition from the diphenylamino groups to the triarylborane center. A structureless 1PA band, similar to that seen in Figure 4.3a, is generally observed for various multipolar triarylborane derivatives [59-61].

As is common in homologous conjugated molecules, the extension of the **B*n*N*n+1*** oligomer results in a red-shift of the lowest energy absorption band, an increase in molar absorptivity, ε_{max}, and an increase in energy gap between the first and second 1PA transitions. The change in 1PA wavelength maxima, $\lambda_{abs}^{(1)}$ from ~400 nm for **B1N2** to 423 nm for **B4N5** is consistent with the change in HOMO/LUMO energy gap estimated via electrochemical methods (see section 4.2.2). The difference in $\lambda_{abs}^{(1)}$ between the longer oligomers (**B3N4** and **B4N5)** is very small, suggesting that the effective conjugation length (n_{ECL}) of the oligomer has been reached. This is also consistent with the results from electrochemical studies mentioned previously (see Table 4.1). A comparable conjugation length of $n_{ECL} = 5$ has been

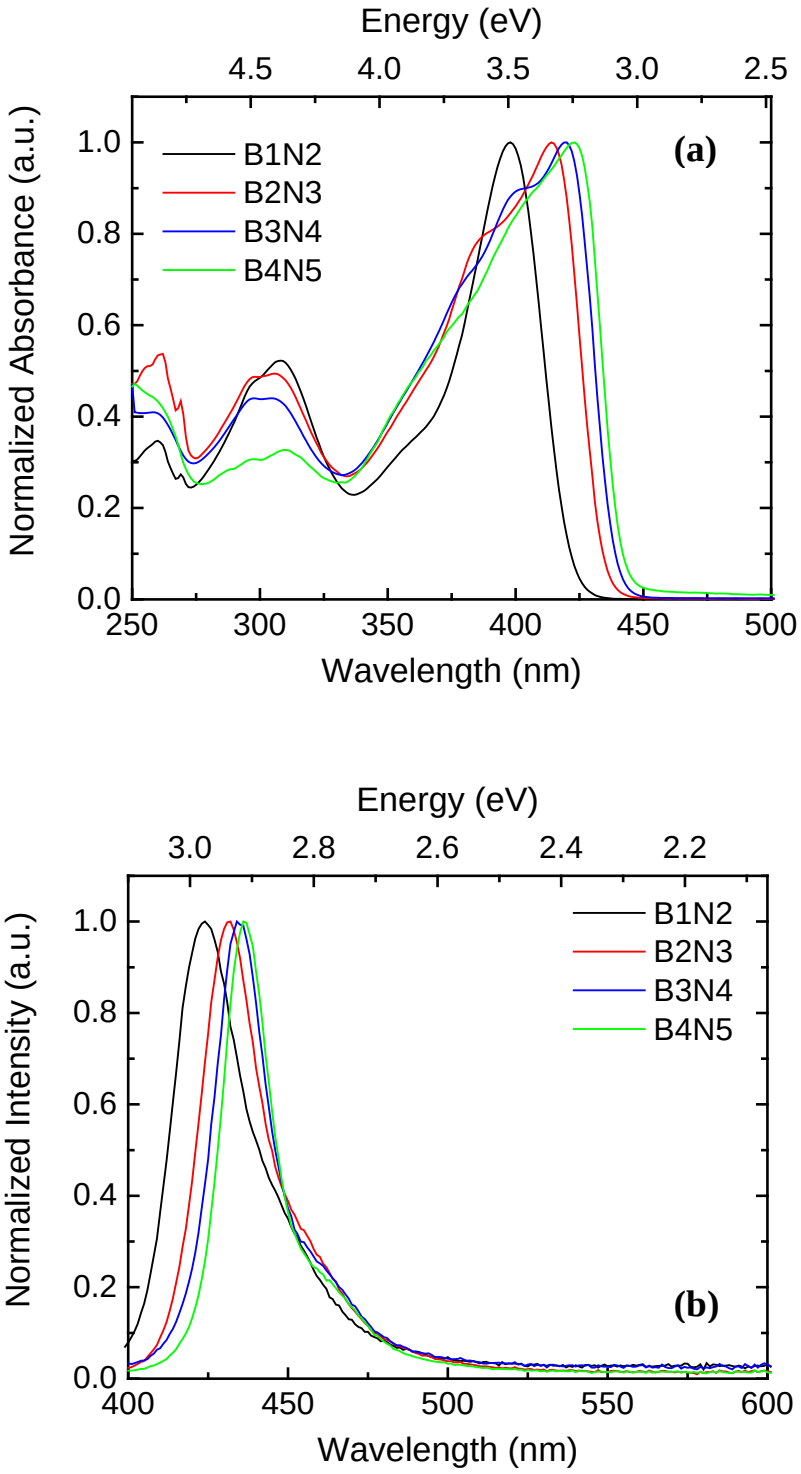

Figure 4.3. Comparison of normalized 1PA (a) and fluorescence (b) spectra of **B*n*N*n*+*1*** oligomers in hexane (excited at $\lambda_{abs}^{(1)}$).

Table 4.2 Experimental one-photon spectroscopic parameters and fluorescence lifetimes **B*n*N*n+1*** oligomers

	B1N2	**B2N3**	**B3N4**	**B4N5**
$\lambda_{abs}^{(1)}$ (nm)[a]	398	414	420	423
ε_{max} (10^4 $M^{-1}cm^{-1}$)[b]	3.9	7.3	9.7	12.0
λ_{fl} (nm) [c]	424	432	435	437
Φ_{fl} [c]	0.77 ± 0.05	0.65 ± 0.06	0.72 ± 0.00	0.72 ± 0.05
τ_{fl} (ns)[d]	2.04	1.89	1.70	1.69
k_r (10^8 s^{-1})[d]	3.79	3.46	4.23	4.24
k_{nr} (10^8 s^{-1})[d]	1.11	1.83	1.65	1.67

[a]One-photon absorption maximum ($\lambda_{abs}^{(1)}$) determined in hexane. [b]Peak molar absorptivity (ε_{max}) determined in toluene. [c]Maximum fluorescence maximum wavelength (λ_{fl}) and fluorescence quantum yield, Φ_{fl} determined in hexane. The error reported is the standard deviation of the fluorescence quantum yields at different concentrations. [d]Fluorescence lifetimes (τ_{fl}) and rate constants for radiative (k_r) and nonradiative (k_{nr}) decay determined in hexane.

reported for the fluoreneborane oligomers **OB*n*** [62] while a corresponding data analysis has to our knowledge not been performed for oligoanilines, **OA*n***.

Photoexcitation of **B*n*N*n+1*** oligomers in hexane resulted in blue emission with the wavelength of maximum fluorescence (λ_{fl}) ranging from ~420-440 nm and large fluorescence quantum yields (Φ_{fl}) of > 0.65 listed in Table 4.2. The emission bands are somewhat narrow in width and there is minimal vibronic structure, suggesting a primarily planar excited state with a small amount of photoinduced ICT character. A bathochromic shift in λ_{fl} was observed with increased chain length. The extension in conjugation in the **B*n*N*n+1*** oligomers has very little effect on Φ_{fl}, whereas a slight decrease in the fluorescence lifetime (τ_{fl}) of the oligomers occurs upon chain extension from ~2 ns for **B1N2** to ~1.7 ns for **B4N5**. The rate constants for the radiative (k_r) and nonradiative (k_{nr}) decays can be estimated from Φ_{fl} and τ_{fl} [63] and are included in Table 4.2. Both the k_r and k_{nr} for the **B*n*N*n+1*** oligomers increase linearly with length suggesting very little change in the radiative and nonradiative pathways from the S_1 state due to the extended conjugation.

4.3.2. Two-Photon Absorption (2PA) Spectroscopy

The 2PA spectra of the **B*n*N*n+1*** oligomers can be viewed in Figure 4.4 with corresponding parameters listed in Table 4.3. The 2PA spectrum of **B1N2** consists of one band in the visible and short near-IR spectral region with a 2PA maximum wavelength ($\lambda_{abs}^{(2)}$) at ~730 nm, along with a weak shoulder to the red of 800 nm corresponding to the $S_0 \rightarrow S_1$ transition via vibronic coupling. There is also a slight increase in δ in the 550-600 nm region, which can be attributed to pre-resonance enhancement due to the nearby one-photon transition [64]. The change in shape and position of the 2PA band is minimal as the oligomer is extended resulting in

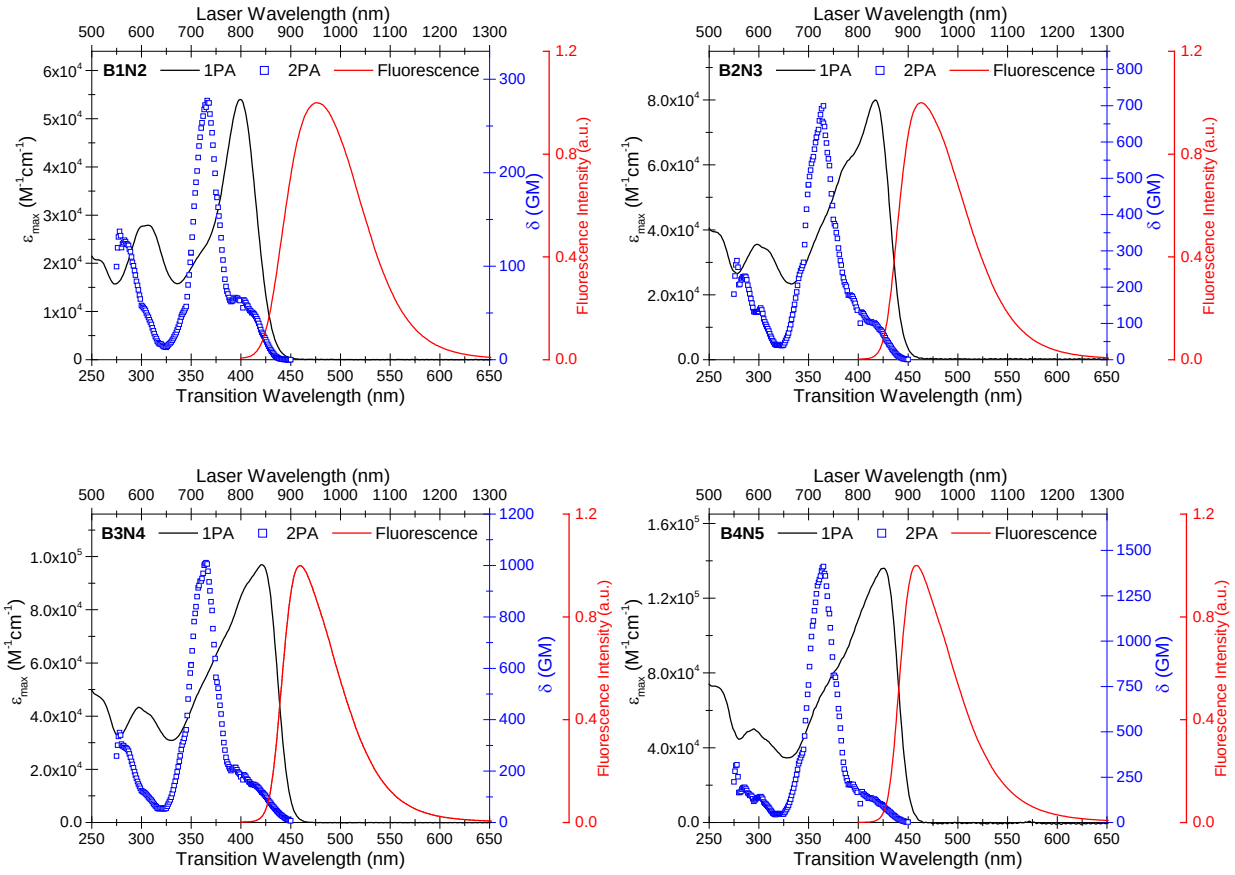

Figure 4.4. 1PA, fluorescence, and 2PEF spectra of linear borazine oligomers in dichloromethane. The solid black (—) indicates the 1PA spectrum; the 2PEF spectrum is represented by blue squares (□); the solid red line (—) is the one-photon fluorescence spectrum (excitation wavelengths are λ_{ex} = 390 nm).

Table 4.3. Experimental two-photon spectroscopic parameters of **B*n*N*n+1*** oligomers in hexane determined via 2PEF methods

	B1N2	**B2N3**	**B3N4**	**B4N5**
$\lambda_{abs}^{(2)}$ (nm) [a]	732	730	730	730
δ_{max} (GM)[a]	280	700	1,000	1,410

[a] Maximum of the two-photon fluorescence excitation spectrum ($\lambda_{abs}^{(2)}$) and peak two-photon absorption cross section (δ_{max}); 1 GM ≡ 1 x 10^{-50} cm^4·s/photon-molecule.

an increased separation of the 2PA and 1PA band positions. The increased $S_2 - S_1$ energy gap suggests stronger donor-acceptor coupling and ICT in the extended oligomers. The maximum 2PA cross section (δ_{max}) is significantly increased as the number of monomer units is increased, with δ_{max} = 1410 GM for **B4N5**. A similar trend of increasing δ has been reported by Perry and coworkers [4] and is a result of an increase in transition dipole moment between the S_0 and S_1 state along with a reduction in the detuning energy.

As shown in Figure 4.5, a strong length dependence in δ_{max} is observed as both parameters increase linearly with the addition of monomer units (*n*), which allows for strong electronic coupling between adjacent units. This is consistent with the idea that the δ is correlated to the distance over which a charge may be transferred [1, 4, 65]. A linear length dependence for ε_{max} is also observed. However, when considering ε_{max}/n and δ_{max}/n, the beginnings of the saturation of the linear and nonlinear absorption properties are observed at $n>2$. If we describe the length dependence of ε_{max} and δ_{max} with a simple power law (see Figure 4.6), we find the exponents to be 0.63 and 1.4, respectively, such that the following relations are determined: $\varepsilon_{max} \propto L^{0.63}$ and $\delta_{max} \propto L^{1.4}$, where L is the length of the oligomer. The saturation values for ε_{max} and δ_{max} are significantly smaller than those reported for heteroaromatic oligomers, such as oligothiphenes for which Thienpont *et al.* suggests demonstrates a saturation of the linear polarizability (α) and the second hyperpolarizability (γ) for $n>7$ [66]. Additionally, our values are smaller than the n_{ECL} = 5 reported for **OB*n*** [62].

The combination of electronic localization along with conformational disorder within the oligomer are possible reasons for the short n_{ECL} observed in **B*n*N*n+1*** oligomers. As opposed to

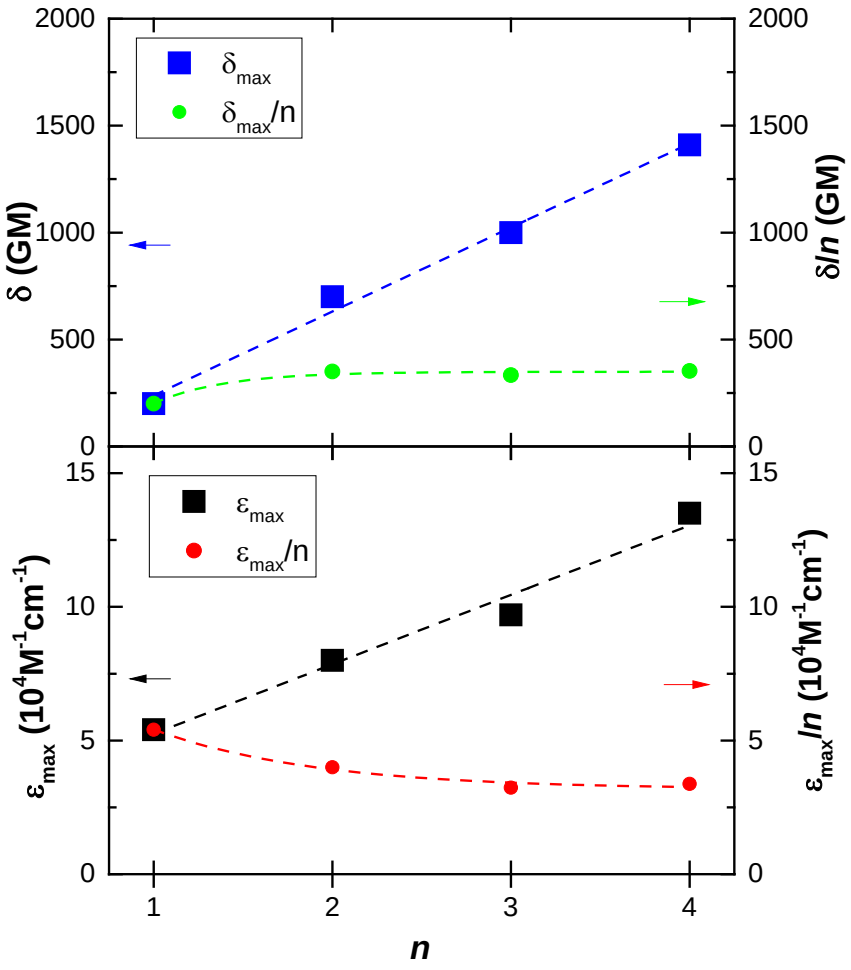

Figure 4.5. The length dependence of ε_{max}, ε_{max} /*n*, δ_{max} and δ_{max} /*n* observed in linear borazine oligomers. The dotted lines are only meant to guide the eye.

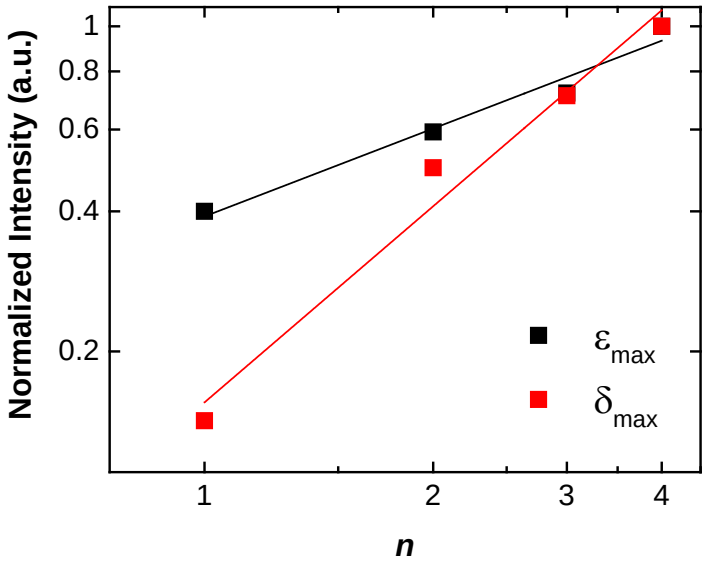

Figure 4.6. Normalized ε_{max} and δ_{max} vs number of monomer units (*n*). The lines represent power-law dependences with exponents of 0.63 and 1.4 for ε_{max} and δ_{max}, respectively.

the fluorene groups of **OB*n***, the phenylene linker between the aryl borane and aryl amine groups allow for twisting throughout the oligomer unit.

4.3.3. Excited-State Absorption (ESA) and Transient Kinetics

In order to understand changes in ESA due to the length of the **B*n*N*n+1*** oligomers, transient absorption (TA) spectroscopy was performed following excitation at 415 nm. The representative TA spectra and kinetics recorded with **B1N2** and **B4N5** in hexane are depicted in Figure 4.7, Figure 4.8, and Figure 4.9.

All linear borazine TA spectra show bleaching in the 1PA band region due to the depletion of ground-state population, which is also referred to as ground state bleaching (GSB).

Negative ΔOD signals to the red of the 1PA band coincide with photoluminescence and were determined to be a result of stimulated emission (SE). Figure 4.8 shows intensity-normalized spectra of **B1N2** in the GSB and SE spectral region recorded at early time delays. The dominant peak corresponds to the 0-0 vibronic transition observed in the steady-state fluorescence and the smaller intensity peak aligns with the $\lambda_{abs}^{(1)}$ of **B1N2**. The evolution of the TA spectra in this region shows a slight but continuous red-shift (~7 nm) of the SE band as the time delay increases to 100 ps, while the GSB band is stationary after 10 ps.

The changes in SE band position can be associated with the structural reorientation in relaxation of the S_1 state. Although boryl groups arranged in main-chain functionalized conjugated systems have been found to be twisted relative to the conjugated π-system [60], the fluorescence spectra of the **B*n*N*n+1*** oligomers suggest a highly planarized geometry in the lowest excited state [67]. Therefore, the changes observed in Figure 4.8 can be interpreted as solvent relaxation from the non-planar Franck-Condon state to the more planar equilibrium region of the S_1 state. Similar ultrafast changes in SE bands have been observed in phenylene ethynylene oligomers which possess an extremely planar geometry in the S_1 state [68].

Strong, broadband ESA over a range of 1150 nm in the visible and near-IR spectral region (ca. 450-1600 nm) is observed for all **B*n*N*n+1*** oligomers. As shown in Figure 4.7, the ESA of all linear borazine oligomers overlaps with the GSB and SE of the chromophores. Comparing the ESA of **B1N2** to **B4N5**, the absorbance maxima at 600 nm and 980 nm lose their structure and prominence in the longer oligomer. **B4N5** also shows a slight increase in ΔOD at ~1550 nm, relative to **B1N2**. Due to the large energy spacing between the band at 1550 nm and

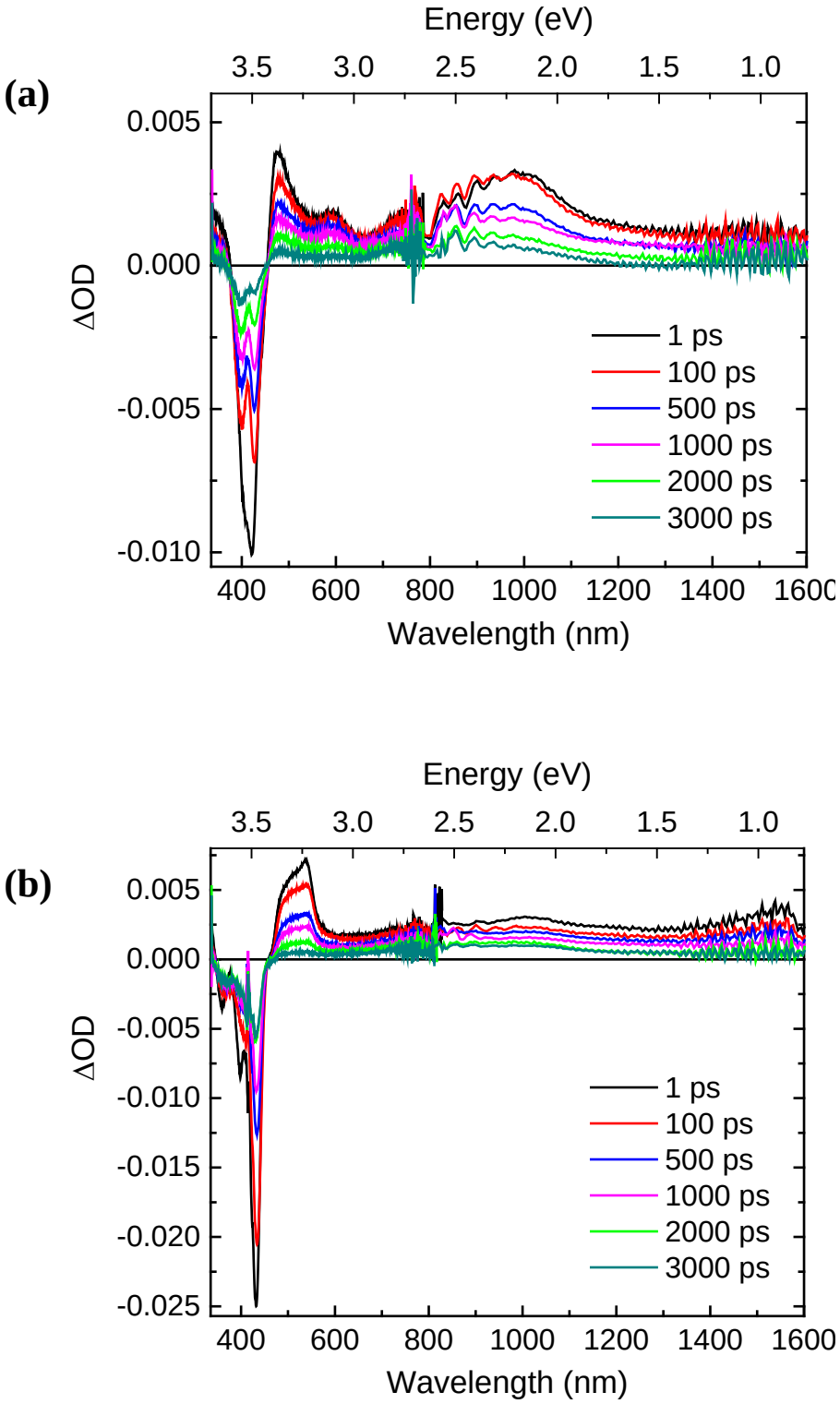

Figure 4.7. Femtosecond TA spectra of **B1N2** (a) and **B4N5** (b) in hexane. The samples were prepared at concentrations of 10^{-5}M and were excited at 415 nm at 500 nJ/pulse.

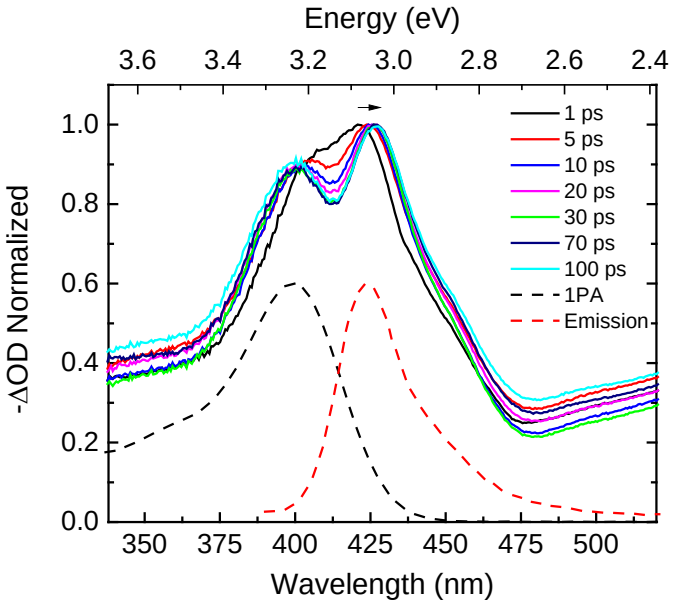

Figure 4.8. Intensity-normalized TA spectra of **B1N2** in the SE region. The 1PA and emission spectra (normalized to 0.6) have been overlaid with the TA spectra for comparison purposes. The sample was prepared in hexane at 75 μM and was excited at 415 nm at 500 nJ/pulse.

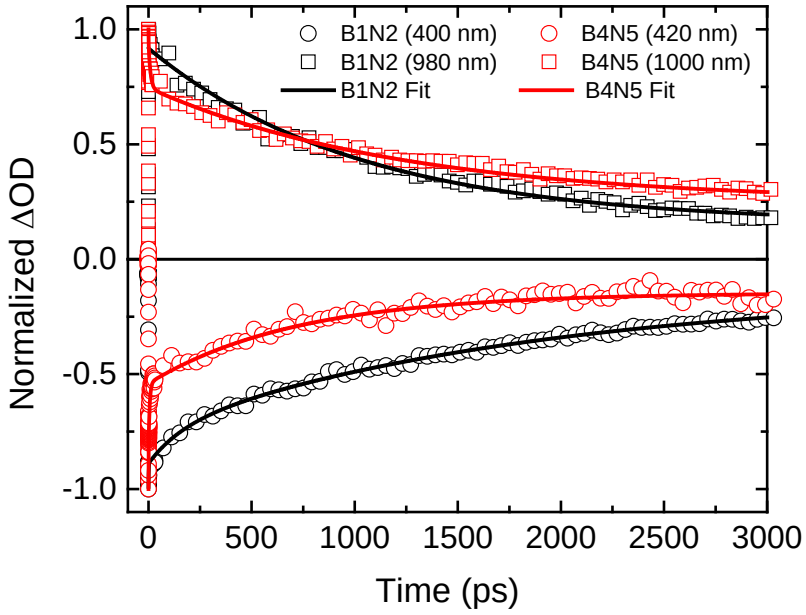

Figure 4.9. Normalized transient kinetics of **B1N2** and **B4N5** in hexane. The multiexponential fits for all kinetic traces are depicted as solid lines and have been overlaid with the experimental data. Samples were prepared at 10^{-5} M concentrations were excited at 415 nm at 500 nJ/pulse.

the shorter ESA features in the visible (19,800 cm^{-1}) and the broad ESA at ~1000 nm (2800 cm^{-1}), the long-wavelength ESA is ascribable to transitions to a different excited-state.

Figure 4.9 shows transient kinetics of the GSB and ESA of **B1N2** and **B4N5**. The ground state recovery kinetics for both oligomers show complex dynamics and were fitted with a triexponential function consisting of short, medium, and long components with a y-offset attributed to an unrecovered (or "infinite") component, relative to the time window of the fs-pulsed pump-probe experiment. For fittings of the GSB, the shortest time component, which can be assigned to the structural relaxation in the chromophore, shows an increase in amplitude and a decrease in time decay comparing **B1N2** to **B4N5** (~1 ps to 100 fs, respectively). A significant decrease in the medium and long time components is also observed as the oligomer is extended, with time constants varying from 160 ps and 1800 ps for **B1N2** to 6 ps and 700 ps for **B4N5**. Both oligomers display a non-recovered offset, which may be attributed to the triplet-state population.

The ESA decay kinetics of **B1N2** and **B4N5** show distinctly different dynamics. The decay of **B1N2** is monoexponential with a lifetime of 1000 ps, while the decay kinetics of **B4N5** is well fitted with a triexponential function and time constants similar to the GSB of the molecule. The comparisons presented in Figure 4.9 would suggest that an increase in length of the oligomer results rapid decay to the more planar S_1 configuration via solvent relaxation. This, in turn, leads to an increase in radiative and/or nonradiative decay to S_0 rather than the generation of the triplet species. This is in accordance to the k_r and k_{nr} values determined for **B4N5**, which are significantly larger than that of **B1N2**.

4.4. Solvent-Based Changes in the Steady-State and Ultrafast Characterization of Linear Borazine Oligomers

Further studies of the conformational and ICT character of linear borazine oligomers, steady-state absorption and emission, time-resolved fluorescence, and fs-TA measurements have been conducted in solvents with varying polarizability.

4.4.1. Solvent-Based Steady-State Absorption and Fluorescence Measurements

While the 1PA of the **B*n*N*n+1*** oligomers shows very little solvent-based changes, a strong positive solvatochromism is observed in the fluorescence of the chromophores, along with significant broadening of the emission band (Figure 4.10). The largest changes are observed in **B1N2**, where λ_{fl} is red-shifted by ~70 nm, comparing hexane to propylene carbonate (PC). Substantial solvatochromic shifts in fluorescence as large as 7300 cm^{-1} have been reported in triarylborane derivatives and are attributed to the large dipole moment of the excited state (~60 D) [61, 69]. The magnitude of the solvatochromic changes in λ_{fl} is reduced in the longer oligomer (**B1N2** vs **B4N5**), suggesting a reduction in ICT character as the oligomer is extended. The Φ_{fl} is also greatly affected due to the solvent medium and is reduced with increasing polarity (Table 4.4).

Interesting solvatochromic effects are observed when considering the changes in emission as the oligomer is lengthened in nonpolar versus polar solvent environments (see Figure 4.11). For example, the bathochromic shift of λ_{fl} with chain extension observed in hexane becomes a hypsochromic shift in the more polar solvents. In addition to the changes in λ_{fl}, the emission band narrows as the oligomer is lengthened in the more polar solvents. The narrowing of the emission band along with the blue-shift of λ_{fl} as the oligomer is extended suggests that there is an increase in planarity in the excited state.

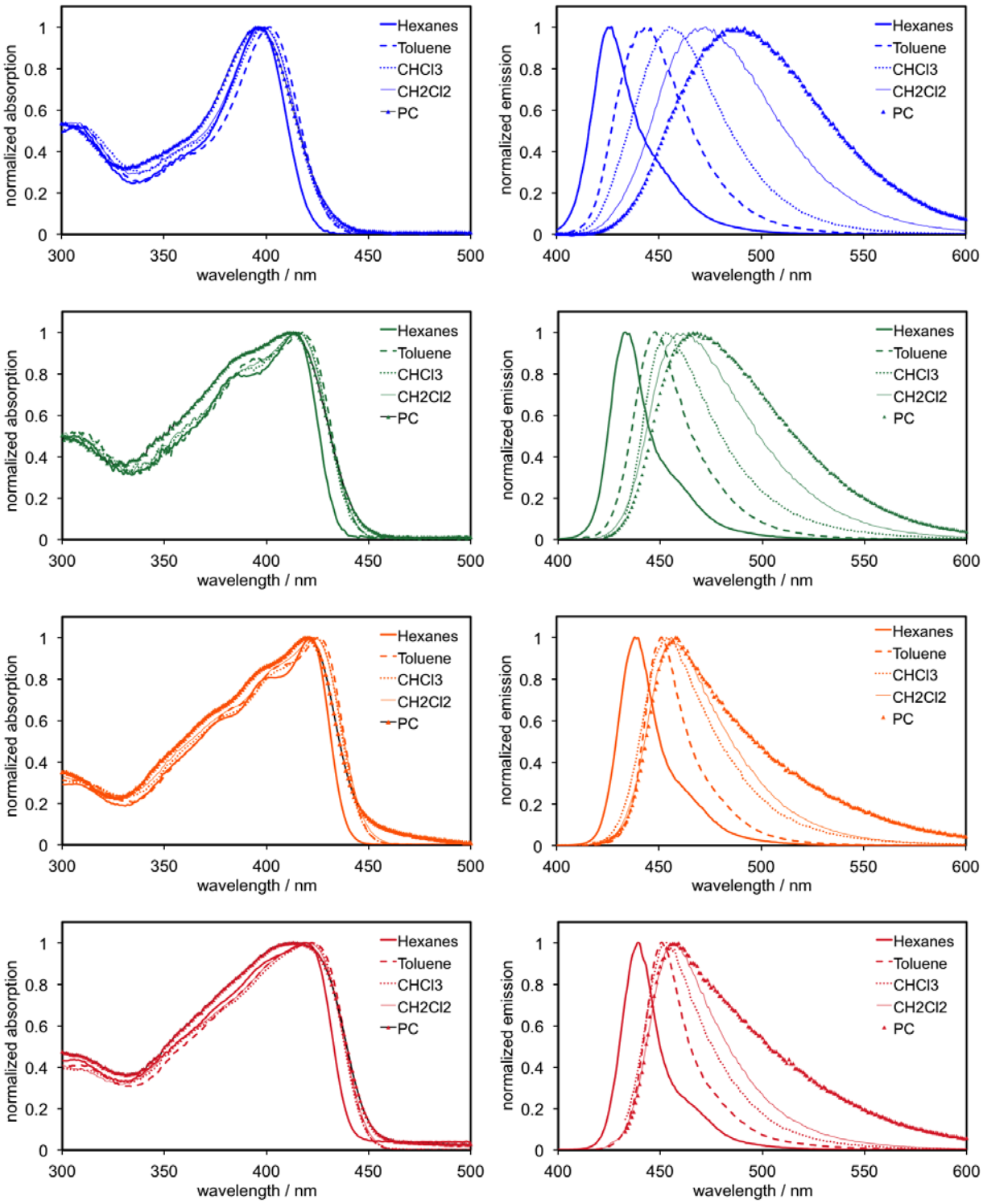

Figure 4.10. Normalized absorption and fluorescence spectra of **B*n*N*n+1*** oligomers in solvents of varying polarity (top to bottom: **B1N2**, **B2N3**, **B3N4**, **B4N5**). This experiment was performed by the group of Frieder Jäkle in the Department of Chemistry at Rutgers University.

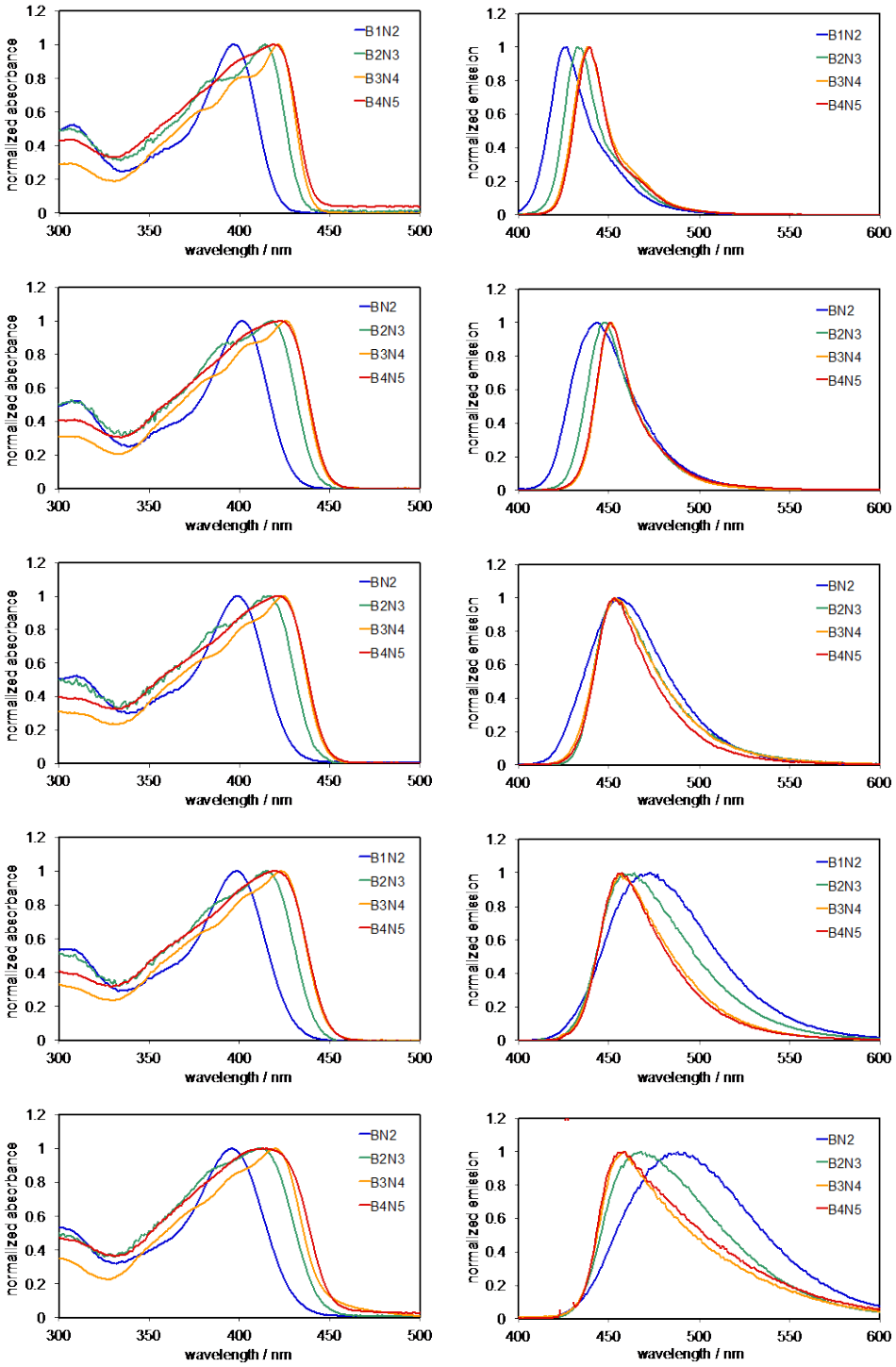

Figure 4.11. Solvatochromism observed in the normalized absorption and fluorescence spectra of the **B*n*N*n+1*** oligomers. Top to bottom: hexane, toluene, $CHCl_3$, CH_2Cl_2, and PC. This experiment was performed by the Frieder Jäkle group in the Department of Chemistry at Rutgers University.

Table 4.4 Experimental fluorescence spectroscopic parameters and fluorescence lifetimes of linear borazine oligomers in select solvents

	B1N2			**B2N3**			**B3N4**			**B4N5**		
	HEX	TOL	DCM	HEX	TOL	DCM	HEX	TOL	DCM	HEX	TOL	DCM
λ_{fl} (nm) [a]	424	442	476	432	431	463	435	435	460	437	436	425
Φ_{fl} [a]	0.77 ± 0.05	0.94 ± 0.06	0.54 ± 0.02	0.65 ± 0.06	0.82 ± 0.04	0.48 ± 0.03	0.72 ± 0.00	0.78 ±0.03	0.51 ± 0.04	0.72 ± 0.05	0.77 ± 0.02	0.48 ± 0.03
τ_{fl} (ns) [b]	2.04	2.40	3.92	1.89	2.11	3.02	1.70	2.15	2.60	1.69	2.09	2.41
k_r (10^8 s)[b]	3.79	3.92	1.22	3.46	3.89	1.69	4.23	3.62	1.96	4.24	3.69	2.24
k_{nr} (10^8 s)[b]	1.11	0.25	1.33	1.83	0.85	1.62	1.65	1.03	1.88	1.67	1.09	1.91

[a] Maximum fluorescence maximum wavelength (λ_{fl}) and fluorescence quantum yield, Φ_{fl}. The error reported is the standard deviation of the fluorescence quantum yields at different concentrations. [b]Fluorescence lifetimes (τ_{fl}) and rate constants for radiative (k_r) and nonradiative (k_{nr}) decay. Hexane, toluene, and dichloromethane have been abbreviated as HEX, TOL, and DCM, respectively. The highlighted hexane spectroscopic properties were taken from Table 4.2 and are presented here for comparison purposes.

4.4.2. Solvent Effects Analyzed via Lippert-Mataga Fitting

The results of solvent-dependent absorption and emission studies of the oligomers can be analyzed using the Lippert-Mataga equation given by [70]

$$\nu_A - \nu_F = \frac{2}{hca^3}\Delta f(\mu_E - \mu_G)^2 \qquad \text{(Eq 4.1)}$$

In this equation ν_A and ν_F are the absorption and emission maxima, respectively, measured in wavenumbers, and ν_A- ν_F is the Stokes shift of the molecule. The symbol h (=6.6256 x 10^{-27} ergs) is Planck's constant, c (=2.9979 x 10^{10} cm/s) is the speed of light, and a denotes the radius of the cavity in which the fluorophore resides. The symbols μ_G and μ_E denote the dipole moments in the ground and excited state, respectively. The variable Δf is the orientational polarizability and is calculated from the permittivity (ϵ) and refractive index (n_s) of the solvent.

$$\Delta f = \frac{\epsilon-1}{2\epsilon+1} - \frac{n_s^2-1}{2n_s^2+1} \qquad \text{(Eq 4.2)}$$

Figure 4.12 depicts the Stokes shift of the **B*n*N*n+1*** oligomers plotted against the orientation polarizability of various solvents. According to Eq.4.1, the slope for each oligomer is correlated with the difference in the dipole moment in the excited state and the ground state (μ_E - μ_G).

A key observation is that the slope of the Lippert-Mataga plots decreases significantly with increasing chain length from **B1N2** to **B4N5**. The very large Stokes shift for **B1N2** is similar to the behavior of dipolar chromophores (for example for Stokes

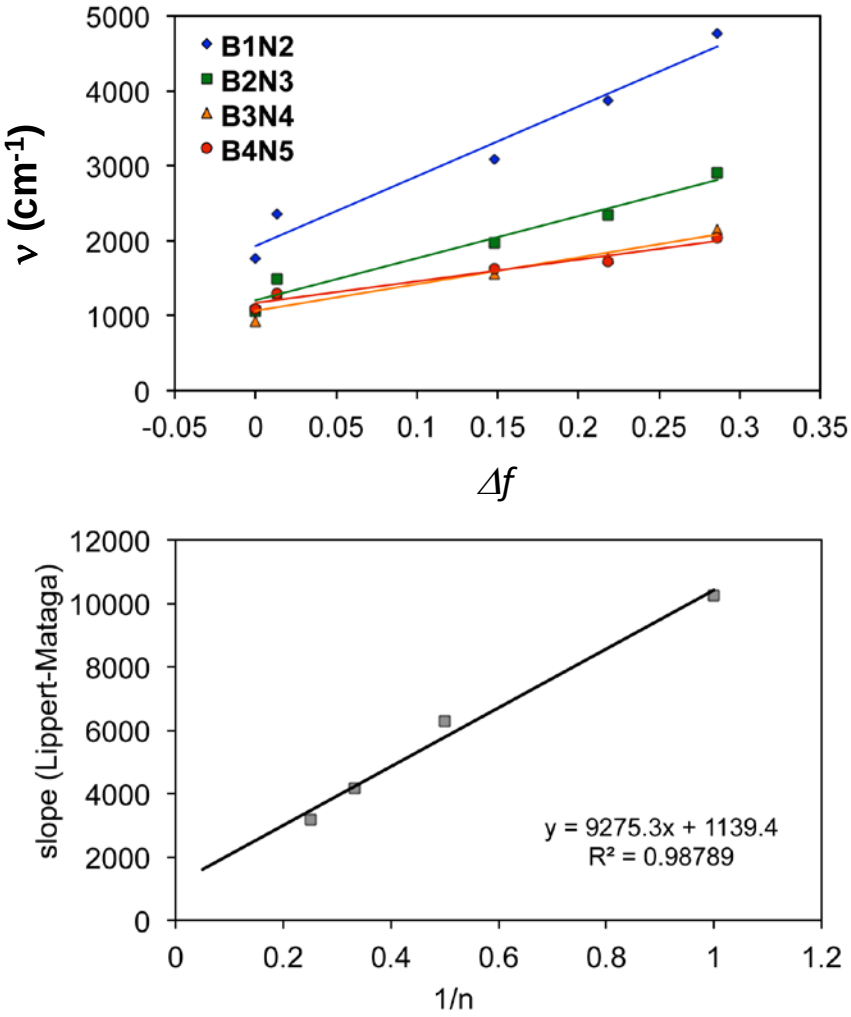

Figure 4.12. (a) Lippert-Mataga plot for the organoborane oligomers (b) Plot of Lippert-Mataga slope overlaid with a linear fit versus the number of repeating units in ***BnNn+1*** oligomers. This study was performed by the Frieder Jäkle group in the Department of Chemistry at Rutgers University.

shift is ~4600 cm^{-1} for 4-(dimesitylboryl)-N,N-diphenylaniline in tetrahydrofuran [60]). The reduction of the Stokes shift with increasing oligomer length is consistent with a decrease in the polarizability of the excited state as the ratio of D to A sites decreases from 2:1 for **B1N2** to 5:4 for **B4N5**.

4.4.3. Solvent-Dependent Time-Resolved Fluorescence Measurements

The results from solvent-based time-resolved fluorescence measurements are shown in Table 4.4. All oligomers show a substantial increase of τ_{fl} in DCM, relative to hexane, the largest of which was observed in **B1N2** where a 2-fold increase in τ_{fl} was determined. The Φ_{fl} of all **B*n*N*n+1*** oligomers is also affected by the solvent environment. Comparing Φ_{fl} values obtained in hexane to those determined in DCM, a reduction of fluorescence is observed as the solvent polarity is increased.

In toluene, there is a slightly different change in emission properties, such that a small increase in Φ_{fl} is observed when the oligomers are prepared in the polarizable solvent. While it is expected that the emission responses of the organoborane oligomers in toluene would be somewhat similar to those observed in hexane, we attribute deviations to the trend of decreasing Φ_{fl} detected in toluene to intermolecular interactions that may occur in the solvent, such as π-π stacking [71]. Given the numerous aromatic groups in the **B*n*N*n+1*** molecular structure, it is possible that π- π interactions between the solvent and the chromophore may lead to optical effects that are not entirely due to the polarity of the solvent medium.

Reductions in Φ_{fl} along with increases in τ_{fl} result in a ~50% decrease in k_r for all oligomers, when comparing hexane to DCM solvents, with the exception of **B1N2** which shows a 30% reduction in k_r. The nonradiative decay rate, however, is unaffected with solvent change.

The results from the steady-state and time-resolved fluorescence measurements reveal important information regarding the S_1-S_0 decay as a factor of solvent polarity. The reduction of k_r and Φ_{fl}, would suggest that the radiative decay processes are less favored in polar solvent environments. This can be attributed to conformational changes in the oligomers as a result of the stabilization of the ICT state by the polar solvent.

4.4.4. Solvent-dependent Excited-state Absorption and Transient Kinetics

Femtosecond TA spectroscopy was performed in various solvents following excitation into the lowest lying one-photon allowed state of all molecules. The TA spectra of the linear borazine oligomers are displayed in Figure 4.13. As shown in Figure 4.13, solvent-induced changes in the ESA of the linear borazines are observed, particularly in the TA spectra of **B1N2**. In hexane and toluene, **B1N2** shows two broad ESA bands with absorbance maxima at 480 nm and 980 nm. In DCM, however, the ESA of **B1N2** overlaps with the SE of the chromophore, resulting in an ESA band with absorption maxima at 435, 700, and 900 nm at time delays >100 ps after the pump pulse. Similar ESA band shapes due to overlapping SE was detected for all oligomers dissolved in DCM. This is consistent with significant red-shift of the emission band that was observed for all oligomers in the more polar solvents.

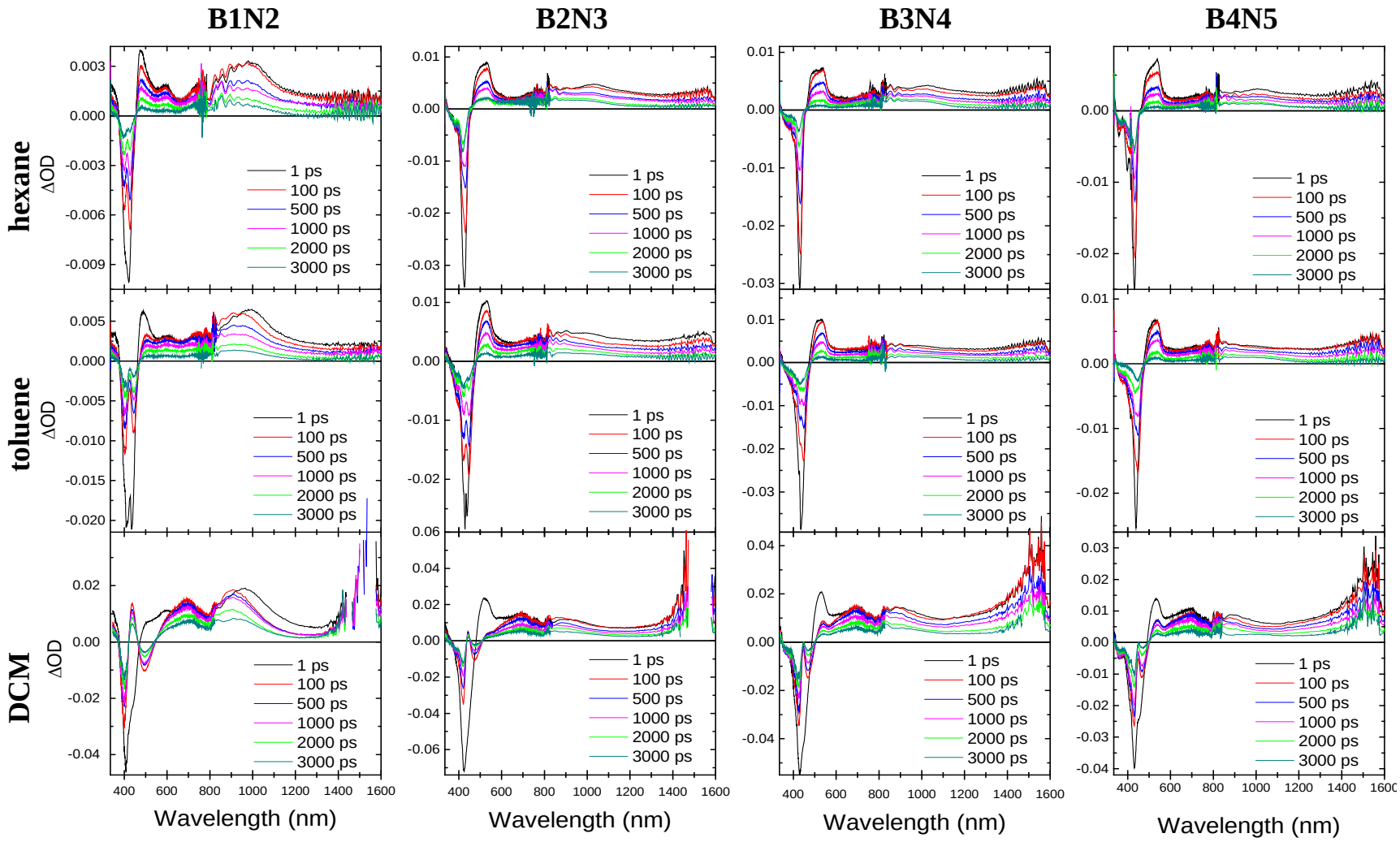

Figure 4.13 Femtosecond transient absorption spectra of the oligomers in hexane, toluene, and dichloromethane (DCM). Excitation wavelengths were 415 nm for all molecules. Concentrations of samples were 10^{-5} M.

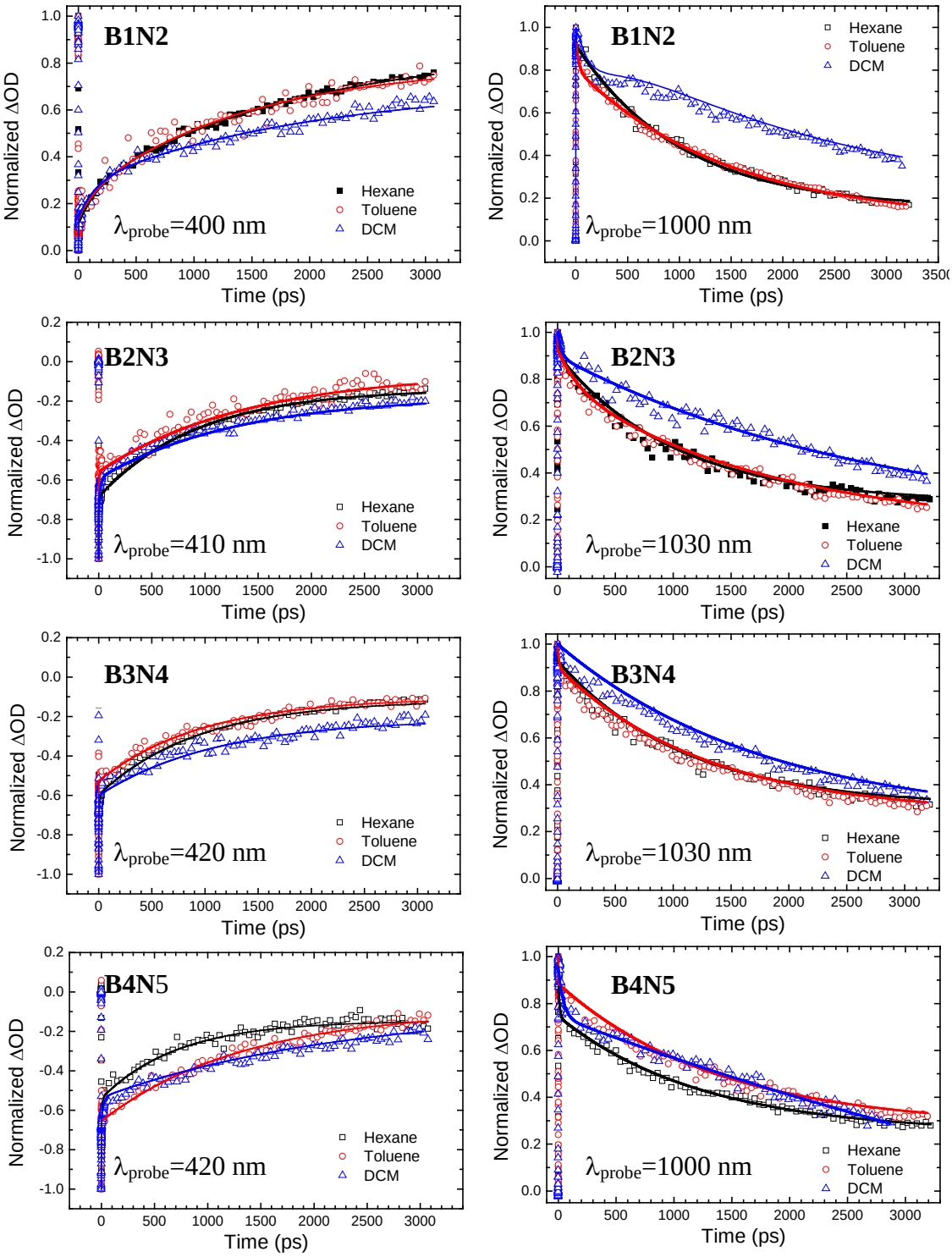

Figure 4.14. Normalized fs-TA kinetics of ***BnNn+1*** oligomers in various solvents. The fits for all kinetic traces are depicted as solid lines and have been overlaid with the experimental data. The oligomer and associated probe wavelength (λ_{probe}) are indicated in the plot. Samples were prepared at 10^{-5} M concentrations were excited at 415 nm at 500 nJ/pulse.

The long-wavelength (1550 nm) ESA band observed in the TA of **B4N5** in hexane is present for all **B*n*N*n+1*** oligomers dissolved in DCM. Although the assignment of this band is presently not conclusive, it is possible that when placed in DCM, significant conformational changes allow for an electronic transition to a lower-energy singlet excited-state. It is also possible that the long-wavelength band is ascribable to the absorption of the **B*n*N*n+1*** radical cation created by charge transfer from the oligomer to solvent. It is known that under high-intensity pulsed excitation chlorinated solvents, such as DCM, allow for the photochemical generation of radical cations of organic molecules and the solvation of electrons [72]. Finally, the 1550 nm band could also be associated with triplet-triplet ESA. Nanosecond TA, power-.dependent TA, and electrochemical measurements are required to definitively assign this transition.

Interesting solvent-based changes are also observed in the fs TA kinetics of the **B*n*N*n+1*** oligomers. For the shorter oligomers dissolved in DCM, larger y-offsets in the ground-state recovery and the excited-state decay are observed, relative to that of hexane. For the longer oligomers, the changes in the y-offsets between the nonpolar and polar solvents are not as drastic. Multiexponential fits of the recovery and decay kinetics show that the increased offset is not due to an increase in the amplitude of the "infinite" component but rather an increase in the time decay of a long-lived component that is closely associated with the τ_{fl} of the oligomers.

4.5. Summary

We have explored the photophysical, 1PA, and 2PA characteristics of a family of linear organoboranes that have a quadrupolar and bent-dipolar structures. The 1PA and emission spectra indicate that there is a large degree of torsion in the ground-state conformation of the

BnNn+1 oligomers. The lowest excited state, however appears to have a much more planar conformation, especially for the longer oligomers. The oligomers exhibit large two-photon cross sections and a 2PA band that extends from the visible to the near-IR region. Broadband singlet-singlet and triplet-triplet ESA from the oligomers was also observed.

Solvatochromic measurements revealed that the optical properties of the linear borazine dyes are highly sensitive to changes in solvent, especially in the emission properties of the dyes. Most notably, the shorter oligomers possess ICT transfer character, resulting in a 70 nm red-shift in the emission band going from nonpolar to polar medium. Additional changes are observed in the excited-state photophysics of the oligomers. The strong two-photon absorptivity of these organoborane chromophores would suggest that this family of oligomers indicates potential utility for several NLO applications. For example, the large δ values coupled with high Φ_{fl} indicates these organoborane oligomers are of interest for two-photon sensing applications. Furthermore, the overlap of the 2PA and ESA bands would suggest the oligomers are potential candidates for OPL applications.

4.6. Experimental Details

Materials. The synthesis of the **B*n*N*n+1*** oligomers was carried out by the Frieder Jäkle group in the Department of Chemistry at Rutgers University. The synthesis details are presented in Appendix A.

Electrochemical measurements were also carried out by the Frieder Jäkle group in the Department of Chemistry at Rutgers University. Cyclic voltammetry (CV) and square wave voltammetry (SWV) experiments were carried out on a BAS CV-50W analyzer. The three-electrode system consisted of an Au disk as working electrode, a Pt wire as secondary electrode

and an Ag wire as a pseudo reference electrode. The voltammograms were recorded with ca. 10^{-3} to 10^{-4} M sample solution in THF with $Bu_4N[PF_6]$ (0.1 M) as the supporting electrolyte for the reduction and in CH_2Cl_2 with $Bu_4N[PF_6]$ (0.1 M) for the oxidation scans. The scans were referenced after the addition of a small amount of ferrocene as an internal standard. The potentials are reported relative to the Fc/Fc^+ couple.

Spectroscopic measurements were performed using hexane, toluene, chloroform, dichloromethane, methanol, acetonitrile, and propylene carbonate (spectroscopic grade, Acros Organics). All solvents were degassed via several freeze-pump-thaw cycles for use with air-sensitive compounds. All solutions were prepared under an atmosphere of prepurified nitrogen using either Schlenk techniques or an inert-atmosphere glove box. Coumarin 540A, (Laser dye grade, Exciton) was used as reference compounds for quantum yield and 2PA cross section measurements.

Spectroscopic Measurements. UV-Vis. absorption spectra were measured with a UV-Vis-NIR scanning spectrophotometer (UV-3101PC, Shimadzu). Peak molar extinction coefficients (ε_{max}) were obtained in toluene from a linear regression analysis of absorbance versus the chromophore concentration using the Beer-Lambert equation. A spectrofluorometer (Fluorolog-2, Spex) was used for the measurement of fluorescence spectra. To obtain fluorescence spectra, all molecules were excited at their one-photon absorption maximum wavelength ($\lambda_{abs}^{(1)}$). All spectra have been corrected via subtraction of the scattering response from the solvent and the instrument's spectral response. Low concentration solutions (10^{-6} M) were used for all steady-state fluorescence measurements to minimize inner filter effects.

Fluorescence quantum yields (Φ_{fl}) were determined using Coumarin 102 in methanol (Φ_{std}=0.87) as a reference compound [73].

Fluorescence lifetimes were measured using a LifeSpec II (Edinburgh Instruments) time-correlated single-photon counting (TCSPC) system. In this measurement, a picosecond-pulsed diode laser (PicoQuant, LDH-P-C-375) with an excitation wavelength of 375 nm was used as an excitation light source. The detection system consisted of a high speed MicroChannel Plate PhotoMultiplier Tube (MCP-PMT, Hamamatsu R3809U-50) and TCSPC electronics.

Femtosecond TA spectra and kinetic traces were measured with a commercially available broadband pump-probe spectrometer (HELIOS, Ultrafast Systems LLC) using a femtosecond Ti:Sapphire regenerative amplifier laser source (Solstice, Spectra-Physics, 800-nm, 3.7-W average power, 100-fs pulse width, 1-KHz repetition rate) and a computer-controlled optical parametric amplifier (OPA) (TOPAS, Spectra-Physics, wavelength range: 266-2290 nm, pulse width: ~75 fs HW1/e) pumped by the amplified laser. The excitation wavelength of 415 nm was generated using the output of OPA. The white-light continuum (WLC, 330-1600 nm) probe beam was produced by focusing less than 5% of the 800 nm amplified beam into a nonlinear crystal in the Helios. A chirp correction function for the WLC probe was determined using measurements of the non-degenerate nonlinear response of carbon tetrachloride and was applied to all transient spectra. All samples for TA measurements were prepared at concentrations of ~10^{-5} M and were stirred continuously during measurements in 2 mm path-length fused silica cuvettes.

2PA cross sections (δ in GM) were determined using an one-arm, dual-channel referential 2PEF technique with the femtosecond-pulsed laser excitation source mentioned

previously. The details of the experimental setup and method of analysis of the data is described elsewhere [74]. The reference standard used in the measurement was Coumarin 540A (Exciton Dayton, OH) in carbon tetrachloride [74]. All samples were prepared under atmosphere in degassed dichloromethane at a concentration of ~10^{-5} M and contained in 1 cm path-length fused silica cuvettes.

4.7. References

[1] Albota, M., Beljonne, D., Brédas, J.-L., Ehrlich, J.E., Fu, J.-Y., Heikal, A.A., Hess, S.E., Kogej, T., Levin, M.D., Marder, S.R., McCord-Maughon, D., Perry, J.W., Röckel, H., Rumi, M., Subramaniam, G., Webb, W.W., Wu, X.-L. and Xu, C., *Design of Organic Molecules with Large Two-Photon Absorption Cross Sections.* Science, 1998. **281**(5383): p. 1653-1656.

[2] Pond, S.J.K., Rumi, M., Levin, M.D., Parker, T.C., Beljonne, D., Day, M.W., Bredas, J.-L., Marder, S.R. and Perry, J.W., *One- and Two-Photon Spectroscopy of Donor-Acceptor-Donor Distyrylbenzene Derivatives: Effect of Cyano Substitution and Distortion from Planarity.* J. Phys. Chem. A, 2002. **106**(47): p. 11470-11480.

[3] Rumi, M., Barlow, S., Wang, J., Perry, J. and Marder, S., *Two-Photon Absorbing Materials and Two-Photon-Induced Chemistry*, in *Photoresponsive Polymers I*, S. Marder and K.-S. Lee, Editors. 2008, Springer Berlin Heidelberg. p. 1-95.

[4] Rumi, M., Ehrlich, J.E., Heikal, A.A., Perry, J.W., Barlow, S., Hu, Z., McCord-Maughon, D., Parker, T.C., Röckel, H., Thayumanavan, S., Marder, S.R., Beljonne, D. and Brédas, J.-L., *Structure-Property Relationships for Two-Photon Absorbing Chromophores: Bis-Donor Diphenylpolyene and Bis(Styryl)Benzene Derivatives.* J. Am. Chem. Soc., 2000. **122**(39): p. 9500-9510.

[5] Oheim, M., Michael, D.J., Geisbauer, M., Madsen, D. and Chow, R.H., *Principles of Two-Photon Excitation Fluorescence Microscopy and Other Nonlinear Imaging Approaches.* Adv. Drug Deliv. Rev., 2006. **58**(7): p. 788-808.

[6] Schafer-Hales, K.J., Belfield, K.D., Yao, S., Frederiksen, P.K., Hales, J.M. and Kolattukudy, P.E., *Fluorene-Based Fluorescent Probes with High Two-Photon Action Cross-Sections for Biological Multiphoton Imaging Applications.* J. Biomed. Opt., 2005. **10**(5): p. 051402-051402-8.

[7] Charlot, M., Porres, L., Entwistle, C.D., Beeby, A., Marder, T.B. and Blanchard-Desce, M., *Investigation of Two-Photon Absorption Behavior in Symmetrical Acceptor-[Small Pi]-Acceptor Derivatives with Dimesitylboryl End-Groups. Evidence of New Engineering Routes for Tpa/Transparency Trade-Off Optimization.* Phys. Chem. Chem. Phys., 2005. **7**(4): p. 600-606.

[8] Strehmel, B., Sarker, A.M. and Detert, H., *The Influence of Σ and Π Acceptors on Two-Photon Absorption and Solvatochromism of Dipolar and Quadrupolar Unsaturated Organic Compounds.* ChemPhysChem, 2003. **4**(3): p. 249-259.

[9] Belfield, K.D., Hagan, D.J., Van Stryland, E.W., Schafer, K.J. and Negres, R.A., *New Two-Photon Absorbing Fluorene Derivatives: Synthesis and Nonlinear Optical Characterization.* Org. Lett., 1999. **1**(10): p. 1575-1578.

[10] Stellacci, F., Bauer, C.A., Meyer-Friedrichsen, T., Wenseleers, W., Marder, S.R. and Perry, J.W., *Ultrabright Supramolecular Beacons Based on the Self-Assembly of Two-Photon Chromophores on Metal Nanoparticles.* J. Am. Chem. Soc., 2002. **125**(2): p. 328-329.

[11] Cao, D.X., Liu, Z.Q., Fang, Q., Xu, G.B., Xue, G., Liu, G.Q. and Yu, W.T., *Blue Two-Photon Excited Fluorescence of Several D-Π-D, a-Π-a, and D-Π-a Compounds Featuring Dimesitylboryl Acceptor.* J. Organomet. Chem., 2004. **689**(13): p. 2201-2206.

[12] Yuan, Z., Collings, J.C., Taylor, N.J., Marder, T.B., Jardin, C. and Halet, J.-F., *Linear and Nonlinear Optical Properties of Three-Coordinate Organoboron Compounds.* J. Solid State Chem., 2000. **154**(1): p. 5-12.

[13] Liu, Z.-Q., Fang, Q., Cao, D.-X., Wang, D. and Xu, G.-B., *Triaryl Boron-Based a-Π-a Vs Triaryl Nitrogen-Based D-Π-D Quadrupolar Compounds for Single-and Two-Photon Excited Fluorescence.* Org. Lett., 2004. **6**(17): p. 2933-2936.

[14] Entwistle, C.D. and Marder, T.B., *Boron Chemistry Lights the Way: Optical Properties of Molecular and Polymeric Systems.* Angew. Chem. Int. Ed., 2002. **41**(16): p. 2927-2931.

[15] Entwistle, C.D. and Marder, T.B., *Applications of Three-Coordinate Organoboron Compounds and Polymers in Optoelectronics.* Chem. Mater., 2004. **16**: p. 4574-4585.

[16] Entwistle, C.D. and Marder, T.B., *Boron Chemistry Lights the Way: Optical Properties of Molecular and Polymeric Systems.* Angew. Chem. Int. Ed., 2002. **41**(16): p. 2927-2931.

[17] Liu, Z.-Q., Shi, M., Li, F.-Y., Fang, Q., Chen, Z.-H., Yi, T. and Huang, C.-H., *Highly Selective Two-Photon Chemosensors for Fluoride Derived from Organic Boranes.* Org. Lett., 2005. **7**(24): p. 5481-5484.

[18] Yuan, Z., Collings, J.C., Taylor, N.J., Marder, T.B., Jardin, C. and Halet, J.-F., *Linear and Non-Linear Optical Properties of Three-Coordinate Organoboron Compounds.* J. Solid State Chem., 2000. **154**: p. 5-12.

[19] Collings, J.C., Poon, S.Y., Le Droumaguet, C., Charlot, M., Katan, C., Palsson, L.O., Beeby, A., Mosely, J.A., Kaiser, H.M., Kaufmann, D., Wong, W.Y., Blanchard-Desce, M. and Marder, T.B., *The Synthesis and One- and Two-Photon Optical Properties of Dipolar,*

Quadrupolar and Octupolar Donor-Acceptor Molecules Containing Dimesitylboryl Groups. Chem. Eur. J., 2009. **15**(1): p. 198-208.

[20] Steeger, M. and Lambert, C., *Charge-Transfer Interactions in Tris-Donor-Tris-Acceptor Hexaarylbenzene Redox Chromophores.* Chem. Eur. J., 2012. **18**(38): p. 11937-11948.

[21] Stahl, R., Lambert, C., Kaiser, C., Wortmann, R. and Jakober, R., *Electrochemistry and Photophysics of Donor-Substituted Triarylboranes: Symmetry Breaking in Ground and Excited State.* Chem. Eur. J., 2006. **12**(8): p. 2358-2370.

[22] Reitzenstein, D. and Lambert, C., *Localized Versus Backbone Fluorescence in N-P-(Diarylboryl)Phenyl-Substituted 2,7- and 3,6-Linked Polycarbazoles.* Macromolecules, 2009. **42**: p. 773-782.

[23] Makarov, N.S., Mukhopadhyay, S., Yesudas, K., Bredas, J.L., Perry, J.W., Pron, A., Kivala, M. and Mullen, K., *Impact of Electronic Coupling, Symmetry, and Planarization on One- and Two-Photon Properties of Triarylamines with One, Two, or Three Diarylboryl Acceptors.* J. Phys. Chem. A, 2012. **116**(15): p. 3781-3793.

[24] Pron, A., Baumgarten, M. and Müllen, K., *Phenylene Bridged Boron-Nitrogen Containing Dendrimers.* Org. Lett., 2010. **12**(19): p. 4236-4239.

[25] Schmidt, H.C., Reuter, L.G., Hamacek, J. and Wenger, O.S., *Multistage Complexation of Fluoride Ions by a Fluorescent Triphenylamine Bearing Three Dimesitylboryl Groups: Controlling Intramolecular Charge Transfer.* J. Org. Chem., 2011. **76**(21): p. 9081-9085.

[26] Entwistle, C.D. and Marder, T.B., *Applications of Three-Coordinate Organoboron Compounds and Polymers in Optoelectronics.* Chem. Mater., 2004. **16**(23): p. 4574-4585.

[27] Jäkle, F., *Lewis Acidic Organoboron Polymers.* Coord. Chem. Rev., 2006. **250**: p. 1107-1121.

[28] Jäkle, F., *Advances in the Synthesis of Organoborane Polymers for Optical, Electronic and Sensory Applications.* Chem. Rev., 2010. **110**: p. 3985-4022.

[29] Doshi, A. and Jäkle, F., *1.27 - Boron-Containing Polymers*, in *Comprehensive Inorganic Chemistry Ii (Second Edition)*, J. Reedijk and K. Poeppelmeier, Editors. 2013, Elsevier: Amsterdam. p. 861-891.

[30] Li, H. and Jäkle, F., *Donor-Pi-Acceptor Polymer with Alternating Triarylborane and Triphenylamine Moieties".* Macromol. Rap. Commun., 2010. **31**: p. 915-920.

[31] Ehrlich, J.E., Wu, X.L., Lee, I.Y.S., Hu, Z.Y., Röckel, H., Marder, S.R. and Perry, J.W., *Two-Photon Absorption and Broadband Optical Limiting with Bis-Donor Stilbenes.* Opt. Lett., 1997. **22**(24): p. 1843-1845.

[32] Geng, Y., Trajkovska, A., Katsis, D., Ou, J.J., Culligan, S.W. and Chen, S.H., *Synthesis, Characterization, and Optical Properties of Monodisperse Chiral Oligofluorenes.* J. Am. Chem. Soc., 2002. **124**: p. 8337-8347.

[33] Pond, S.J.K., Tsutsumi, O., Rumi, M., Kwon, O., Zojer, E., Brédas, J.-L., Marder, S.R. and Perry, J.W., *Metal-Ion Sensing Fluorophores with Large Two-Photon Absorption Cross Sections: Aza-Crown Ether Substituted Donor-Acceptor-Donor Distyrylbenzenes.* J. Am. Chem. Soc., 2004. **126**(30): p. 9291-9306.

[34] Mishra, A., Ma, C.-Q. and Bäuerle, P., *Functional Oligothiophenes: Molecular Design for Multidimensional Nanoarchitectures and Their Applications.* Chem. Rev., 2009. **109**(109): p. 1141-1276.

[35] Zhang, L., Colella, N.S., Liu, F., Trahan, S., Baral, J.K., Winter, H.H., Mannsfeld, S.C.B. and Briseno, A.L., *Synthesis, Electronic Structure, Molecular Packing/Morphology Evolution, and Carrier Mobilities of Pure Oligo-/Poly(Alkylthiophenes).* J. Am. Chem. Soc., 2013. **135**(2): p. 844-854.

[36] Sadighi, J.P., Singer, R.A. and Buchwald, S.L., *Palladium-Catalyzed Synthesis of Monodisperse, Controlled-Length, and Functionalized Oligoanilines.* J. Am. Chem. Soc., 1998. **120**: p. 4960-4976.

[37] Wegner, G., Müllen, K. and Eds, *Electronic Materials: The Oligomer Approach*. 1996, Weinheim, Germany: VCH. 250.

[38] Gierschner, J., Cornil, J. and Egelhaaf, H.-J., *Optical Bandgaps of P-Conjugated Organic Materials at the Polymer Limit: Experiment and Theory.* Adv. Mater., 2007. **19**(2): p. 173-191.

[39] Chen, P.K., Lalancette, R.A. and Jäkle, F., *Π-Expanded Borazine: An Ambipolar Conjugated B-Pi-N Macrocycle.* Angew. Chem. Int. Ed., 2012. **51**(32): p. 7994-7998.

[40] Lai, M.-Y., Chen, C.-H., Huang, W.-S., Lin, J.T., Ke, T.-H., Chen, L.-Y., Tsai, M.-H. and Wu, C.-C., *Benzimidazole/Amine-Based Compounds Capable of Ambipolar Transport for Application in Single-Layer Blue-Emitting Oleds and as Hosts for Phosphorescent Emitters.* Angew. Chem. Int. Ed., 2008. **47**(3): p. 581-585.

[41] Shirota, Y. and Kageyama, H., *Charge Carrier Transporting Molecular Materials and Their Applications in Devices.* Chem. Rev., 2007. **107**(4): p. 953-1010.

[42] Wang, H., Wang, J., Yan, X., Shi, J., Tian, H., Geng, Y. and Yan, D., *Ambipolar Organic Field-Effect Transistors with Air Stability, High Mobility, and Balanced Transport.* Appl. Phys. Lett., 2006. **88**(13): p. -.

[43] Anthopoulos, T.D., de Leeuw, D.M., Cantatore, E., Setayesh, S., Meijer, E.J., Tanase, C., Hummelen, J.C. and Blom, P.W.M., *Organic Complementary-Like Inverters Employing Methanofullerene-Based Ambipolar Field-Effect Transistors.* Appl. Phys. Lett., 2004. **85**(18): p. 4205-4207.

[44] Cravino, A., *Conjugated Polymers with Tethered Electron-Accepting Moieties as Ambipolar Materials for Photovoltaics.* Polym. Int., 2007. **56**(8): p. 943-956.

[45] Thelakkat, M., Schmitz, C., Hohle, C., Strohriegl, P., Schmidt, H.-W., Hofmann, U., Schloter, S. and Haarer, D., *Novel Functional Materials Based on Triarylamines-Synthesis and Application in Electroluminescent Devices and Photorefractive Systems.* Phys. Chem. Chem. Phys., 1999. **1**(8): p. 1693-1698.

[46] Kisselev, R. and Thelakkat, M., *Synthesis and Characterization of Poly(Triarylamine)S Containing Isothianaphthene Moieties.* Macromolecules, 2004. **37**(24): p. 8951-8958.

[47] Yamaguchi, S., Akiyama, S. and Tamao, K., *Colorimetric Fluoride Ion Sensing by Boron-Containing Pi-Electron Systems.* J. Am. Chem. Soc., 2001. **123**(46): p. 11372-11375.

[48] Yamaguchi, S., Akiyama, S. and Tamao, K., *A New Approach to Photophysical Properties Control of Main Group Element Pi-Electron Compounds Based on the Coordination Number Change.* J. Organomet. Chem., 2002. **652**: p. 3-9.

[49] Wade, C.R., Broomsgrove, A.E.J., Aldridge, S. and Gabbai, F.P., *Fluoride Ion Complexation and Sensing Using Organoboron Compounds.* Chem. Rev., 2010. **110**(7): p. 3958-3984.

[50] Jiang, C., Zhao, T., Yuan, P., Gao, N., Pan, Y., Guan, Z., Zhou, N. and Xu, Q.-H., *Two-Photon Induced Photoluminescence and Singlet Oxygen Generation from Aggregated Gold Nanoparticles.* ACS Applied Materials & Interfaces, 2013. **5**(11): p. 4972-4977.

[51] Pammer, F. and Jäkle, F., *3-Vinylborane-Functionalized Oligothiophenes: Isomer-Dependent Electronic Structure and Fluorescence Enhancement Upon Anion Binding.* Chem. Sci., 2012. **3**: p. 2598-2606.

[52] Cheng, F., Bonder, E.M. and Jäkle, F., *Electron-Deficient Triarylborane Block Copolymers: Synthesis by Controlled Free Radical Polymerization and Application in the Detection of Fluoride Ions.* J. Am. Chem. Soc., 2013. **135**(46): p. 17286–17289.

[53] Branger, C., Lequan, M., Lequan, R.M., Barzoukas, M. and Fort, A., *Boron Derivatives Containing a Bithiophene Bridge as New Materials for Non-Linear Optics.* J. Mater. Chem., 1996. **6**: p. 555-558.

[54] Jia, W.L., Bai, D.R., McCormick, T., Liu, Q.D., Motala, M., Wang, R.Y., Seward, C., Tao, Y. and Wang, S.M., *Three-Coordinate Organoboron Compounds Bar2r (Ar = Mesityl, R = 7-Azaindolyl- or 2,2'-Dipyridylamino-Functionalized Aryl or Thienyl) for Electroluminescent Devices and Supramolecular Assembly.* Chem. Eur. J., 2004. **10**(4): p. 994-1006.

[55] Jia, W.L., Moran, M.J., Yuan, Y.Y., Lu, Z.H. and Wang, S.N., *(1-Naphthyl)Phenylamino Functionalized Three-Coordinate Organoboron Compounds: Syntheses, Structures, and Applications in Oleds.* J. Mater. Chem., 2005. **15**(32): p. 3326-3333.

[56] Li, F., Jia, W., Wang, S., Zhao, Y. and Lu, Z.-H., *Blue Organic Light-Emitting Diodes Based on Mes2b [P-4,4'-Biphenyl-Nph(1-Naphthyl)]*. J. Appl. Phys., 2008. **103**(3): p. 034509/1-034509/6.

[57] Hudson, Z.M. and Wang, S., *Impact of Donor-Acceptor Geometry and Metal Chelation on Photophysical Properties and Applications of Triarylboranes.* Acc. Chem. Res., 2009. **42**(10): p. 1584-1596.

[58] Suresh, D., Gomes, C.S.B., Gomes, P.T., Di Paolo, R.E., Macanita, A.L., Calhorda, M.J., Charas, A., Morgado, J. and Teresa Duarte, M., *Syntheses and Photophysical Properties of New Iminopyrrolyl Boron Complexes and Their Application in Efficient Single-Layer Non-Doped Oleds Prepared by Spin Coating.* Dalton Trans., 2012. **41**(28): p. 8502-8505.

[59] Chen, P., Lalancette, R.A. and Jäkle, F., *Applying the Oligomer Approach to Luminescent Conjugated Organoboranes.* J. Am. Chem. Soc., 2011. **133**(23): p. 8802-8805.

[60] Makarov, N.S., Mukhopadhyay, S., Yesudas, K., Brédas, J.-L., Perry, J.W., Pron, A., Kivala, M. and Müllen, K., *Impact of Electronic Coupling, Symmetry, and Planarization on One- and Two-Photon Properties of Triarylamines with One, Two, or Three Diarylboryl Acceptors.* J. Phys. Chem. A, 2012. **116**(15): p. 3781-3793.

[61] Kitamura, N. and Sakuda, E., *Spectroscopic and Excited-State Properties of Tri-9-Anthrylborane I: Solvent Polarity Effects.* J. Phys. Chem. A, 2005. **109**(33): p. 7429-7434.

[62] Chen, P.K., Lalancette, R.A. and Jäkle, F., *Applying the Oligomer Approach to Luminescent Conjugated Organoboranes.* J. Am. Chem. Soc., 2011. **133**(23): p. 8802-8805.

[63] Demas, J., *Excited State Lifetime Measurements*. 1983, New York: Academic Press, Inc.

[64] Hales, J.M., Hagan, D.J., Stryland, E.W.V., Schafer, K.J., Morales, A.R., Belfield, K.D., Pacher, P., Kwon, O., Zojer, E. and Brédas, J.L., *Resonant Enhancement of Two-Photon Absorption in Substituted Fluorene Molecules.* J. Chem. Phys., 2004. **121**(7): p. 3152-3160.

[65] Shuai, Z. and Brédas, J.L., *Static and Dynamic Third-Harmonic Generation in Long Polyacetylene and Polyparaphenylene Vinylene Chains.* Phys. Rev. B, 1991. **44**(11): p. 5962-5965.

[66] Thienpont, H., Rikken, G.L.J.A., Meijer, E.W., ten Hoeve, W. and Wynberg, H., *Saturation of the Hyperpolarizability of Oligothiophenes.* Phys. Rev. Lett., 1990. **65**(17): p. 2141-2144.

[67] Wakamiya, A., Mori, K. and Yamaguchi, S., *3-Boryl-2,2′ -Bithiophene as a Versatile Core Skeleton for Full-Color Highly Emissive Organic Solids.* Angew. Chem. Int. Ed., 2007. **46**(23): p. 4273-4276.

[68] Duvanel, G.G., J.; Schuwey, A.; Gossauer, A.; Vauthey, E., *Ultrafast Excited-State Dynamics of Phenyleneethynylene Oligomers in Solution.* Photochem. Photobiol. Sci., 2007. **6**: p. 956-963.

[69] Sakuda, E., Ando, Y., Ito, A. and Kitamura, N., *Extremely Large Dipole Moment in the Excited Singlet State of Tris{[P-(N,N-Dimethylamino)Phenylethynyl]Duryl}Borane.* J. Phys. Chem. A, 2010. **114**(34): p. 9144-9150.

[70] Lakowicz, J.R., *Principles of Fluorescence Spectroscopy*. 2007: Springer.

[71] Martinez, C.R. and Iverson, B.L., *Rethinking the Term "Pi-Stacking".* Chem. Sci., 2012. **3**(7): p. 2191-2201.

[72] Wintgens, V., Valat, P. and Garnier, F., *Photochemical Generation of Radical Cations from Thiophene Oligomers.* The Journal of Physical Chemistry, 1994. **98**(1): p. 228-232.

[73] Jones, G., II, Jackson, W.R., Choi, C.Y. and Bergmark, W.R., *Solvent Effects on Emission Yield and Lifetime for Coumarin Laser Dyes. Requirements for a Rotatory Decay Mechanism.* J. Phys. Chem., 1985. **89**(2): p. 294-300.

[74] Makarov, N.S., Campo, J., Haley, M.M. and Perry, J.W., *Rapid, Broadband Two-Photon-Excited Fluorescence Spectroscopy and Its Application to Red-Emitting Reference Compounds.* Opt. Express, 2011. **1**(4): p. 551-563.

CHAPTER 5

NONLINEAR OPTICAL PROPERTIES OF TWO-PHOTON ABSORBING CHROMOPHORES IN THE PRESENCE OF SILVER NANOPARTICLES

5.1. Introduction

Metal nanoparticles (NP) have the ability to exhibit surface plasmon resonance (SPR) upon irradiation, arising from the collective oscillations of the electrons in the conduction band of the NP [1, 2]. Thus, metal NP can act as electric field intensifiers that may considerably enhance the linear and nonlinear optical properties of a material. This is particularly attractive in nonlinear processes such as two-photon absorption (2PA), wherein two photons are simultaneously absorbed by a material. Interest in materials that exhibit 2PA has been driven by the development of potential applications, such as three-dimensional (3D) fluorescence microscopy [3], 3D microfabrication [4], photodynamic therapy [5], and optical power limiting (OPL) [6]. Although substantial efforts have been directed towards developing materials with large 2PA cross sections (δ), the 2PA process is inherently weak and requires high excitation with a focused beam.

Several researchers have demonstrated the ability of metal nanostructures to increase the two-photon absorptivity or two-photon excited fluorescence (2PEF) intensity of organic chromophores [7-9]. Kano et al. report that the presence of plasmon resonance results in a 90-times enhancement of the 2PEF signal from LD490/PMMA mixture deposited on planar silver film [10]. Glass and coworkers report of a 150-fold

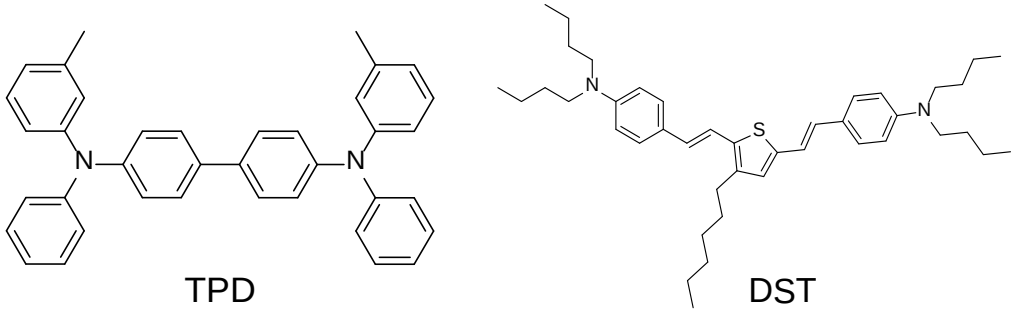

Figure 5.1. Molecular structure of the two bis-donor chromophores considered in this work: **TPD** and **DST**.

enhancement from Rhodamine B molecules adsorbed onto silver particle films [11]. Perry and coworkers report a 2PEF enhancement factor as large as 10^5 for thiol containing dyes, attached to silver nanoparticle fractal clusters [12]. Exploiting 2PA enhancement effects due to SPR in photonic applications (such as those mentioned earlier in this dissertation) would allow for the potential of greater sensitivity and lower laser intensities to be utilized in various two-photon activated processes.

The exploitation 2PA enhancement effects due to SPR is of particular interest for photonic applications, such as OPL via two-photon initiated processes. In this work, we explore the notion of plasmon-enhanced OPL. It is our hypothesis that small sized metal nanoparticle aggregates dispersed at moderate concentration in a concentrated chromophoric solution could allow for both significant changes in the photophysics of the chromophore and the enhancement of nonlinear absorption of laser pulses. Here, we investigate the photophysical and nonlinear optical properties of two bis-donor chromophores, (bis(diarylamino)biphenyl (**TPD**) and bis(di-n-butylamino)distyryl,n-hexylthiophene (**DST**), with and without the presence of AgNPs (see Figure 5.1). We also examine and compare the OPL properties of the 2PA dyes and dye/AgNP aggregates

solutions. Results from this study provide insight into the effectiveness of metal nanoparticles composite solution towards enhanced optical pulse suppression.

5.2. Photophysical Characterization of TPD and DST

5.2.1. One- and Two-Photon Absorption and Fluorescence Spectra

Figure 5.2 shows the one-photon absorption (1PA), 2PA, and fluorescence spectra of **TPD** and **DST**. The one-photon absorption wavelength maximum ($\lambda_{abs}^{(1)}$) of **DST** (447 nm) is red-shifted with respect to that of **TPD** (355 nm), consistent with the thiophene heterocycle being more electron-rich than the biphenyl π-bridge. The chromophores show strong linear absorption with similar peak molar extinction coefficients (ε_{max}) on the order of ~5 x 10^4 $M^{-1}cm^{-1}$. **TPD** and **DST** are also highly fluorescent (η> 0.7) and have structured fluorescence emission spectra, characterized by a progression of peaks and shoulders, all of which suggest a relatively planar conformation of the lowest singlet excited state of the bis-donor chromophores.

Significant differences are observed in the 2PA characteristics of the dyes. As shown in Figure 5.2a, **TPD** shows modest 2PA in the visible spectral region with a 2PA cross section (δ) of ~90 GM (1 GM ≡ 1 x 10^{-50} cm^4·s/photon-molecule) at a wavelength ($\lambda_{abs}^{(2)}$) of 550 nm, not far from the peak wavelength. The 2PA of **DST** is much stronger than that of **TPD**, where a δ_{max} of ~570 GM at ~730 nm is observed. Additionally, the 2PA band of **DST** is much broader than that of **TPD** and extends into the near-IR region. Replacing biphenyl π-bridge conjugated vinyl linkers between terminal donor units with the more electron-rich thiophene heterocycle significantly enhances 2PA response of the molecule [13, 14].

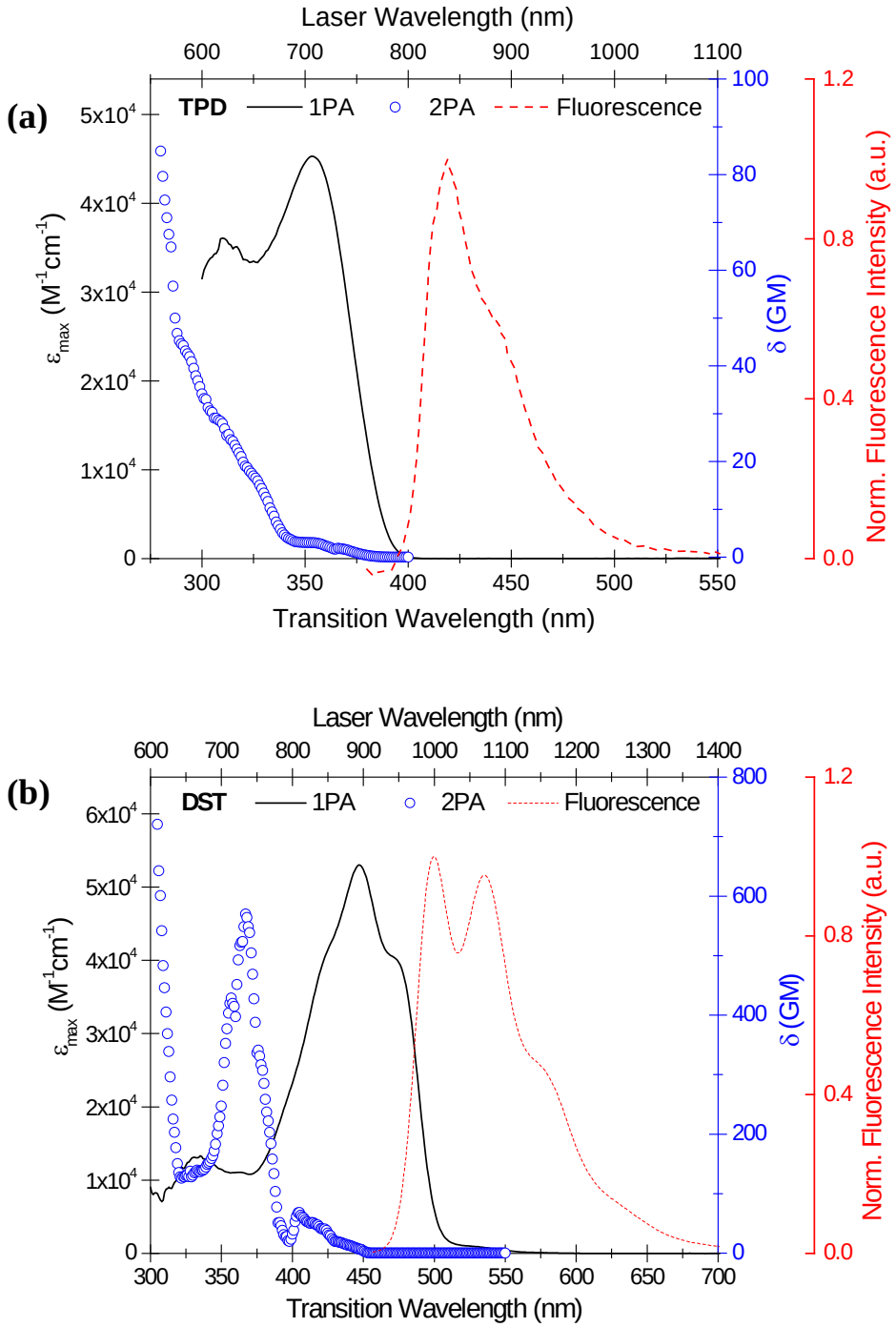

Figure 5.2. 1PA, fluorescence, and 2PEF spectra of **TPD** (a) and **DST** (b) in toluene. The solid black (—) indicates the 1PA spectrum; the 2PEF spectrum is represented by blue squares (□); the solid red line (—) is the one-photon fluorescence spectrum (excitation wavelengths for fluorescence experiments are $\lambda_{abs}^{(1)}$).

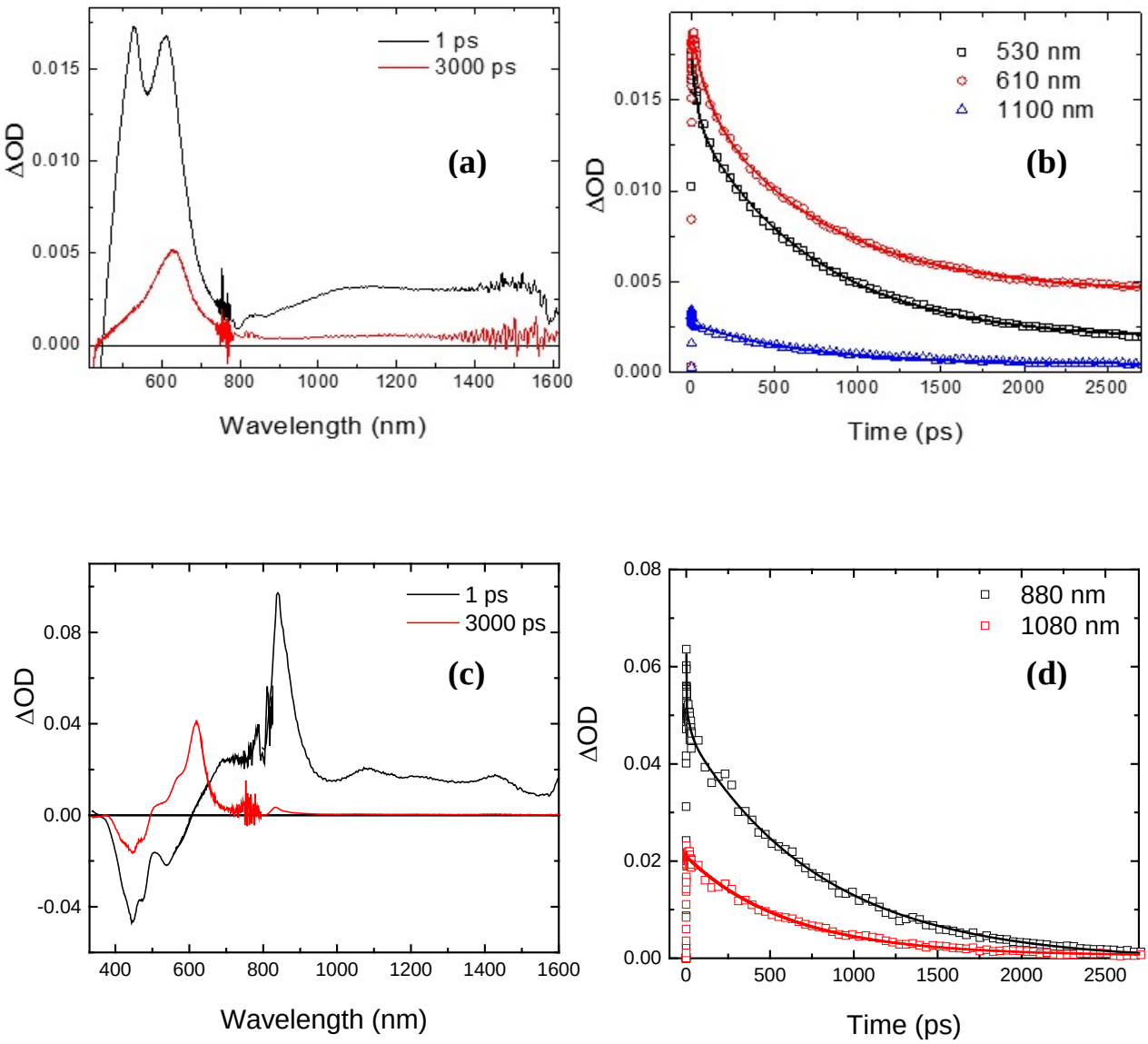

Figure 5.3. Representative femtosecond TA spectra and kinetics of **TPD** (a and b) and **DST** (c and d) in toluene. Multiexponential kinetic fits are represented as solid lines and are overlaid with the experimental data. Excitation wavelengths were 350 nm and for 420 nm for **TPD** and **DST**, respectively. Samples were prepared at 10^{-4} M and were excited at ~600 nJ/pulse.

5.2.2. Excited-State Absorption (ESA) and Transient Kinetics

In order to determine the ESA and dynamics of the two bis-donor chromophores, transient absorption (TA) spectroscopy was performed following excitation into the lowest lying one-photon allowed state of both dyes. Representative TA spectra and kinetics of **TPD** and **DST** obtained via femtosecond excitation are displayed in Figure 5.3.

As shown in Figure 5.3a, **TPD** exhibits strong singlet-singlet ESA with a structured band in the visible and a broader ESA band in the near-IR region. The singlet-singlet ESA of **DST** is also highly structured and is characterized by a well-defined peak at ~840 nm as well as vibronic structure in the near-IR. The singlet ESA kinetic traces of **TPD** are depicted in Figure 5.3b and well reproduced by a biexponential function with short and long-lived decay components of 40 ps and 730 ps. **DST** shows slightly more complicated ESA dynamics, with kinetic decays that are best fit with a triexponential function with decay lifetimes of 0.34 ps, 20 ps, and 800 ps.

The singlet-singlet ESA decays and triplet-triplet ESA in the visible is observed in both chromophores. The singlet-singlet and triplet-triplet ESA features of both **TPD** and **DST** overlap with their 2PA bands, suggesting these chromophores may exhibit effective OPL via 2PA-ESA processes in the visible and near-IR region.

5.3. Solubility Characteristics of TPD and DST

Noticeable solubility differences are observed between the two bis-donor 2PA chromophores. **TPD** was determined to be moderately soluble toluene, for which a maximum concentration of 100 mM was obtained. Because of the relatively low δ values

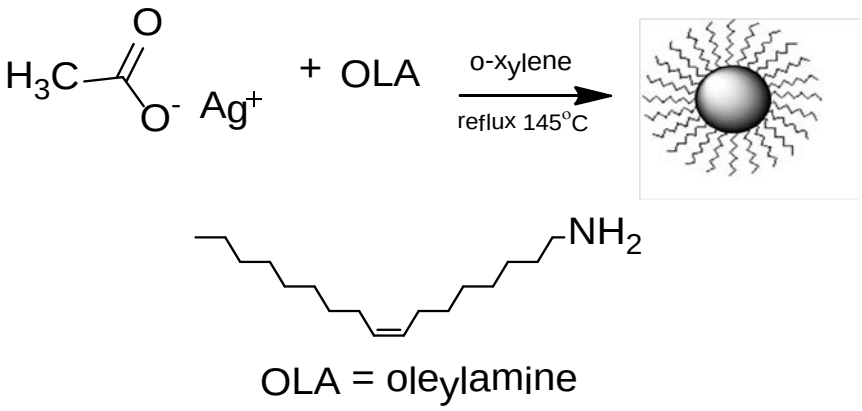

Figure 5.4. Synthesis of AgNPs in the presence of oleylamine (OLA) under reflux conditions.

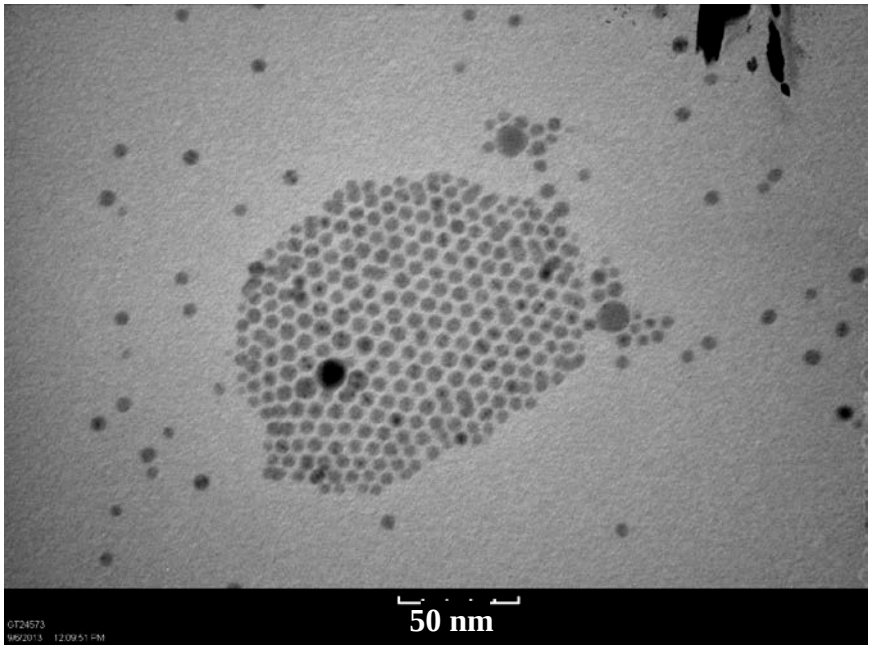

Figure 5.5. TEM image of AgNPs synthesized via the Hiramatsu method [15]. TEM images were provided by Mr. Lucas Johnstone of the Perry Research Group in the Center for Organic Photonics at the Georgia Institute of Technology.

of the chromophore, the solubility of **TPD** is a limiting factor for its usefulness in 2PA-based application.

DST, however, exhibits exceptional solubility, over 1 M in several organic solvents. Moreover, the **DST** chromophores shows little aggregation in the 1PA spectrum, such that reasonably high transmissions (>60%) are obtained in small pathlength cells. This is very encouraging for the potential use of **DST** for 2PA applications, particularly for OPL device

applications. The high solubility of the DST dye, along with the reasonably large δ values, offer the potential of greater sensitivity, thus allowing for lower laser intensities to be utilized in various two-photon activated processes.

5.4. Synthesis of Silver Nanoparticles and Their Aggregates

To investigate whether enhanced nonlinear absorption by plasmonic effects can give rise to enhanced solution-based OPL of pulsed laser systems, it is necessary to develop methods for the preparation of organic soluble aggregates of metal nanoparticles. AgNPs were prepared via a modified synthetic method reported by Hiramatsu et al. [15], which produces homogenous nanoparticles on a large scale with weakly bound protecting ligands (see Figure 5.4). This synthetic method produces 18 nm AgNPs with a narrow size distribution that are highly soluble in toluene (Figure 5.5). AgNP dissolved in toluene show a strong plasmon band at ~440 nm (see Figure 5.6).

In order for plasmon enhancement in the nonlinearity of a chromophore to occur, the 2PA of the dye must overlap with the plasmon resonance spectrum of the metal nanostructure. The 2PA bands of **TPD** and **DST** are at longer wavelengths than the AgNP plasmon absorption band at 440 nm. Therefore methods were used to increase the

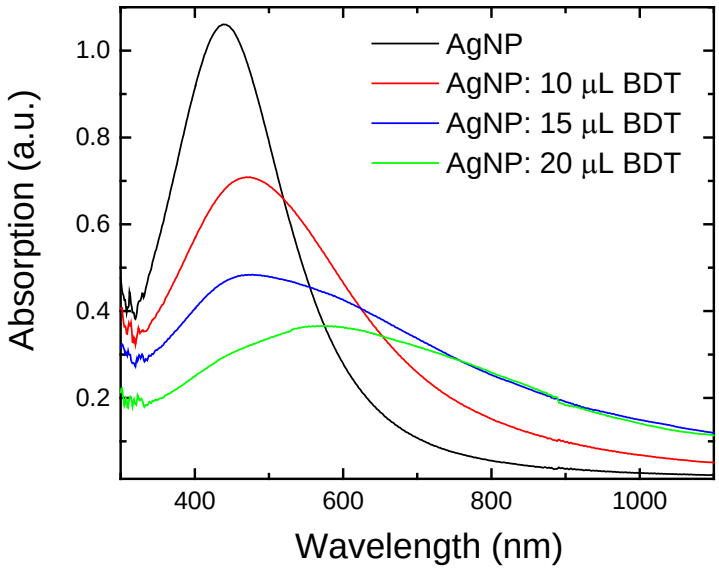

Figure 5.6. 1PA of AgNP dissolved in toluene with different additions of BDT.

size of the AgNPs by creating aggregates of the nanoparticles, thereby shifting the plasmon absorption band to longer wavelengths. Adding an aggregation inducing ligand to a solution of solvated AgNPs, such as benzene-1,4-dithiol (BDT), results in a fast exchange of ligands from the weakly bound OLA to the BDT. BDT provides two anchoring groups which result in the crosslinking of AgNPs. The resulting nanoparticle aggregates, which we denote as AgNP*, are linked in a branching arrangement and are mildly soluble in organic solvents (Figure 5.7). Figure 5.6 shows the changes in 1PA as differing amounts of BDT are added to the AgNP solution. Because of the reduction in concentration of single AgNP and the increase in concentration of aggregate metal structures, the strong plasmon absorption

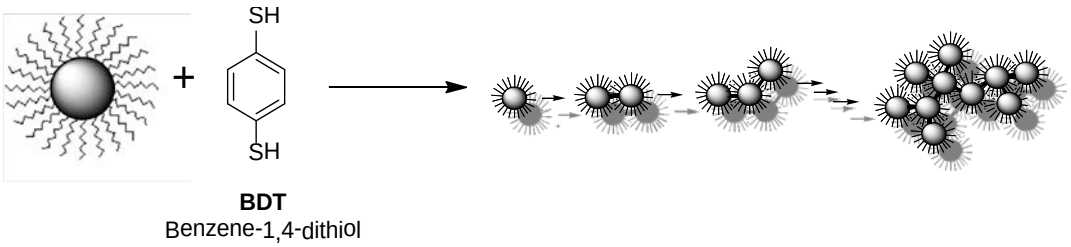

BDT
Benzene-1,4-dithiol

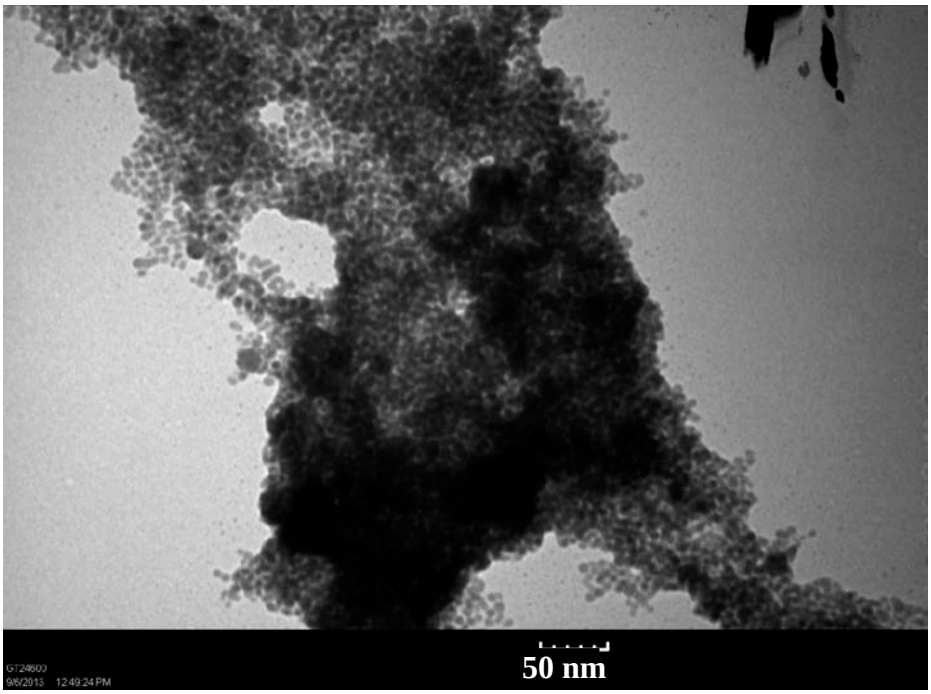

Figure 5.7. Cartoon depiction (top) and TEM image (bottom) of aggregated AgNPs obtained via aggregation-inducing BDT. TEM images were provided by Mr. Lucas Johnstone of the Perry Research Group in the Center for Organic Photonics at the Georgia Institute of Technology.

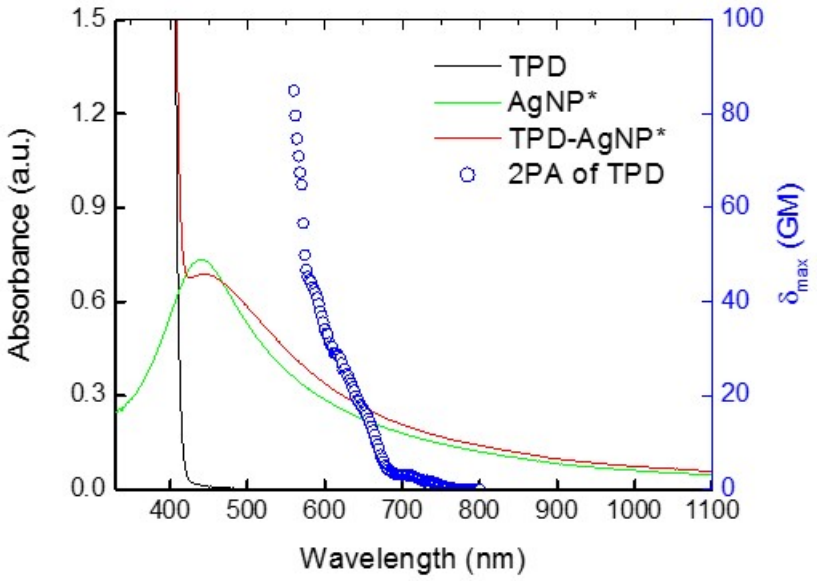

Figure 5.8. 1PA of **TPD**, AgNP*, and **TPD**-AgNP* composite solution. The 2PA of **TPD** is overlaid with the 1PA of the samples as a reference.

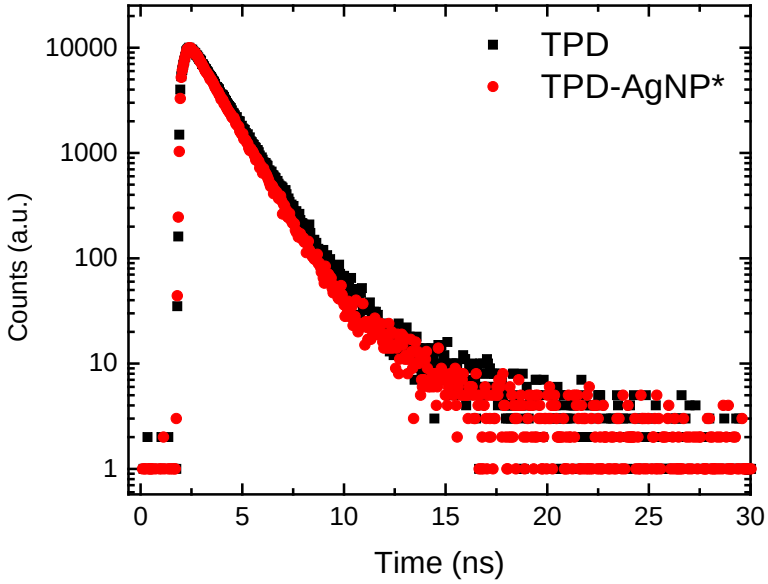

Figure 5.9. Normalized fluorescence decays collected at 375 nm excitation for toluene solutions of **TPD** and **TPD**-AgNP* solutions.

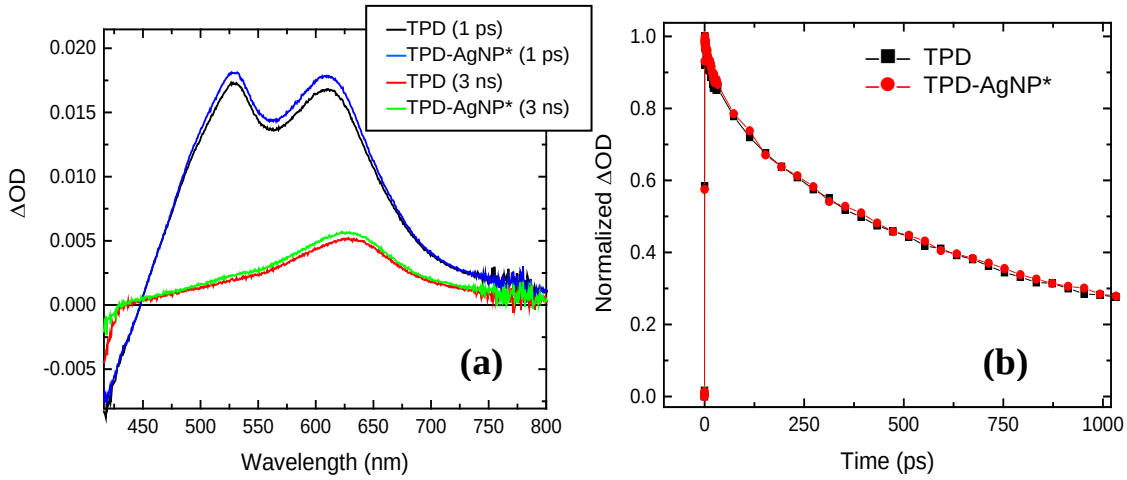

Figure 5.10. Representative TA spectra (a) and kinetic decay (b) of **TPD** and **TPD**-AgNP aggregate solutions. Samples were prepared in toluene and were excited at 350 nm at 500 nJ/pulse.

band at 440 nm was reduced and the plasmon absorption band was broadened and extends to wavelengths >1100 nm.

5.5. Photophysical characterization of TPD in the presence of AgNP Aggregates

The 1PA spectra of **TPD**, AgNP*, and **TPD**-AgNP* prepared in toluene are presented in Figure 5.8. **TPD** solutions were prepared at their highest concentration possible (100 mM) as a means to increase the dye-nanoparticle interaction. The addition of BDT to the AgNP solution resulted in a broad plasmon absorption band that overlaps well with the 2PA of **TPD**.

Time-resolved fluorescence and fs-TA measurements were performed on AgNP*-**TPD** composite solutions in order to understand how the photophysics of the dye is affected by the presence of metal particles. Figure 5.9 depicts the fluorescence decay of **TPD** and **TPD**-AgNP* composite solutions. Analysis of the decay curve measured for a

toluene solution of **TPD** revealed a monoexpontential decay lifetime of 1.3 ns. Adding AgNP* to the **TPD** solution results in very little change in the fluorescence decay curve. The fluorescence decay curve of the **TPD**-AgNP* solution is fit with a monexponential decay and shows a slight reduction in decay time to 1.1 ns, relative to neat the **TPD** solution.

The results of TA measurements performed on solutions of neat **TPD** and **TPD**-AgNP aggregates are shown in Figure 5.10. Similar to the time-resolved fluorescence measurements, very little change was observed in the TA spectra of **TPD** in the presence of AgNP*. There is a slight difference in the intensity of the ESA bands; however, this can be attributed to the plasmon absorption in this spectral region. No considerable changes were also noted in the ESA decay kinetics comparing the **TPD** neat solution to the **TPD**-AgNP aggregate composite solution.

The lack of changes in the excited-state absorption and decay of **TPD** in the presence of metal nanoparticles and their aggregates is contrary to what has been reported by other authors. Particularly, Malicki et al. report of large changes in the photophysics associated with gold nanoparticles coated with **TPD**-based thiols with alkyl spacers between the chromophore and the surface of the nanoparticle [16]. The authors find that positioning the **TPD** in close proximity of the gold nanoparticle via short alkyl linkers results in significant changes to the ultrafast dynamics of the excited states of the dye, including significant quenching of the fluorescence decay lifetime and the formation of a **TPD**-cation species upon excitation. The lack of changes in our **TPD**-AgNP* composite solution would suggest that the free chromophores are not close enough to experience

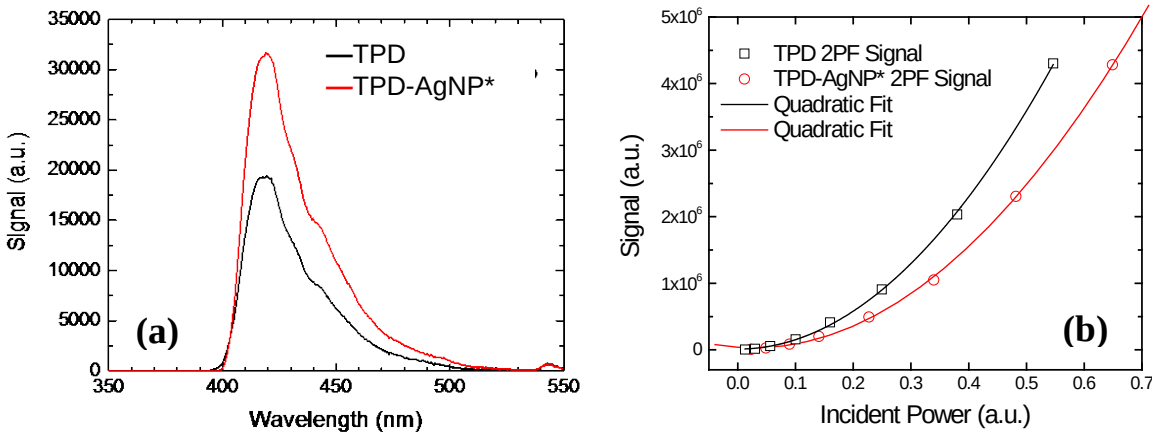

Figure 5.11. Two-photon induced fluorescence (2PEF) signal (a) and power dependence of 2PEF signal at 420 nm after excitation at 650 nm. Samples were prepared in toluene with **TPD** at 100 mM.

quenching or photooxidation due to energy or electron transfer to the metal nanoparticle [17, 18].

5.6. Plasmon Enhancement in the Nonlinear Behavior of TPD

As a means to determine the plasmon effect on the nonlinear absorption of **TPD**, the two-photon excited fluorescence (2PEF) signal was monitored after exciting directly into the 2PA band of the material (650 nm). For 2PEF measurements, the sample cell pathlength was reduced to 1 mm to reduce attenuation of the excitation beam due to plasmon absorption in the 2PA spectral region. As shown in Figure 5.11a, a substantial 1.6-enhancement in 2PEF signal is observed comparing the **TPD**-AgNP* solution to the neat **TPD** solution. Power-dependent measurements shown in Figure 5.11b confirm that the fluorescence signal is purely due to two-photon excitation. This increase in 2PEF would suggest stronger 2PA from the TPD chromophores due to plasmon enhancement effects.

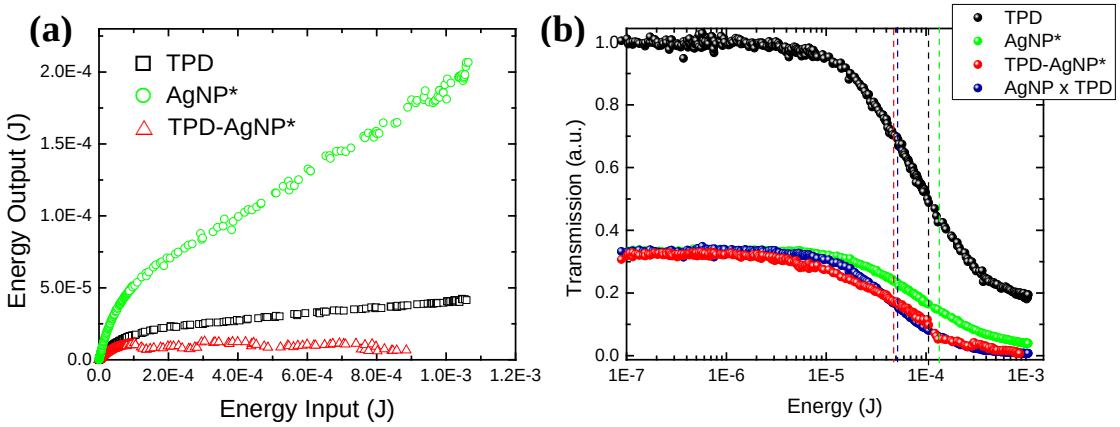

Figure 5.12. OPL curves of 100 mM solution of **TPD** (black), AgNP aggregates (green), the composite mixture of 100 mM solution of **TPD** and AgNP aggregates (red) and the product of **TPD** solution with suspension of AgNP aggregates (navy). The top plot (a) depicts the OPL curves in terms of input and output energy, while the bottom plot (b) shows the transmission dependence on the incident energy. The E_{Th} for each solution is displayed as a vertical dotted line.

Table 5.1. Energy threshold (E_{Th}) and figure-of-merit (*FOM*) values for optical limiting studies at 532 nm on solutions of **TPD**, AgNP aggregates, **TPD**-AgNP aggregate composite, and the product of **TPD** and AgNP aggregate energy-dependent curves in toluene

	TPD	**AgNP***	**TPD-AgNP***	**Product of TPD and AgNP***
E_{Th}	100 μJ	132 μJ	47 μJ	53 μJ
FOM	5.2	11	44	5.6

5.7. Optical limiting of TPD in the presence of AgNP Aggregates

The influence of AgNP* on the OPL of nonlinear medium has been studied using nanosecond laser excitation at 532 nm with the beam focused in the center of a 1 cm cuvette. **TPD** solutions were prepared in toluene at concentrations of 100 mM. AgNP* prepared using BDT as the aggregating agent were dispersed in toluene at a concentration chosen to obtain reasonable transmittance at 532 nm.

We can compare the OPL performance of the chromophore and metal nanoparticle co-solutions by quantifying the nonlinear response in terms of the energy threshold (E_{Th}) value and optical pulse suppression figure-of-merit (FOM) given by the following equations

$$E_{Th} = T_{Lin}/2 \quad \text{(Eq 5.1)}$$

$$FOM = T_{Lin}/T_F \quad \text{(Eq 5.2)}$$

where T_{Lin} is the linear transmittance at the excitation wavelength and T_F is the final transmittance of the sample before saturation or optical breakdown. The E_{Th} values are displayed in Figure 5.12b as dotted vertical lines. The values are also displayed in Table 5.1.

TPD solutions show high transparencies (~99%) at 532 nm, which is a desirable characteristics for an optical limiting material. The energy-dependent transmittance curves of the **TPD** neat solution are characterized by a high turn-on energy and a subsequent steep reduction of the transmittance. Such energy-dependent curves are indicative of a limiting mechanism involving 2PA-ESA, which is expected given the overlap of the 2PA and ESA bands of the material. Optical suppression is also observed in AgNP* solutions and is likely attributed to nonlinear scattering; however, as shown in

Figure 5.12a, the suppression of the output energy from the AgNP* solution does not compare to that observed with neat **TPD**. The FOM values, however, suggest that overall suppression is greater in AgNP* solutions compared to the neat **TPD** solutions. This is primarily due to the relatively low T_{Lin} of AgNP* solutions.

As shown in Figure 5.12a, the composite mixture shows a reduction in E_{Th} relative to that of the AgNP* and neat **TPD** in solution. The product of the **TPD** and AgNP aggregated OPL curves is shown in Figure 5.12b. Assuming there is no interaction between the chromophore and the nanoparticles, the product of the individual components should overlap with the curve of the **TPD**-AgNP aggregate co-solution. Indeed, there is good agreement between the two OPL curves, suggesting that no enhancement of OPL occurs and that the improved response is a combination of the two limiting processes of **TPD** and AgNP*. The results from the OPL measurements would suggest that no considerable enhancement of OPL is achieved in the **TPD**-AgNP* solution in comparison to the neat **TPD** solution. This is somewhat puzzling as a 1.6-enhancement in 2PEF (hence an enhancement in the 2PA of the chromophore) was observed when **TPD** was in the presence of AgNP aggregates (see Figure 5.11a). One reason that no enhancement of OPL was observed can be attributed to the low T_{Lin} of the dye-nanoparticle composite solution. 2PA-intiated processes occur high intensity in a small local volume. The high attenuation of the composite solution may prevent efficient two-photon excitation of **TPD** molecules, thus minimizing the concentration of dye molecules that will undergo 2PA-ESA.

Another possible reason for the absence of plasmon-enhanced OPL may be attributed to the low δ values and low solubility of the **TPD** dye. The maximum 2PA

cross section of **TPD** is relatively small compared to other D-π-D chromophores. Additionally, the maximum concentration of **TPD** in toluene is 100 mM. In order to realize the benefits of plasmon-enhanced OPL, the dyes and nanoparticles must be in close enough proximity to interact, thus, additional 2PA dyes must be considered that are highly soluble, possess reasonably strong two-photon cross sections, and can exhibit OPL in a small pathlength sample cell in order to reduce attenuation from the AgNP plasmon absorption.

5.8. Optical Power Limiting of DST

To determine the optical limiting capabilities of **DST**, experiments were performed using nanosecond- pulsed excitation on solutions at four representative wavelengths covering the visible and near-IR spectral region. The OPL curves are shown in Figure 5.13. Because the dye is a viscous liquid at room temperature, extremely high concentrations of 1.5 M of **DST** solutions in toluene were achieved. OPL Measurements were performed in a 1 mm pathlength cell.

DST shows exceptionally high linear transmittances (T_{Lin} > 65%) at high concentrations for all wavelengths considered in the OPL measurement. Attenuation due to nonlinear absorption begins at reasonably low energies, particularly at 620 nm, where deviation from the linear transmission is observed at ~1 μJ and a E_{Th} of 13 μJ was determined. The optical suppression of the nanosecond pulses was substantial throughout the visible and near-IR region with FOM as large as 24 or a suppression of 18 dB.

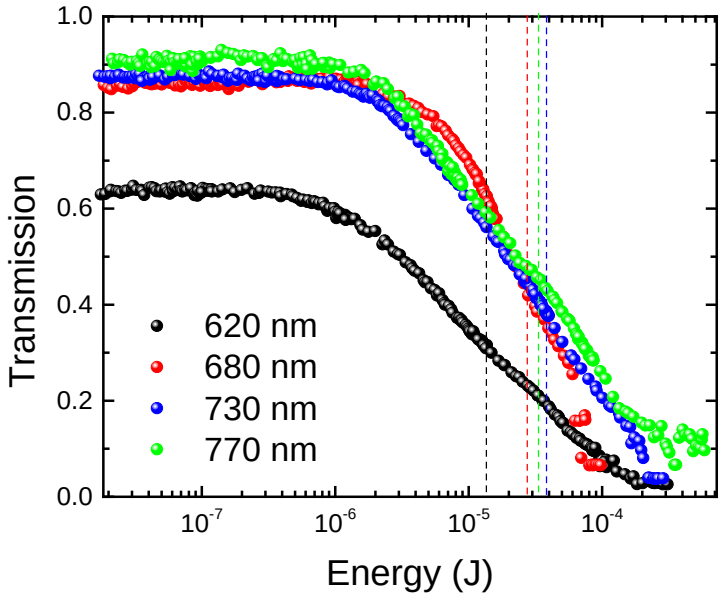

Figure 5.13. Ns-pulsed OPL of solutions of **DST** at various wavelengths across the visible and near-IR spectral region. The **DST** was prepared in toluene at 1.5 M and placed in a 1 mm sample cell. The E_{Th} for each solution is displayed as a vertical dotted line.

Table 5.2. Energy threshold (E_{Th}) and figure-of-merit (*FOM*) values for wavelength-dependent optical limiting studies on solutions of **DST** (1.5 M) in toluene

	620 nm	**680 nm**	**730 nm**	**770 nm**
E_{Th}	13 μJ	28 μJ	38 μJ	33 μJ
FOM	24	3.4	11	5.6

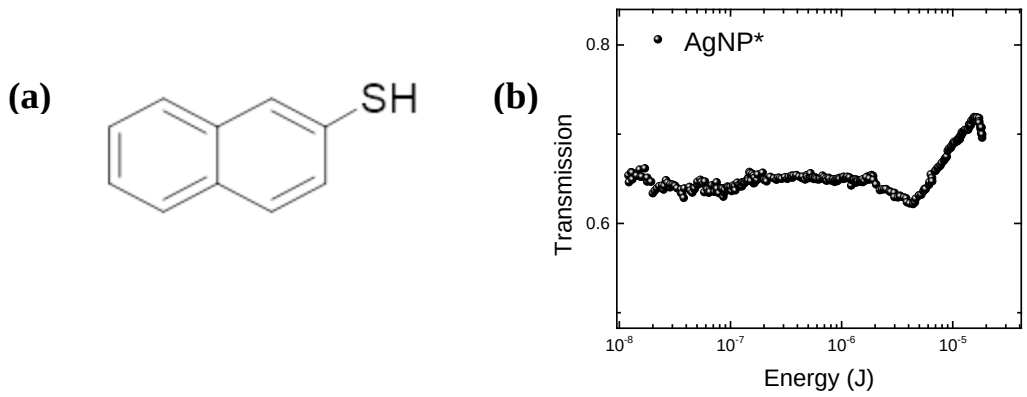

Figure 5.14. (a) Molecular structure of 2-napthalenethiol (NPT) and the energy-dependent curves of AgNP aggregates created via NPT in toluene after nanosecond-pulsed excitation at 730 nm.

The energy-dependent transmittance curves of **DST** at 620 nm are characterized by relatively low T_{Lin} values along with a gradual reduction in transmittance as the input energy is increased, suggesting a 1PA-ESA contribution to the limiting mechanism. At longer wavelengths, the OPL curves show high T_{Lin} values along steep reduction of the transmittance at higher energies, which are indicative of a limiting mechanism involving 2PA-ESA.

5.9 Preparation of AgNP Aggregates with Plasmon Absorption in the near-IR

OPL measurements of **DST** solutions show that effective 2PA-based limiting occurs in the longer wavelength (>680 nm). In order to study the proposed plasmon-enhanced OPL of the **DST** chromophore, AgNP* that exhibit plasmon absorption at longer wavelengths were synthesized. Because AgNP* created with the use of BDT show plasmon

absorption at relatively shorter wavelengths ($\lambda_{abs}^{(1)}$= 500-600 nm), a different aggregating agent was utilized. 2-napthalenethiol (NPT) has been shown to create metal nanoparticle

aggregates that absorb at longer wavelength due to the π- π stacking of the NPT, and was used to create AgNP aggregates that show plasmon absorption in the near-IR.

To achieve substantial plasmon absorption in the near-IR in a 1 mm pathlength cell, high concentrations of the AgNP aggregates were required. Unfortunately, the aggregates do not show good solubility at these concentrations. Nanosecond-pulsed OPL measurements of the AgNP aggregates made using NPT were performed at 730 nm, during which the nanoparticle aggregates showed saturable absorption. The instability of the nanoparticles in solution along with their saturable absorption behavior at high intensities suggest that AgNP aggregates created using this method are not effective for OPL. An alternative is to use a different aggregating agent that would allow for better stability at high concentrations. Another alternative is to use a different metal nanoparticle with a plasmon absorption closer to the 2PA band of **DST**, such as gold nanoparticles.

5.10. Summary

In summary, we have presented the photophysical and nonlinear characterization of 2PA dyes in the presence of silver nanoparticles and their aggregates for the possibility of plasmon-enhanced OPL. AgNPs that are highly soluble in organic solvents were synthesized. Aggregates of these AgNPs created by a ligand exchange with an aggregating agent exhibit plasmon absorption from the visible to the near-IR spectral region. The overlap of the plasmon absorption band with that of the 2PA band of our candidate 2PA dyes allowed for an exploration into the optical effects of on the photophysical and nonlinear absorption properties of 2PA dyes in the presence of metal nanoparticle aggregates. In the case of **TPD**, time-resolved fluorescence and TA

measurements revealed that the dye-nanoparticle interaction was not strong such that no appreciable changes in photophysics was observed. Two-photon induced fluorescence measurements did, however, show a 1.6-increase in the 2PEF signal of the chromophore, suggesting a considerable increase in 2PA due to the presence of the nanoparticle. OPL studies showed that **TPD** in the presence of AgNP aggregates exhibited effective OPL of ns pulses, with a reduction of threshold energy relative to solutions of the neat chromophore. Further analysis of the energy-dependent curves revealed that the co-solution of dye and nanoparticle overlaid well with the product of the individual components, suggesting there is effectively no interaction between the dye and the nanoparticle that would result in enhanced suppression.

Additional experiments were performed on a liquid dye, **DST**, which showed exceptional high solubility of 1.5 M in toluene. AgNP aggregates were created that exhibited a plasmon absorption band that overlaid with the 2PA of **DST**; however, the nanoparticle aggregates were unstable at the high concentrations necessary for OPL in a small pathlength cell. Furthermore, the AgNP aggregates showed saturable absorption at high energy. Future work would include creating highly soluble and photostable nanoparticle aggregates to better pair with the exception **DST** dye.

5.11. Experimental Details

Materials. The silver nanoparticles were synthesized according to a modified method reported by Hiramatsu and coworkers [15]. The details of the synthesis method is described elsewhere [19]. Solutions of silver nanoparticles dissolved in toluene at a concentration of ~40mg/L were obtained from the synthetic process. BDT-silver nanoparticle aggregates were created by additing 50 μL of a BDT stock solution of 15 mM prepared in toluene to 30 μL of the AgNP stock solution, along with 100 μL of toluene. NPT-silver aggregate solutions were prepared in a similar fashion, using 200 μL of a 10 mM NPT stock solution prepared in toluene, along with 200 μL of the AgNP stock solution. BPT and NPT were purchased from Aldrich.

Spectroscopic measurements were performed using toluene (spectroscopic grade, Acros Organics). Coumarin 485, (Laser dye grade, Exciton) was used as reference compounds for quantum yield and 2PA cross section measurements [20].

Spectroscopic Measurements. UV-Vis. absorption spectra were measured with a UV-Vis-NIR scanning spectrophotometer (UV-3101PC, Shimadzu). Peak molar extinction coefficient (ε_{max}) values were obtained in toluene from a linear regression analysis of absorbance versus the chromophore concentration using the Beer-Lambert equation. A spectrofluorometer (Fluorolog-2, Spex) was used for the measurement of fluorescence spectra. To obtain fluorescence spectra, all molecules were excited at their one-photon absorption maximum wavelength ($\lambda_{abs}^{(1)}$). All spectra have been corrected via subtraction of the scattering response from the solvent and the instrument's spectral response. Low concentration solutions (10^{-6} M) were used for all steady-state fluorescence measurements to minimize inner filter effects.

Fluorescence lifetimes were measured using a LifeSpec II (Edinburgh Instruments) time-correlated single-photon counting (TCSPC) system. In this measurement, a picosecond-pulsed diode laser (PicoQuant, LDH-P-C-375) with an excitation wavelength of 375 nm was used as an excitation light source. The detection system consisted of a high speed MicroChannel Plate PhotoMultiplier Tube (MCP-PMT, Hamamatsu R3809U-50) and TCSPC electronics.

Femtosecond TA spectra and kinetic traces were measured with a commercially available broadband pump-probe spectrometer (HELIOS, Ultrafast Systems LLC) using a femtosecond Ti:Sapphire regenerative amplifier laser source (Solstice, Spectra-Physics, 800-nm, 3.7-W average power, 100-fs pulse width, 1-KHz repetition rate) and a computer-controlled optical parametric amplifier (OPA) (TOPAS, Spectra-Physics, wavelength range: 266-2290 nm, pulse width: ~75 fs HW1/e) pumped by the amplified laser. The excitation wavelength was generated using the output of OPA. The white-light continuum (WLC, 330-1600 nm) probe beam was produced by focusing less than 5% of the 800 nm amplified beam into a nonlinear crystal in the Helios. A chirp correction function for the WLC probe was determined using measurements of the non-degenerate nonlinear response of carbon tetrachloride and was applied to all transient spectra. All samples for TA measurements were prepared at concentrations of ~10^{-5} M (unless otherwise noted) and were stirred continuously during measurements in 2 mm path-length fused silica cuvettes.

2PA cross sections (δ in GM) were determined using a one-arm, dual-channel referential 2PEF technique with the femtosecond-pulsed laser excitation source mentioned previously. The details of the experimental setup and method of analysis of

the data is described elsewhere [20]. All samples were prepared under atmosphere in degassed dichloromethane at a concentration of ~10^{-5} M and contained in 1 cm path-length fused silica cuvettes.

5.12. References

[1] Kelly, K.L., Coronado, E., Zhao, L.L. and Schatz, G.C., The Optical Properties of Metal Nanoparticles: The Influence of Size, Shape, and Dielectric Environment. J. Phys. Chem. B, 2002. **107**(3): p. 668-677.

[2] Link, S. and El-Sayed, M.A., Spectral Properties and Relaxation Dynamics of Surface Plasmon Electronic Oscillations in Gold and Silver Nanodots and Nanorods. J. Phys. Chem. B, 1999. **103**(40): p. 8410-8426.

[3] Zipfel, W.R., Williams, R.M. and Webb, W.W., Nonlinear Magic: Multiphoton Microscopy in the Biosciences. Nature biotechnol., 2003. **21**(11): p. 1369-1377.

[4] Zhou, W., Kuebler, S.M., Braun, K.L., Yu, T., Cammack, J.K., Ober, C.K., Perry, J.W. and Marder, S.R., An Efficient Two-Photon-Generated Photoacid Applied to Positive-Tone 3D Microfabrication. Science, 2002. **296**(5570): p. 1106-1109.

[5] Collins, H.A., Khurana, M., Moriyama, E.H., Mariampillai, A., Dahlstedt, E., Balaz, M., Kuimova, M.K., Drobizhev, M., Yang, V.X. and Phillips, D., Blood-Vessel Closure Using Photosensitizers Engineered for Two-Photon Excitation. Nature Photon., 2008. **2**(7): p. 420-424.

[6] Ehrlich, J.E., Wu, X.L., Lee, I.Y.S., Hu, Z.Y., Röckel, H., Marder, S.R. and Perry, J.W., Two-Photon Absorption and Broadband Optical Limiting with Bis-Donor Stilbenes. Opt. Lett., 1997. **22**(24): p. 1843-1845.

[7] Cohanoschi, I. and Hernández, F.E., Surface Plasmon Enhancement of Two- and Three-Photon Absorption of Hoechst 33 258 Dye in Activated Gold Colloid Solution. J. Phys. Chem. B, 2005. **109**(30): p. 14506-14512.

[8] Cohanoschi, I., Yao, S., Belfield, K.D. and Hernández, F.E., Effect of The Concentration of Organic Dyes on Their Surface Plasmon Enhanced Two-Photon

Absorption Cross Section Using Activated Au Nanoparticles. J. Appl. Phys., 2007. **101**(8): p. 086112.

[9] Wang, Y., Xie, X. and Goodson, T., Enhanced Third-Order Nonlinear Optical Properties in Dendrimer−Metal Nanocomposites. Nano Lett., 2005. **5**(12): p. 2379-2384.

[10] Kano, H. and Kawata, S., Two-Photon-Excited Fluorescence Enhanced by a Surface Plasmon. Opt. Lett., 1996. **21**(22): p. 1848-1850.

[11] Glass, A.M., Wokaun, A., Heritage, J.P., Bergman, J.G., Liao, P.F. and Olson, D.H., Enhanced Two-Photon Fluorescence of Molecules Adsorbed on Silver Particle Films. Phys. Rev. B, 1981. **24**(8): p. 4906-4909.

[12] Wenseleers, W., Stellacci, F., Meyer-Friedrichsen, T., Mangel, T., Bauer, C.A., Pond, S.J.K., Marder, S.R. and Perry, J.W., Five Orders-of-Magnitude Enhancement of Two-Photon Absorption for Dyes on Silver Nanoparticle Fractal Clusters. J. Phys. Chem. B, 2002. **106**(27): p. 6853-6863.

[13] Shuai, Z. and Brédas, J.L., Static and Dynamic Optical Nonlinearities in Conjugated Polymers: Third-Harmonic Generation and The DC Kerr Effect in Polyacetylene, Polyparaphenylene Vinylene, and Polythienylene Vinylene. Phys. Rev. B., 1992. **46**(8): p. 4395-4404.

[14] Reinhardt, B.A., Brott, L.L., Clarson, S.J., Dillard, A.G., Bhatt, J.C., Kannan, R., Yuan, L., He, G.S. and Prasad, P.N., Highly Active Two-Photon Dyes: Design, Synthesis, and Characterization toward Application. Chem. Mat., 1998. **10**(7): p. 1863-1874.

[15] Hiramatsu, H. and Osterloh, F.E., A Simple Large-Scale Synthesis of Nearly Monodisperse Gold and Silver Nanoparticles with Adjustable Sizes and with Exchangeable Surfactants. Chem. Mat., 2004. **16**(13): p. 2509-2511.

[16] Malicki, M., Hales, J.M., Rumi, M., Barlow, S., McClary, L., Marder, S.R. and Perry, J.W., Excited-State Dynamics and Dye-Dye Interactions in Dye-Coated Gold Nanoparticles with Varying Alkyl Spacer Lengths. Phys. Chem. Chem. Phys., 2010. **12**(23): p. 6267-6277.

[17] Ghosh, S.K. and Pal, T., Photophysical Aspects of Molecular Probes Near Nanostructured Gold Surfaces. Phys. Chem. Chem. Phys., 2009. **11**(20): p. 3831-3844.

[18] Thomas, K.G. and Kamat, P.V., Chromophore-Functionalized Gold Nanoparticles. Acc. Chem. Res., 2003. **36**(12): p. 888-898.

[19] Haske, W., Photophysics of Bis(Diarylamino)Biphenyl Dyes Adsorbed on Silver Nanoparticles, in School of Chemistry and Biochemistry, Ph.D. Thesis, August 2010, Georgia Institute of Technology.

[20] Makarov, N.S., Campo, J., Haley, M.M. and Perry, J.W., Rapid, Broadband Two-Photon-Excited Fluorescence Spectroscopy and its Application to Red-Emitting Reference Compounds. Opt. Express, 2011. **1**(4): p. 551-563.

CHAPTER 6

CONCLUSIONS AND FUTURE OUTLOOK

This dissertation presented the investigation of a set of conjugated molecules and polymer systems in order to understand their photophysical and nonlinear optical absorption response, as well as to show their usefulness in NLO applications, particularly optical power limiting (OPL).

As described in Chapter 1, conjugated organic materials show large nonlinearities, offer the ability for facile structural modification and processability in comparison with inorganic semiconductors. The material properties of organic conjugated systems allow for potential fabrication of NLO devices via relatively low cost solution processing. For these reasons, studies of the molecular and bulk optical properties of organic conjugated systems are essential to further the use of organic materials for NLO applications.

In Chapter 3, we discuss a structure modification approach towards increasing the efficacy of conjugated organic polymers for OPL. The addition of conjugated side-arms in a cruciform-like configuration to a PPE polymer backbone resulted in significant changes in the 1PA, 2PA, ESA band positions and bandwidths, as well as the photophysics of the co-polymers. These changes resulted in improved optical suppression of nanosecond laser pulses, as well as the bandwidth over which 2PA-ESA processes can occur efficiently, relative to the unsubstituted PPE polymer. These structure-property correlations provide a means for tailoring the optical properties of conjugated polymer systems for OPL applications. Although, the FOMs determined in Chapter 3 are far from those required for commercial-viable OPL devices, the cruciform design strategy can be applied to different conjugated polymer systems, such as poly(phenylene vinylene), that are more easily processable and possess stronger nonlinearities that PPEs.

Consequently, we suggest that further improvement of conjugated polymer 2PA and ESA properties may be achieved that could lead to much larger FOMs, and furthermore, in conjunction with optimized optical limiter device designs, the OPL FOM may be appreciably enhanced.

In Chapter 4, we investigated the intermolecular charge transfer and 2PA properties of a set of organoborane oligomers. These systems provided a set of $p\pi$-conjugated oligomer systems, that have alternating donor and acceptor units with both a quadrupolar and dipolar charge distribution, although the 2PA spectra evidence the dominance of the quadrupolar character on the 2PA properties. 2PA cross sections for the longest oligomer reached a sizable value of ~ 1400 GM, which could have utility in sensing and photonic applications. The scaling of the 2PA cross section as a function of the number of oligomeric units was determined. 2PA cross sections for the longest oligomer reached a sizable value of ~ 1400 GM, which could have utility in sensing and photonic applications. Furthermore, our studies showed that the degree of charge transfer character in these systems diminished with increasing number of oligomers. Future studies could utilize these oligomers in two-photon excited fluorescence in the detection of groups that can coordinate with the triarylborane and triarylamine groups, such as cyanide anion, borane or organoboranes, and others. There are also possibilities for detection of H_2 via heterolytic dissociation or for storage of H_2.

In Chapter 5, we studied the changes in the photophysics and nonlinear response of quadrupolar 2PA dyes due to presence of metal nanoparticles. While little changes were observed in the photophysics of the dye-nanoparticle composite solutions, an increase in two-photon excited fluorescence was detected. Optical limiting measurements revealed a significant reduction in threshold energy that can be attributed to the combination of limiting process of 2PA dyes and nanoparticles. In Chapter 5, we also investigated characterize a highly soluble 2PA chromophore, DST, that shows exceptional solubility in a variety of organic solvents and exhibits broadband optical suppression of nanosecond laser pulses in the visible and near-IR region. The silver

nanoparticle aggregates studied in this work proved to be ineffective for pulse suppression at high concentrations in the visible region.

Future studies that include the use of better controlled silver nanoparticle assemblies that provide much stronger local field enhancements at the wavelength of the 2PA-ESA processes. The use of alternative metal nanoparticles, such as gold nanoparticles, whose plasmon band overlaps well with the 2PA band of the DST chromophore could prove most intriguing. Another potential avenue for future research would include the use of smaller (~3 nm) nanoparticles to minimize the volume fraction of metal and reduce optical scattering, which has been a problem with the 18 nm silver nanoparticles.

APPENDIX A

SYNTHETIC INFORMATION OF LUMINESCENT DONOR-ACCEPTOR-DONOR TYPE BORAZINE OLIGOMERS

A.1. Introduction

This work discussed in Chapter 5 is part of a collaborative effort between Ariel Marshall and Dr. San-hui Chi of the Joseph Perry group at the School of Chemistry and Biochemistry at the Georgia Institute of Technology and Xiaodong Yin and Dr. Pangkuan Chen of the Frieder Jäkle group in the Department of Chemistry at Rutgers University. The synthesis of the oligomers and additional was conducted by the Jäkle group and is included here for additional background on this set of oligomers (Chart A.1).

A.2. Synthesis of Oligomers

Retrosynthetic analysis of the targeted ambipolar oligomers (**B*n*N*n+1***) suggests that chain extension to give larger oligomers should be readily achieved by activation of the trimethylsilyl end-capped triarylamine building block with BBr_3 as a boron source in a Si/B exchange reaction, followed by selective Sn/B exchange using two equiv of the bifunctional reagent **1-SiSn** (Scheme A.1). Subsequent stabilization of the boron center is accomplished by introducing bulky aryl groups using the copper reagent TipCu (Tip = 2,4,6-triisopropylphenyl) in refluxing toluene. Standard isolation of the crude samples followed by purification using preparative size-exclusion column chromatography on Bio-beads^{TM} and subsequent recrystallization afforded the spectroscopically pure oligomers as pale-yellow

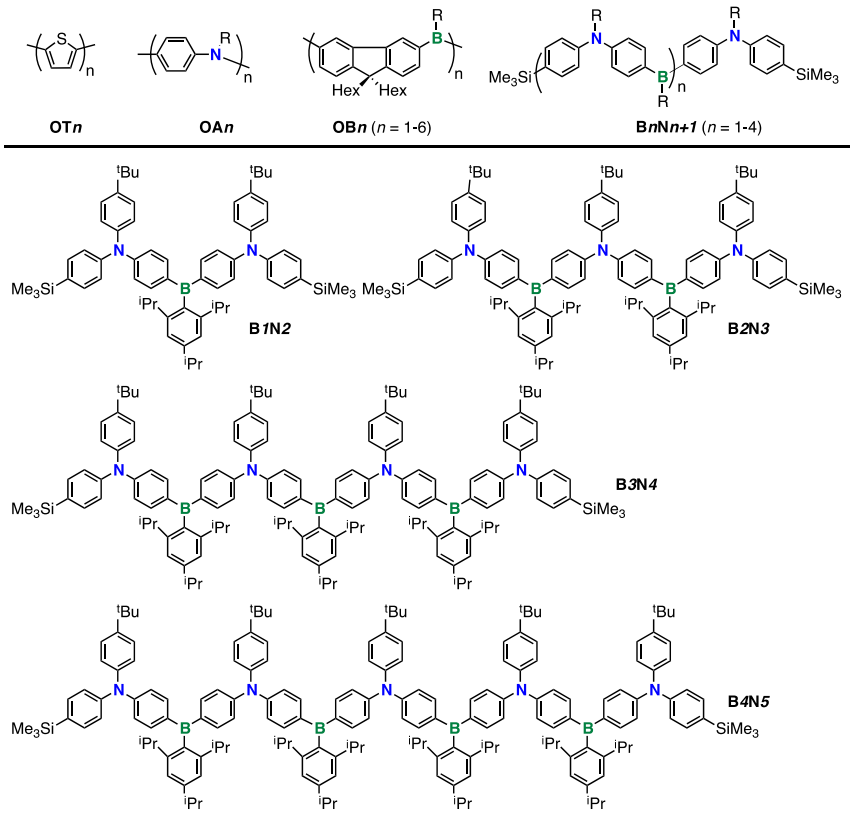

Figure A.1. Examples of well-defined conjugated oligomers with electron donor and electron acceptor moieties and structures of **B*n*N*n+1***oligomers.

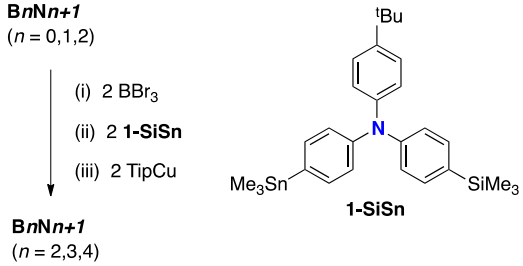

Figure A.2. Chain extension of D-A-D type linear oligomers ***BnNn+1***

powdery solids in good yields. The products are reasonably stable in air and moderately soluble in non-polar aliphatic hydrocarbons, but well soluble in chlorinated and aromatic solvents.

The structures of the oligomers were verified by high-resolution MALDI-MS, which in all cases showed the molecular ion peaks (Table A.1). Monodisperse GPC traces ($Đ$ = 1.01) ascertained the high purity of the samples (Figure A.1). The number average molecular weights (M_n) match the corresponding calculated values very well, although they are measured relative to narrow low molecular polystyrene standards.

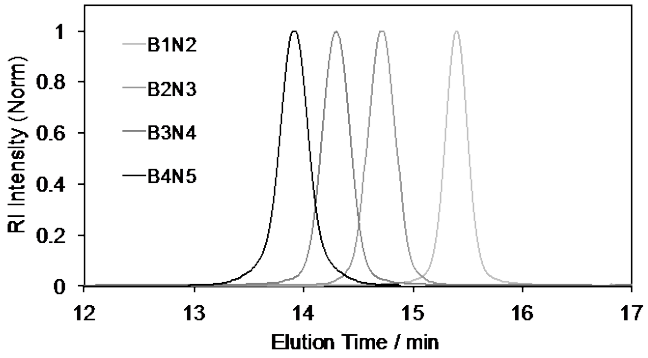

Figure A.3. GPC-RI traces for oligomers (THF, 1 mL min^{-1}).

Table A.1. Summary of GPC-RI and MALDI-MS Data

	Formula	M_{th}	M_{MS}	$M_{n,\,GPC}$	$M_{w,\,GPC}$	$Đ$ [a]
B1N2	$C_{65}H_{83}BN_2Si_2$	958.62	958.62	992	1003	1.01
B2N3	$C_{102}H_{127}B_2N_3Si_2$	1471.98	1471.98	1608	1622	1.01
B3N4	$C_{139}H_{171}B_3N_4Si_2$	1985.34	1985.33	2078	2109	1.01
B4N5	$C_{176}H_{215}B_4N_5Si_2$	2498.70	2498.68	2807	2838	1.01

[a] $Đ = M_{n,\,GPC} / M_{w,\,GPC}$

Spectroscopic characterization by multinuclear NMR corroborated the proposed structures. Integration of the proton signals in the ^{1}H NMR spectra of the higher oligomers confirmed gradual chain elongation (Figure A.2). For example, the integral ratio between the protons due to the Tip groups at 6.96 ppm and the terminal phenylene protons adjacent to the silyl groups at 7.40 ppm increases from 2:4 (**B1N2**) to 4:4 (**B2N3**), 6:4 (**B3N4**) and 8:4 (**B4N5**). Two-dimensional NMR data were acquired for **B1N2**, and NOE correlations between the aromatic protons and the *t*-Bu, $SiMe_3$, and *i*-Pr substituents allow for unequivocal signal assignments. The presence of broad ^{11}B NMR signals at ca. 70 ppm is consistent with boron in a tricoordinate environment and the number of quadrupole-broadened (Figure A.3), boron-bound carbons in the ^{13}C NMR matches the expected one. Sharp singlet peaks at ca. –4 ppm in the ^{29}Si NMR spectra correspond to the trimethylsilyl moieties attached to the terminal aryl groups.

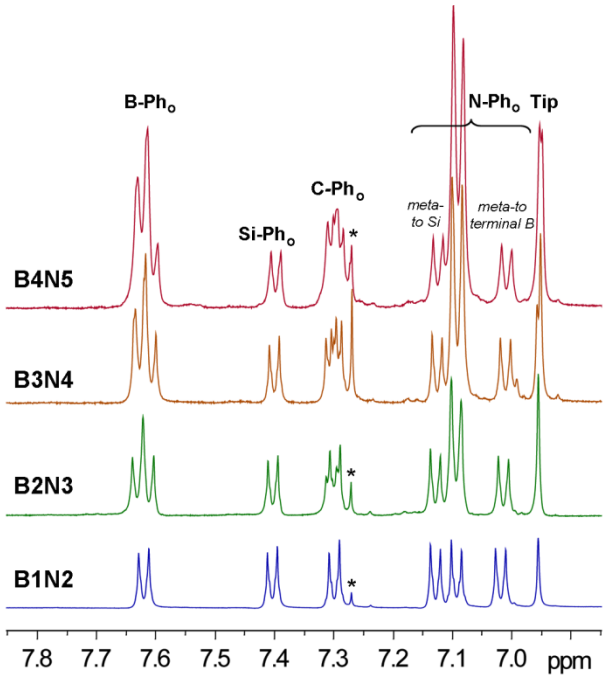

Figure A.4. Aromatic region of the ^{1}H NMR spectra for **B*n*N*n+1*** ($CDCl_3$).

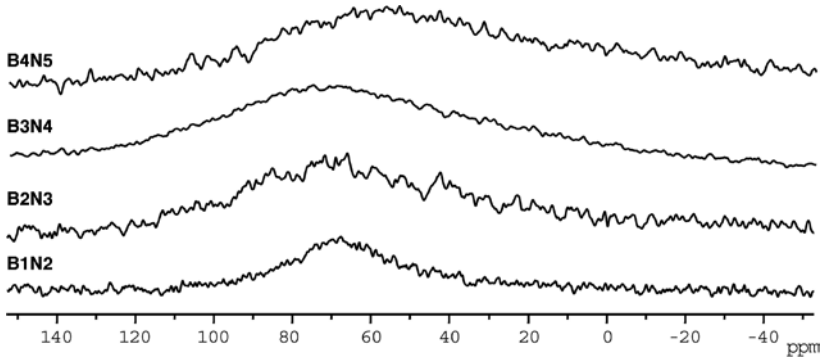

Figure A.5. Overlay of the ^{11}B NMR spectra of oligomers **B*n*N*n+1*** ($CDCl_3$, 25 °C).

VITA

Ariel Marshall was born in Benton, Arkansas. She completed her undergraduate work at the University of Central Arkansas where she received her Bachelor of Science in Chemistry in 2008. For her Ph.D. pursuit, Ariel matriculated into the Georgia Institute of Technology School of Chemistry and Biochemistry. Currently, she is a research assistant in Prof. Joseph Perry's laboratory where her research focuses on the structural, electronic and optical properties of organic conjugated small molecule and polymer systems with potential applications in electronics, photonics and photovoltaics.